THE

JOHNS HOPKINS

UNIVERSITY

DEPARTMENT

OF

PHYSICS

ORIGINAL CONTAINS
COLOR ILLUSTRATIONS

Final Report

APOLLO 17
ULTRAVIOLET SPECTROMETER
EXPERIMENT (S-169)

Task I. Principal Investigator Services

Wm. G. Fastie, Principal Investigator

July 30, 1974
                                                     Baltimore, Maryland 21218

THE JOHNS HOPKINS UNIVERSITY

DEPARTMENT OF PHYSICS
HOMEWOOD CAMPUS
BALTIMORE, MARYLAND 21218

July 30, 1974

To: Distribution

From: Wm. G. Fastie, Principal Investigator

Subject: Final Report.   PI Contract - MA-093T, NASA/MSC
           Contract NAS 9-11528.   Task I. Principal Investigator
           Services.

        We submit herewith a contractual deliverable item pre-
pared in accordance with DRD No. MA-093T.   Distribution is as
indicated below, in accordance with contract instructions.

                                        Wm. G. Fastie

WGF:ec

Distribution:

    5 Copies NASA/JSC, L. McFadin
    5   "   "   "   , N. Hardee
    4   "   "   "   , Technical Library, Attn. Retha Shirkey
    1 Copy   "   "   , E. Smith
    1   "   "   "   , Enoch Jones
    1   "   "   "   , A. Lemons
    1   "   "   "   , John Wheeler
    1   "   NASA, Floyd Roberson
    1   "   "   , G. Esenwein, Jr.
    1   "   NASA/GSFC, J. Diggins
    1   "   ONRRR/JHU, W. Girkin
    1   "   APL/JHU, T. Wyatt
    1   "   JHU, A. Ashton

FINAL REPORT

APOLLO 17

ULTRAVIOLET SPECTROMETER EXPERIMENT

(S-169)

Task I. Principal Investigator Services

Wm. G. Fastie, Principal Investigator

The Johns Hopkins University
Department of Physics
Baltimore, Maryland 21218

July 30, 1974

TABLE OF CONTENTS

I. Introduction

We summarize in this report the activities of the scientific
team in preparing the UVS experiment, supporting the flight activities,
reducing the data, and analyzing and publishing the scientific findings.

The data reduction is now complete.   All information needed
for future public use of the data and the data tapes have been filed
in the National Data Center. Although considerable analysis and
publication have been accomplished, substantial future work in this area
is anticipated.

For easy reference reprints or preprints of several of our pub-
lications   are attached as addenda to this report.

II. Scientific Objectives of the UVS Experiment

The prime mission for the spectrometer was to study resonance
reradiation of lunar atmospheric constituents for the purpose of deter-
mining the density and composition of the lunar atmosphere. As discussed
in the referenced publications, the resonance reradiation method is a
highly sensitive one and for most of the atomic species that were
expected to be present in the lunar atmosphere is capable of detecting
densities in the range from 10 to 10^3 atoms per cc.

Other objectives include the measurement of the far UV lunar albedo
which was accomplished by determining the brightness of reflected solar
radiation; the study of far UV radiation from stars and from the direction
of the galactic poles, from interplanetary dust, and from rich clusters of
galaxies, with particular emphasis on determination of the absolute spec-
tral brightness of several ultraviolet stars; the study of the distribution

of atomic hydrogen in the solar system by observing the distribution of Lyman α (1216 A) resonance reradiation over the celestial sphere; the study of ultraviolet radiation of the earth's atmosphere, including the search for a geotail; a study of ultraviolet zodiacal light emissions from the inner solar atmosphere, which observation used the limb of the Moon to cut off solar radiation; and to study light emitted by gases and/or particles released by the Apollo spacecraft.

All of the above scientific objectives were accomplished by the experiment, as summarized in Section V and in the referenced and addended publications.

III. Description and Operation of Ultraviolet Spectrometer

The spectrometer is a large Ebert grating instrument with mechanical scanning to cover the spectral range from 1180 to 1680 A. No external optics were employed to illuminate the slit, the instrument observing over a field of 1/25th of a steradian. Exit slit mirrors[1] were employed to increase the instrumental sensitivity. A complete and detailed description of the spectrometer has been published[2] and is addended.

The spectrometer was mounted in a fixed position in the scientific instrument module. The normal mode of observation in lunar orbit was to look approximately downward at the Moon. There were other modes in which the spacecraft was positioned in fixed position with respect to galactic coordinates or in cyclical modes in which a segment of the sky could be repeatedly observed. These modes are more fully described in reference 2.

IV. Instrument Preparation and Performance

A great deal of effort was expended to provide a highly precise absolute calibration of the spectrometer because the scientific analysis required absolute spectrophotometer intensity measurements. A special calibration facility was constructed.[3] In addition, the instrument was cross-calibrated at the Vacuum Optical Bench facility at Goddard Space Flight Center. Before the mission a simulation test was run in the calibration facility where the expected light intensities to which the instrument would be subjected during the flight were passed into the spectrometer to determine the stability of the calibration. During the flight the prototype spectrometer was also operated in the calibration facility in a simulated fashion but with the feedback of the actual observed signals from space to determine the stability of calibration. It was also possible in flight to track the sensitivity of the instrument by repeated observations of the same target. A small amount of degradation was observed in flight and an equivalent amount was observed during the simulated laboratory operation. In this way we have obtained intensity measurements throughout the flight with very high absolute precision.

Instrument performance during flight was almost exactly as anticipated with the exception of the fact that the dark count rate of the photomultiplier tube was about 10 to 20 times higher than anticipated. This increased count rate has been analyzed[4] as being due to unexpectedly high fluorescence of the photomultiplier window, produced by high energy

cosmic protons. The high background count thus produced degraded the ability of the instrument to see very weak light signals by about a factor of 3, but the detectivity was still extremely high as indicated in Table I.

V. Scientific Results

A. Lunar Atmosphere

Previous lunar atmosphere studies had indicated that the total pressure at the lunar surface was very low, but probably high enough to be detected by the UVS. In particular, it was anticipated that atomic hydrogen would be present at a level of about 6000 atoms/cc because of solar protons bombarding the lunar dust. Also xenon, the heaviest gas and the gas which would degas most slowly, might be present. In addition, residual volcanization would be expected to produce H, C, N, O and CO, all of which were detectable to very low limits.

None of the atomic or molecular species to which the UVS was sensitive were detected during the mission. The most surprising facet of this result is that the atomic hydrogen upper limit of about 10 atoms/cc is almost 3 orders of magnitude below the anticipated level. As reported in the Preliminary Science Report[5] and in Science[6] we conclude that solar protons are converted to molecular hydrogen by first collecting an electron at the lunar surface and then recombining with another neutral hydrogen atom. The expected H_2 concentration in this effect is just below the limit of detection for H_2 of the UVS. In the last two references the full implications of these observations

are discussed in full detail. The implication of these data with regard to degassing rates from the lunar surface will be discussed in detail.[7] The low level of lunar atmosphere determined by the UVS is in very good quantitative agreement with the Apollo 17 mass spectrometer measurement of Hoffman et al.[8] and Hodges et al.[9]

Table I below summarizes the upper limits which have been determined for all of the species studied, lists the preflight predictions and in the final column lists the upper limit of gases in the spacecraft environment as discussed in Section E below.

Table I

Species	Density at Lunar Surface (atoms/cc)	Predicted Instrument Limit	Spacecraft** Environment Limit
H	< 10	1	< 10^8
O	< 100[†]	27	<1x 10^9
N	<1200*	480*	<1x 10^{10}
C	< 120*	27*	<1x 10^9
Kr	<10000	2000	
Xe	<1000	540	
H_2	<6x10^3	—	<1x 10^{11}
CO	<2x10^4	—	<1.3 x 10^{11}

†Value published in Ref. 5 was in error.

*Values published in Ref. 2 and 5 have been reevaluated using more recent solar flux data.

**Total column density. If all the gas were in a 10 meter uniform density cloud, the density per cc would be 10^{-3} of values shown.

B. Lunar Albedo

While in lunar orbit the instrument made many measurements of the

brightness of the lunar surface from which the lunar albedo could be determined. The most important result of these measurements is that the terrae, which are brighter than the maria in the visible, are darker than the maria in the far ultraviolet. On-going lunar dust sample studies in this laboratory are attempting to determine the physical reason for this reversal in contrast. At first glance it appears that the effect could be explained if maria material has a higher refractive index than terrae material because the refractive index is the dominating physical property that determines far ultraviolet reflectivity of opaque materials, whereas in the visible region the diffuse reflectivity is controlled by the body color of the minerals. A preliminary discussion of albedo measurements was presented in the Preliminary Science Report,[5] and was presented at the Fifth Lunar Science Conference.[10] A far UV albedo map will be published in the Fifth Lunar Science Conference Proceedings.[11] The first results of the laboratory lunar dust sample studies have been published.[12]

The nature of the albedo measurements suggests that future lunar orbiting missions should carry a far ultraviolet photometer with better angular resolution and greater lunar surface coverage than was possible on the Apollo 17 mission.

C. Zodiacal Light

During the lunar orbiting phase of the Apollo 17 mission the lunar horizon was used as a mask to permit the UVS to look very close to the sun in an attempt to detect zodiacal light in the far ultraviolet for the purpose of extending and confirming far ultraviolet zodiacal light

measurements that were made by OAO-2.[13] Significant signals were obtained but the sun at the time of the measurement was in a very bright part of the Milky Way which produced a signal which must be subtracted to determine the magnitude of the zodiacal light. The necessary data handling to accomplish this has not been completed.

D. Astronomical Observations

Transearth coast provided an opportunity for a number of astronomical measurements, including (1) the absolute brightness in the far ultraviolet of several well-isolated bright stars; (2) the study of the weak emission from high galactic latitude regions; (3) a search for redshifted Lyman α radiation from clusters of galaxies; and (4) a general ultraviolet sky map.

Good measurements were obtained on the spectral brightness of six stars.[14,15] These measurements are in good agreement with theoretical calculations and will be very useful to provide absolute calibration of future ultraviolet astronomical experiments. The spectrometer observed a much lower signal at high galactic latitudes than had been observed by previous rocket observations,[14] suggesting that some source in the earth's upper atmosphere produces a false signal. The Apollo 17 cosmic background measurement was the first sensitive and reliable one made from deep space. Further analysis of these data is in progress.

No redshifted Lyman α emission was detected from the Coma cluster of galaxies or from the Virgo cluster, indicating that an excess of hydrogen in the clusters does not explain the apparent mass defect.

Since the UVS could be operated during sleep mode in a transearth coast while the spacecraft was spinning, a significant portion of the sky was mapped in the far ultraviolet. A large amount of data reduction and analysis is required to reduce these data to map form and this work has not yet been completed. The end product of this study will be to determine the origin of the ultraviolet radiation at various galactic latitudes: what portion is direct radiation from stars, and what portion is ultraviolet light scattered by interstellar dust.

E. Spacecraft Environment

The high sensitivity of the UVS to the most common atomic and molecular gas species which might be released by the spacecraft provided an opportunity to determine significant upper limits to equilibrium concentration. No species were detected in normal spacecraft operation, and no solar scattering by dust particles was observed. The upper limit to the density of gaseous components is given in the last column of Table I. These limits, determined both in lunar orbit and in trans-earth coast, indicate a much higher vacuum in the spacecraft environment than had been predicted.

Once during transearth coast the UVS was operated during a waste water dump, a urine dump and during a molecular hydrogen purge of a fuel cell. The urine dump included H_2O and produced a complicated UV fluorescent spectrum which we are analyzing.

Within a few seconds of the onset of the H_2 purge, a fluorescent spectrum of molecular hydrogen was observed. This emission disappeared

within a few seconds of the completion of the purge. These spectra have been analyzed.[16] They show very good agreement in absolute brightness and spectral distribution with theoretical calculations. These spectra are important experimental facts for applying the UV fluorescence technique to the measurement of the H_2 density in the lunar atmosphere (see Section VA) in galactic clouds, in comets and in planetary atmospheres.

F. Distribution of Atomic Hydrogen in the Solar System and in the Earth's Atmosphere

The UV sky survey during transearth coast provided a unique opportunity to measure the extended solar system atmosphere by studying the distribution of Lyman α (1216 A) radiation over the celestial sphere without interference from the earth's extended hydrogen atmosphere. These measurements had been made previously by OGO-5.[17,18] The Ly α intensities measured by Apollo agree quantitatively with the earlier observations. Further analyses to more accurately determine the distribution of solar system hydrogen are in progress. This research has as one of its purposes the study of the interaction between the solar system atmosphere and the interplanetary medium.

As Apollo 17 approached the earth, data were obtained on the distribution of Ly α radiation by the extended atmosphere of the earth. These data are currently being studied to determine whether there is a hydrogen tail on the side of the earth away from the Sun. The Apollo data quantitatively agree with earlier measurements by Mariner IV[19] in

the range 5 to 10 earth radii.

The far UV spectrum of the earth's ionosphere and lower exosphere was obtained while the spacecraft was far from the earth.[20] These data are being compared with similar measurements by rockets for the purpose of establishing the quantitative significance of observations of the far UV spectra of other planets.

VI. Information in National Data Center

All of the data transmitted by the UVS has been deposited in the National Data Center in the form of data tapes and with the data format information necessary to interpret the data tapes. In addition, copies of the preliminary science report (Addendum D) and of this final report have been filed. The data format information is reproduced in Addendum J together with information about the sensitivity decrease during lunar orbit, the background count rate and its variation, and the instrumental light scattering signal during transearth coast. The scattered light information is only significant in searching for very small signals and arises from solar system Ly α radiation scattered by the grating.

VII. Conclusion

Most of the scientific objectives for the Apollo 17 UVS were successfully accomplished, despite the uncooperative nature of the lunar atmosphere. A significant portion of the scientific data has been analyzed and published in scientific journals. Beyond this conclusion of the current program, much additional scientific analysis will be accomplished.

VIII. REFERENCES

[*   Asterisk indicates reprint is addended to report.]

1.   Wm. G. Fastie, Exit Slit Mirrors for the Ebert Spectrometer, Appl. Optics 11, 1960 (1972).

*2.   Wm. G. Fastie, The Apollo 17 Far Ultraviolet Spectrometer Experiment, The Moon 7, 49 (1973).

*3.   Informal Report, Spectrophotometric Calibration in the Far Ultraviolet (Wm. G. Fastie and D. E. Kerr).

*4.   Informal Report, Analysis of Background Counts Recorded by the Apollo 17 Far Ultraviolet Spectrometer Experiment (Prepared by Wm. G. Fastie).

*5.   NASA SP-330 Apollo 17 Preliminary Science Report 23.1 to 23.10 Ultraviolet Spectrometer Experiment.

*6.   Wm. G. Fastie et al., A Search for Far-Ultraviolet Emissions from the Lunar Atmosphere, Science 182, 710-711 (1973).

7.   G. E. Thomas et al., to be published.

8.   J. Hoffman et al., Composition and Physics of the Lunar Atmosphere (Presented at the 16th Cospar Meeting, May, 1973).

9.   R. Hodges et al., The Lunar Atmosphere Icarus 21, 415-426 (1974).

10.   R. L. Lucke et al., Far Ultraviolet Mapping from Apollo 17 (Presented at the Fifth Lunar Science Conference, 1974).

*11.   Far Ultraviolet Albedo Map. To be published in Lunar Science V.

12.   R. L. Lucke et al., Far Ultraviolet Reflectivity of Lunar Dust Samples: Apollo 11, 12 and 14. Astron. J. 78, 262-267 and 283 (1973).

13.   Lillie, C. F., OAO-2 Observations of the Zodiacal Light. The Scientific Results from the Orbiting Astronomical Observatory (OAO-2) NASA SP-310, 95-108 (1972).

14. Wm. G. Fastie et al., Astrophysical Observation from Rockets and Satellites. To be published in Proceedings of the Royal Society (1974).

*15. R. C. Henry et al., Low-Resolution Ultraviolet Spectroscopy of Several Hot Stars from Apollo 17. To be published.

*16 P. D. Feldman and Wm. G. Fastie, Fluorescence of Molecular Hydrogen Excited by Solar Extreme Ultraviolet Radiation, Ap J. 185, No. 2, Part 2, L101-104 (1973).

17. G. E. Thomas and R. F. Krassa, OGO-5 Measurements of the Lyman Alpha Sky Background, Astron. Astrophys. 11, 218 (1971).

18. J. L. Bertaux and J. E. Blamont, Evidence for Extra Terrestrial Lyman-alpha Emission: The Interstellar Wind, Astron. Astrophys. 11, 200 (1971).

19. L. Wallace et al., Mariner 5 Measurements of the Earth's Lyman-Alpha Emission, J. Geophys. Res. 75, 3769 (1970).

20. P. D. Feldman et al., Far Ultraviolet Observation of the Earth's Airglow from Apollo 17, Trans. Am. Geophys. Union 54, 401 (1973).

THE APOLLO 17 FAR ULTRAVIOLET SPECTROMETER EXPERIMENT*

WM. G. FASTIE

Dept. of Physics, The Johns Hopkins University, Baltimore, Md., U.S.A.

Abstract. The Apollo 17 command service module in lunar orbit will carry a far ultraviolet scanning spectrometer whose prime mission will be to measure the composition of the lunar atmosphere. Additional observations will include the spectral lunar albedo, the temporary atmosphere injected by the engines of the lunar exploration module, the solar system atmosphere, the galactic atmosphere and the spectra of astronomical sources, including the Earth. A detailed description of the experimental equipment which observes the spectral range 1180 to 1680 Å, the observing program and broad speculation about the possible results of the experiment, are presented.

1. Introduction

The Apollo 17 spacecraft, scheduled to be launched on December 6, 1972 will include in the scientific instrument module of the lunar orbiting service module, a large and highly sensitive far ultraviolet spectrometer which will cyclically scan the spectral region 1180 to 1680 Å every 12 seconds with a spectral resolution of 10 Å. A number of lunar, solar system and galactic observations will be made, the prime objective being to measure the lunar atmospheric emissions in an attempt to determine the density, composition, and temperature of the lunar atmosphere.

Our present knowledge of the lunar atmosphere indicates an atomic density level for all constituents below 10^5 to 10^7 atoms cc^{-1} at the lunar surface. At these levels of density scattering of solar radiation at the resonance lines of most of the atoms which are likely to be present in the lunar atmosphere requires the highest achievable instrumental sensitivity. The fact that the measurement of a very weak atmospheric emission must be made when the spacecraft is in sunlight and is also illuminated by the lunar surface, requires the use of very efficient optical baffling. The sensitivity requirement and the baffling requirement have led to the design of a large Ebert spectrometer, which is described in Section 3 and which incorporates several new features. It should be noted that the instrumentation has been optimized for atmospheric observations in the far ultraviolet and although significant galactic and solar system observations can also be made, the instrument is not optimized for some of these objectives.

The technique of observing atomic resonance line reradiation of solar far ultraviolet flux provides a very sensitive method of detection of atmospheric atomic species. The method takes advantage of the very large solar flux, the high cross-section for

---

* Paper dedicated to Professor Harold C. Urey on the occasion of his 80th birthday on 29 April 1973.

excitation at the atomic resonance lines and the long path lengths available in planetary atmospheres.

There are many operational and geometrical factors which affect the lunar atmosphere observing program. Several observing modes are required to obtain all of the data needed to determine the atmospheric parameters. For example, we must observe the dark lunar surface beyond the sunlit terminator while the atmosphere above the surface is still illuminated and we must observe the lunar atmosphere at near 90° zenith angle and at other angles against the galactic background. The solar system observations and galactic observations require other observing modes. The manner in which these observations are accomplished is described in Section 5.

2. The Lunar Atmosphere

The most definitive information about the density of the lunar atmosphere has been obtained with cold cathode pressure gauges on the lunar surface (Johnson, 1971). These measurements indicate that the maximum lunar atmospheric density on the illuminated side probably does not exceed 10^7 atoms per cc at the lunar surface and that the minimum density on the lunar dark side is greater than 10^5 atoms cc. Thus the lunar atmosphere is an exosphere with the lunar surface defining the exobase and therefore controlling the 'temperature' of the atmosphere. More specifically, there are no collisions between the atmospheric molecules or atoms. Gravitationally trapped neutral particles leave the lunar surface with a velocity which is probably determined by the local lunar surface temperatures, travel in ballistic orbits with a typical flight time of a few hundred seconds and return to the lunar surface, where the process is repeated. Eventually these particles will be ionized by the extreme ultraviolet solar radiation and can then escape from the Moon by spiraling about the magnetic field lines imbedded in the solar wind, if they do not first collide with the lunar surface and become neutralized by electron capture.

Because of the weak gravitational field of the Moon the lighter atmospheric species have a chance to escape from the Moon (the lunar escape velocity is 2.3 km^{-1}). In particular all hydrogen atoms which leave the lunar surface with the average velocity acquired from a 400 K surface (2.9 km s^{-1}) will not return.

Chemical reactions and gaseous absorption at the lunar surface can also represent a sink for pulses of gases introduced on the Moon. For example, the many tons of gas which have been introduced by the Apollo landings have undoubtedly been largely held in the lunar surface.

The sources of the lunar atmosphere are threefold; the solar wind, lunar degassing and radiogenic gases (argon and radon) formed by lunar radioactivity. A thorough discussion of the possible equilibrium concentrations of the lunar atmospheric species has been presented by Johnson (1971).

The UVS experiment has been designed to optimize the observation of atomic hydrogen and Xenon by spending about 45% of each spectral cycle scanning the resonant emissions of these two species. Since protons are the main component of the

solar wind we would expect an equilibrium concentration of H of about 10^3 atoms cc^{-1} at the lunar surface if most protons charge exchange at the lunar surface and escape. On the other hand if most of the protons charge exchange and form hydrogen molecules before leaving the surface they will not be detectable at 1216 Å (Lyα) with the UV spectrometer until they are dissociated in the atmosphere by extreme ultraviolet radiation. Primordial hydrogen atoms are certainly no longer present on the Moon because of the ease with which they can gravitationally escape. Thus the observation of atomic hydrogen in the lunar atmosphere will determine the lunar-solar relationship which will be of significance in lunar surface geology as well as in developing concepts about the origin and maintenance of planetary atmospheres.

Optimization for xenon detection at 1470 Å is planned on the basis that this heaviest of the naturally occurring gases would probably be the most resilient to the loss processes, which have reduced the primordial lunar atmosphere density to at least 10^{-12} of the density at the surface of the Earth. The solar wind xenon source is at a level that the solar wind electromagnetic field will substantially remove it; (Johnson, 1971) that is, solar wind xenon ions which charge exchange and thermalize at the lunar surface and enter the atmosphere, are ionized by extreme ultraviolet solar radiation, and escape the Moon by spiralling about the solar wind field lines. Thus the detection of xenon in the lunar atmosphere would represent an important parameter in determining the Moon's geological and atmospheric history.

Other atomic atmospheric species which might be detected by the UVS as resonance reradiation are carbon (1657 Å), oxygen (1304 Å), nitrogen (1200 Å), and krypton (1236 Å). The atmospheric species whose resonance lines are not within the UVS range are helium (584 Å), neon (744 Å), argon (1048 Å) and radon (1786 Å). The solar resonance reradiation detection method requires a solar emission line or solar continuum at the resonance line, and for Ne and Ar the Sun is so weak that instrumentation to detect their resonance reradiation at lunar density levels is beyond the state of the art. Although Helium can be detected by resonance reradiation at 584 Å, where the Sun is relatively bright, at lunar density levels detection of this radiation requires much different photometric equipment which is not capable of measuring other atmospheric species at the level of detection of which the UVS is capable. Radon is detectable by the resonance method, but the 3.8 day radioactive lifetime of radon precludes its buildup in detectable quantities. Moreover, the Apollo 16 alpha particle spectrometer provides a more sensitive radon sensor. Localized lunar radon at density levels much below the UVS sensitivity levels has been reported.

Thus the UVS experiment is capable of searching for all of the atomic species for which there is a reasonable chance of detection with the exception of helium. Any carbon, nitrogen and oxygen which may be released in the lunar atmosphere would probably become bound in the surface by chemical reaction or by absorption after a few collisions with the surface. These species will undoubtedly be present at least for a few hours in the lunar atmosphere as products of combustion of the lunar lander engine and will probably be detected by the UVS for several lunar orbits during the mission.

3. Description of Instrumentation

A. GENERAL PRINCIPLES

Because most of the expected UV emissions from the lunar atmosphere will be very weak, we have attempted to optically and electronically optimize the flight spectrometer. It is well known (e.g. Fastie, 1952) that the signal in photoelectrons per s $^{-1}$ delivered by a Littrow or near Littrow grating spectrometer is given by the formula

$$S_\lambda(\text{pe s}^{-1}) = kA_g \frac{L}{F} Q_\lambda T_\lambda, \tag{1}$$

where k is a constant which includes the source function, the slit width and the spectral dispersion; A_g is the grating area; L is the slit length; F is the spectromteer focal length; Q_λ is the quantum efficiency of the detector; T_λ is the optical transmission.

For the Apollo 17 spectrometer we have employed the largest available diffraction grating which was specially ruled for this purpose by Bausch and Lomb Optical Company and which has an optical efficiency at least twice as good as previously available gratings. We have employed the largest available photomultiplier tubes with high quantum efficiency and have designed an optical system which permits the use of a slit length to focal length ratio which provides almost a threefold improvement in output signal. By choosing a grating with the highest possible dispersion, and employing a wide spectral slit width, (which is a compromise between sensitivity and spectral resolution) we have maximized the value of k. We have also employed an electronic detector system which counts the photoelectron pulses and discriminates against electronic noise and dark current.

As a result of these several factors we have produced an instrument for the Apollo 17 mission which is at least an order of magnitude more sensitive than previous far ultraviolet spectrometers which have been used for rockets, satellites and planetary flyby missions to study planetary atmospheres.

B. DESCRIPTION OF OPTICAL-MECHANICAL SYSTEM

Figure 1 is a plan view of the spectrometer optical system. This type of instrument was conceived by Hermann Ebert (1889), buried by Kayser (1900), and resurrected in 1949 (Fastie, 1952a, b). It was first used in a space experiment in 1960 (Fastie et al., 1962) and has been widely used by many space scientists in the past decade (e.g. Barth, 1969a), Barth et al. (1969b), Crosswhite et al. (1962), Donahue and Fastie (1964), Fastie et al. (1964). In addition to its high optical efficiency, the Ebert optical system is optically simple, can achieve high spectral resolution (Fastie et al., 1958) and has a folded optical system which provides a compact instrument with a high degree of mechanical stability; all of which qualities enhance the attractiveness of the system for space applications.

As shown in Figure 1 light entering the slit reflects from one-half of the spherical Ebert mirror and goes to the diffraction grating. The diffracted light from the grating goes to the other half of the Ebert mirror which focuses the spectrum at the exit slit
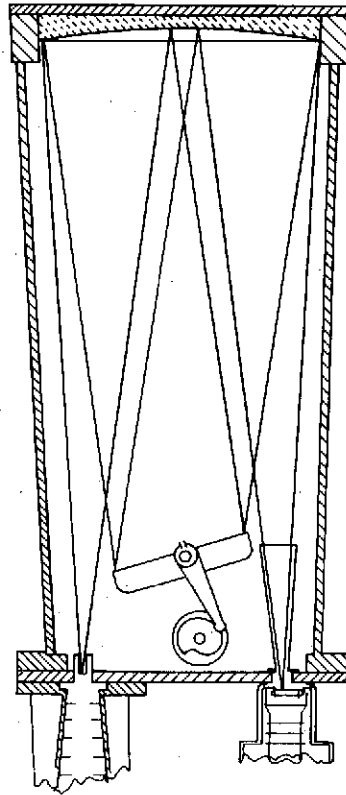
Fig. 1. Plan view of spectrometer optical system.

plane. The monochromatic light passes through the slit and strikes the photocathode of the detector. The entrance slit is longer than the exit slit, and the long spectral image thus produced is 'folded' by the exit slit mirrors to increase the monochromatic photon density passing through the slit.

The grating is mounted in a housing which contains shafts on each end about which the grating can rotate. Two bearing plates which are mounted to the slit plate provide ball-bearing mounts to support the grating shaft. A synchronous motor, gear reducer and cam mechanism to cyclically rotate the grating through its spectral range are also supported on the slit plate. The cam is designed to scan linearly in wavelength range 1180 to 1680 Å at about 75 Å per s except for two 50 Å regions centered on 1216 Å (atomic hydrogen) and 1470 Å (Xenon) which are linearly scanned at 16.6 Å s^{-1}. An optical fiducial marker monitors each cam rotation so that wavelength synchronization for all wavelengths can be accomplished throughout the mission. Photoelectron counts are accumulated for 0.1 s and the count is transmitted to the spacecraft data system as a 16 bit binary word. The optical, optical-mechanical, and electrical properties of the instrument are listed in Table I. Figure 2 is an exploded isometric view of the spectrometer.
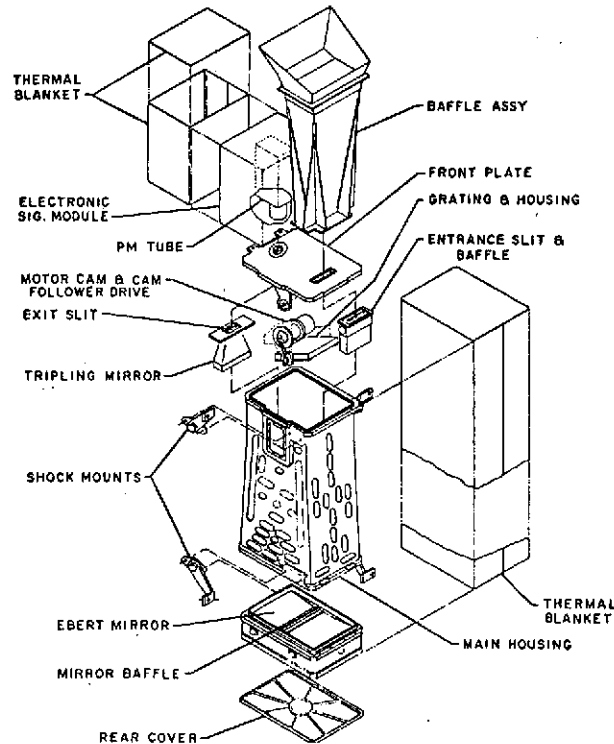
Fig. 2. Exploded isometric view of spectrometer.

The external entrance slit baffle is shown in Figure 3. The principle of this type of baffle has been previously described. In summary, the inner section of the baffle is positioned so that light scattered by it must also be scattered by the entrance slit jaws or by the inner parts of the spectrometer in order to reach the grating. The second section of the baffle is angled so that light scattered from it cannot reach the entrance slit unless it is scattered from the inner section, and so on. This type of baffle is so effective that it cannot be experimentally evaluated in air because of Rayleigh scattering. In a rocket test of a preprototype of the Apollo instrument, studies were made at solar angles which were smaller than will be encountered in lunar orbit. No scattered light was detected.

The exit slit mirror system not only increases the monochromatic signal delivered to the detector photocathode but also provides means by which loss of resolution due to curvature of spectrum can be reduced to a negligible value. The design of the exit slit system and the description of the required adjustments have been presented elsewhere. In summary, the exit slit mirrors are placed at opposite ends of the 2.2 cm long exit slit at such an angle that they reflect the end sections of the 57 mm long entrance slit image onto the exit slit as shown in an elevation view in Figure 4. In order to keep this reflected image in focus, the entrance slit must be in three linear

TABLE I

Optical and optical-mechanical parameters

|	
Focal length (F)	500 mm
Spectral resolution (including aberrations)	11.5 Å
Slit width	2 mm
Entrance slit length	57 mm
Grating area	104 cm^2
Grating spacing	3600 grooves mm^{-1}
Spectral dispersion at exit slit	5 Å mm^{-1}
Scan period	12 s
Total weight	37 lb.
Rectilinear volume (including baffle)	1 cu. ft.
Total power requirements	7 W
Telemetry rate	160 bits per s
Optical transmission (typical)	
1216 Å	20%
1470 Å	25%
1608 Å	20%
Quantum efficiency (typical)	
1216 Å	12%
1470 Å	10%
1608 Å	4%
Photocathode diameter	25 mm
Dark count rate (after pulse discrimination)	0.5 counts s^{-1}
Peak sensitivity for cm^2 col emission rate of 10^6 photon s^{-1} (1 Rayleigh)	75 photoelec s^{-1}
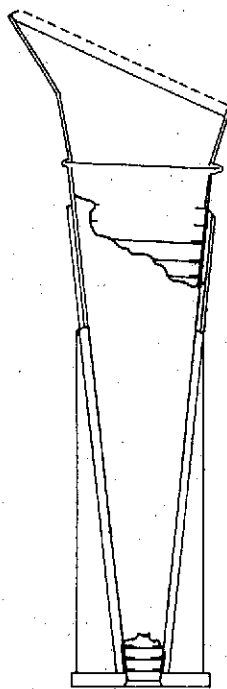
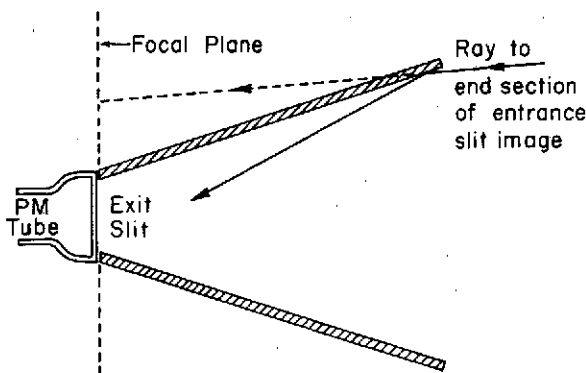Fig. 3.   External entrance slit baffle.

- Fig. 4. Elevation view of exit slit mirrors.

sections as shown in Figure 4 with the ends of the entrance slit inside the focal plane. The exit slit mirrors are used at very high angles of incidence where evaporated Al which has been oxidized in air exhibits high reflectivity in the far ultraviolet.

The Ebert mirror and the diffraction grating are coated in vacuum with Al and overcoated with MgF_2 to provide a high optical efficiency.

The signal in photoelectrons per second which will be produced by a monochromatic source which has sufficient angular extent to fill the monochromator optical system is given by the equation

$$S(\text{pe s}^{-1}) = B_\lambda^s \frac{A_s A_g}{F^2} Q_\lambda T_\lambda, \tag{2}$$

where B_λ^s is the source brightness in photons per second per sq cm per steradian and the other quantities have been defined earlier.

An atmospheric source which is optically thin and which emits over a solid angle of 4π steradians and which appears to have a brightness B_λ^s will emit $4\pi\, B_\lambda^s$ photons per sq cm column. Conversely a sq cm column emission rate of 10^6 photons per s will appear to have a surface brightness of $10^6/4\pi$ photons s^{-1}. Aeronomists use the brightness unit of Rayleigh to define a source of 10^6 photons s^{-1} cm^{-2} col.

C. ELECTRONIC CIRCUITRY

A schematic diagram of the photomultiplier tube circuitry is shown in Figure 5. Electrons which are produced by photons striking the photocathode are multiplied by the dynode string to produce a nominal pulse of 5×10^6 electrons in about 10 nanoseconds at the collector. This electron pulse is rejected by the pulse amplifier and discriminator circuit if it contains less than 5×10^5 electrons, otherwise it is converted to a low impedance square wave voltage pulse with about 1.8 μs width. Each pulse is stored in a 16 bit counter. The discrimination greatly reduces electronic noise and provides a true measure of the PMT dark count which is about 0.5 counts^{-1}. Each tenth second the accumulated stored count is transferred to a second register, and
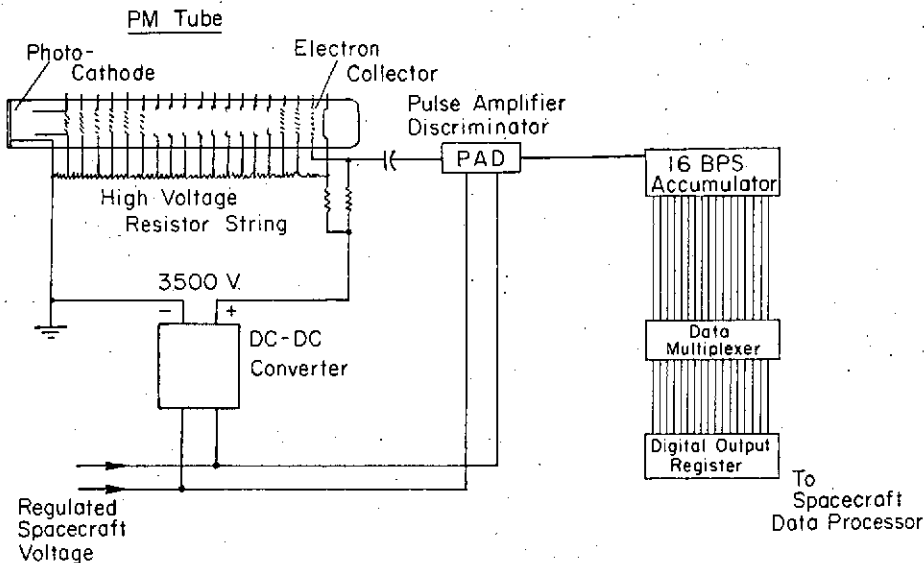
Fig. 5. Photomultiplier detector electronic schematic diagram.

during the next tenth second the second register is read out by the spacecraft data system which either telemeters the signal immediately to Earth receiving stations or, if the spacecraft is in Earth shadow, stores the information on tape for transmission to Earth during a portion of the lunar orbit when the Earth is in view.

An optical fiducial detector associated with the synchronous wavelength drive cam is used to provide a signal to begin the photoelectron count at precisely the same wavelength each spectral scan. This technique provides an opportunity to sum any desired group of the approximately 25000 spectra which will be acquired during the mission without loss of spectral resolution. During the 0.5 s flyback period of the cam follower arm a five word recognition pattern is transmitted which simplifies computer handling of the data.

Further information is separately transmitted about instrument status, such as supply voltage levels and temperature. A shutter is part of the spacecraft system and has been provided to protect the spectrometer from direct sunlight and from spacecraft attitude control jets. This shutter, special spacecraft attitudes and instrument power will be controlled on board by the astronaut crew who will verbally transmit these aspects of instrument status to the control center at Houston. The astronaut crew consists of Commander Gene Cernan, Commander Roland Evans and Dr H. H. Schmitt.

During a 1.8 μs period after the pulse amplifier discriminator has received a pulse from the photomultiplier tube, it is incapable of responding to another pulse. Therefore, when the photon flux becomes large enough that there is a significant probability that more than one photoelectron will occur during a 1.8 μs period, the observed count rate C_0 is less than the true count rate C, according to the statistical equation

$$C_T = \frac{C_0}{1 - C_0\tau}$$

(3)

or

$$\frac{1}{C_T} = \frac{1}{C_0} - \tau,$$

where τ is the dead time of the circuit.

For $\tau = 1.8$ μs and for a very large signal the observed count will approach 555, 535 counts per second. For example for 10^7 true counts per second, the observed count rate will be 526420. On the other hand the observed count rate will track the true count rate very closely, at low intensity levels, departing by only 1% at 5500 counts per second.

Thus the circuitry provides a linear response at the low count levels expected from the lunar atmosphere but can provide an extended range to measure the very large solar signal reflected from the Moon. The 16 bit counter has a maximum capacity of 65,536 counts just above the maximum counting capacity of the circuitry for a 100 ms period.

4. Sensitivity of Resonance Reradiation Method

The number of photoelectrons detected by the Apollo 17 UVS resulting from atomic resonance reradiation of an optically vertical emitting column is given by the equation

$$S(\text{photoelectrons s}^{-1}) = F_s^\lambda \sigma_\lambda N_0 H E_\lambda,$$

(4)

where F_s^λ is the solar flux in photons cm^{-2} s^{-1} Å^{-1}; σ_λ is the atomic cross-section; N_0 is the density at the base of the column; H is the scale height of the atomic species*; E is the instrumental optical and electronic conversion efficiency.

The parametric values for the atmospheric atoms of interest are listed in Table II. From the spacecraft orbital altitude of 100 km, at which height virtually all of the lunar xenon is below the spacecraft, a vertically downward observational path provides a xenon signal of 2.7×10^{-4} photoelectrons per unit xenon density at the lunar surface. If we assume that the background count rate from all sources (dark count, solar scattered radiation, galactic scatter from the dark side lunar surface) is 2 pe per second, assume a total xenon line observation time of 100 s and use the criterion that the signal to noise ratio must be one for positive detection, we can calculate the expected minimum detectable xenon concentration from the statistical formula

$$\frac{S}{N} = \frac{S(\text{pe s}^{-1})\,T}{\sqrt{(S + B)\,T}},$$

(5)

---

* The exospheric scale height is the vertical distance above the bottom of the column over which the number density of the observed specie decreases to $1/e$ of its value at the base of the column. In a constant gravitation field H can be calculated from the relationship $H = kT/mg$ where k is Boltzmann's constant, T is the atmospheric temperature at the base of the exosphere (in this case the lunar surface) m is the atomic mass and g is the gravitational constant.

TABLE II

Sensitivity to atomic species in lunar atmosphere

Atom	λ(Å)	Solar flux (photon cm^{-2} s^{-1} Å)	σ_λ ($\times 10^{15}$)	Scale height (cm)	Optical efficiency ($\times 10^5$)	Fraction of atoms below 100 km	Count rate for unit surface density	Minimum detectable concentration at surface
Hydrogen	1216 Å	4×10^{11}	5.5*	3×10^8	8.0	0.033	1.75 s^{-1}	1.0
Xenon	1470 Å	3×10^8	5.0	2×10^6	8.3	0.99	2.7×10^{-4} s^{-1}	5.4×10^2
Oxygen	1304 Å	1.7×10^{10}	0.47	1.9×10^7	8.5	0.41	5.3×10^{-3}	2.7×10^1
Nitrogen	1200 Å	6×10^6	4.5	2.1×10^7	7.8	0.38	1.7×10^{-5}	8.6×10^3
Carbon	1657 Å	5×10^{11}	4.1	2.5×10^7	2.5	0.33	4.3×10^{-1}	3.4×10^0
Krypton	1236 Å	1.2×10^7	2.3	3.5×10^6	8.1	0.94	7.8×10^{-5}	2×10^3

* Based on Equation (5), $T = 100$ s $S/N = 1$, $B = 2$ counts s^{-1}, except for Hydrogen $B = 200$ counts s^{-1}. Assumes observation of column below spacecraft against dark terminator.

where B is the background count rate and T is the observation time. For the assumed conditions the minimum detectable Xenon concentration at the lunar surface would be about 500 atoms cc^{-1}, about 4 orders of magnitude below the present upper limit.

For hydrogen, the scale height is much greater than the spacecraft altitude which means that the hydrogen density below the spacecraft is substantially constant. Because the Sun is very bright at the hydrogen resonance wavelength, the minimum detectable atomic hydrogen signal against a background count of 2 per second would be 0.1 atoms per cc at the lunar surface; however at the hydrogen wavelength the galactic signal scattered from the Moon's dark side is expected to produce a background count of about 500 counts s^{-1} which, on the basis of Equation (5) gives a minimum detectable hydrogen concentration of about $1\ cc^{-1}$, which is well below the expected minimum concentration.

A 30 times larger signal from hydrogen in the lunar atmosphere can be obtained by observing outward from the Moon, but this mode of observation must be made against the full galactic background of about 200 Rayleighs which results in a higher minimum detectable limit.

The expected minimum detectable limits for the atomic constituents of the lunar atmosphere are listed in Table II.

It should be emphasized that the resonance reradiation method of detection provides an absolute measurement. All of the parameters of Equation (5) are known or can be measured to a high degree of accuracy; that is F_s^λ, the solar flux in the far ultraviolet is well known, and will in fact be remeasured with a rocket borne spectrometer during the Apollo 17 mission, the atomic resonance scattering coefficient σ_λ has been accurately determined in the laboratory for the relevant gases, and the instrumental factor E_λ has been the subject of very careful measurements during the preparation for the mission.

5. Observing Program

The Apollo 17 spacecraft will spend most of its time in lunar orbit at a 100 km altitude with the scientific instrument module axis maintained fixed with the local vertical. The spacecraft nose will either be pointed in the direction of flight or 180° to that direction. The UVS is mounted in a fixed position in the spacecraft with its optical axis pointed 23° forward of the SIM bay axis and 18° to starboard and with the entrance slit aligned approximately perpendicular to the nadir and to the direction of flight. The lunar orbital direction is such that the spacecraft flies into darkness on the lunar sunrise terminator which is visible from the Earth throughout the mission. Thus when the spacecraft nose is pointed in the direction of flight the entire field of view of the UVS is directed at the unilluminated lunar surface before the spacecraft crosses the lunar sunrise terminator and can observe the illuminated atmosphere against the dark lunar background until the spacecraft enters the shadow which occurs about 600 km beyond the terminator, providing 400 s of observation time and about 30 spectral scans with varying shadow height. The shadow height variation provides a means of determining the scale height of the various atmospheric species.

As the spacecraft emerges from the dark and crosses the lunar sunset terminator another 400 s of lunar atmospheric observation will be possible, and will be obtained with minimum interference from the illuminated lunar surface when the spacecraft nose is pointed 180° to the direction of motion.

Because of the large temperature differential between the dark and the illuminated surface, it is anticipated that the lunar sunrise terminator (spacecraft sunset terminator) will show a denser atmosphere and lower atmospheric temperature than observed at the lunar sunset terminator.

During the bright side crossing, the UV data, combined with solar data obtained from a rocket during the mission will provide information about the far UV lunar albedo and its variation. These measurements will be compared with laboratory measurements currently in progress on lunar dust samples, and with samples returned from Apollo 17.

During lunar orbit, the spacecraft will occasionally be oriented so that the UV spectrometer observes an emitting column at a variety of lunar aspect angles including one parallel to the lunar surface, which enhances the atmospheric signal for carbon, nitrogen and oxygen by about a factor of 10, but against a stellar background which will be measured during the return flight to Earth.

When the spacecraft is in shadow, the spacecraft can be oriented to permit observations of the hydrogen atmosphere which extends to several lunar radii. This observation will permit a determination of the lunar hydrogen scale height. From within the shadow it will also be possible to observe the solar atmosphere at distances much closer to the Sun than have previously been possible, permitting a study of the extended solar atmosphere and of the zodiacal light.

During the return flight to Earth a large number of astronomical objects, including the Earth and the Moon, will be observed. Of particular interest will be a careful search for a hydrogen geotail and a study of the extended solar atmosphere.

Acknowledgements

(mirrors). Mr Louis McFadin, Manned Spacecraft Center, Houston, is the experiment manager, and Mr Nat Hardee, assisted by Mr Paul Blackmon, MSC, Houston is science experiment manager. Mr James Diggins, Goddard Space Flight Center served as optical consultant to MSC and also conducted calibration checks of the UVS with the Vacuum Optical Bench facility at GSFC. In this laboratory, much of the scientific studies and calibration work was performed by Professors Donald E. Kerr and H. M. Crosswhite, Dr R. C. Schaeffer, Mr L. J. Hruška, Mr Robert Richardson, Mr M. D. Chedester, Mr Heinz Weiser, Mr Robert Lucke and Mr L. W. Green.

Note added in proof. The spectrometer operated most satisfactorily throughout the Apollo 17 mission. All observational objectives were accomplished. An unexpectedly high background count of about 25 pulses per second (tentatively attributed to cosmic radiation) increased the minimum detectable concentration values shown in Table II by a factor of 3 or 4. None of the observable atomic species were present as major (10% to 100%) or minor (1% to 10%) constituents of the presumed lunar atmosphere of 10^6–10^7 cc^{-1}. Hydrogen was present as a trace constituent but in less than 10% of the predicted amount. Identification of other trace constituents must await computer analysis. Lunar albedo observations, solar system, galactic and Earth observations were performed and provided significant data whose analyses must await spacecraft attitude information.

References

Barth, C. A.: 1969a, *Appl. Opt.* **8**, 1295.

Barth, C. A., Fastie, W. G., Hord, C. W., Pearce, J. B., Kelly, K. K., Stewart, A. I., Thomas, G. E., Anderson, G. P., and Raper, O. F.: 1969b, *Science* **165**, 1004.

Crosswhite, H. M., Zipf, E. C., Jr., and Fastie, W. G.: 1962, *J. Opt. Soc. Am.* **52**, 643.

Donahue, T. M. and Fastie, W. G.: 1964, in P. Muller (ed.) *Space Res.* **4**, (Proceedings of the Fourth International Space Science Symposium Warsaw, June 3–12, 1963).

Ebert, H.: 1889, *Wied. Ann.* **38**, 489.

Fastie, W. G.: 1952a, *J. Opt. Soc. Am.* **42**, 641.

Fastie, W. G.: 1952b, *J. Opt. Soc. Am.* **42**, 647.

Fastie, W. G., Crosswhite, H. M., and Gloersen, P.: 1962, *J. Opt. Soc. Am.* **52**, 643.

Fastie, W. G., Crosswhite, H. M., and Heath, D. F.: 1964, *J. Geophys. Res.* **69**, 4129.

Johnson, Francis S.: 1971, *Rev. Geophys. Space Phys.* **9**, 813.

Kayser, H.: 1900, *Handbuch der Spektroscopie*, Vol. 1.

Spectrophotometric Calibration Techniques in the Far Ultraviolet

Wm. G. Fastie and Donald E. Kerr

The Johns Hopkins University
Department of Physics
Baltimore, Maryland 21218

Spectrophotometric Calibration Techniques in the Far Ultraviolet

Wm. G. Fastie and Donald E. Kerr

The Johns Hopkins University

Abstract

The problems associated with precision spectrophotometric measurements in the far ultraviolet region are discussed. The techniques and the equipment employed to absolutely calibrate a far ultraviolet spectrometer which was flown on Apollo 17 are described. National Bureau of Standards calibrated photoelectric diodes were used as reference standards. A complete vacuum optical facility, which included a premonochromator and stable UV light sources, was developed to calibrate the flight instrument. Absolute photometric calibrations in the range 1200 to 1700 A were performed with an absolute accuracy of ± 10%.

I. Introduction

There are an increasing number of laboratory and space experiments which require that the spectral brightness of light sources in the vacuum ultraviolet region be measured to a high precision. The techniques and equipment which have been developed to fulfill this need are described in this paper. The specific motivation for the development

was to calibrate a scanning photoelectric spectrophotometer which performed a wide variety of far UV observations on the Apollo 17 mission.[1,2] The facility has subsequently been employed to absolutely calibrate a number of rocket and satellite photoelectric spectrophotometers in the spectral range 1150 to 2500 A.

No standard source exists for the spectral region below 2500 A. It has been general practice therefore to separately calibrate the spectrometer photomultiplier tube against a thermopile, and/or a nitric oxide ionization cell and/or a fluorescent film of sodium salicylate coated on the face of a blue sensitive photomultiplier tube,[3] and to separately measure the optical transmission of the spectrometer. Synchrotron radiation as a standard source has also been employed.[4,5] The use of branching ratios in atomic spectra as a means of relative far UV calibrations has been often suggested but seldom used, because of difficulties in experimentally establishing that the spectral source fulfills the necessary physical conditions (no self-absorption, temperature equilibrium, no quenching, equality of discharge tube wall reflectivity and window transmission). Polarization properties of far UV spectrometers have seldom been studied. The fact that each experimenter must employ a variety of techniques to perform a calibration has led to large errors in measured brightnesses of far UV sources, generally a factor of two either way, with the exception of the Ly α 1216 A radiation of atomic hydrogen. A flowing gas nitric oxide

ionization cell[3] at this wavelength has a quantum efficiency of 81%, and its use as a standard for calibrating detectors has permitted very high precision measurements of Ly α radiation.

The techniques for providing very high precision calibration have recently been simplified by the National Bureau of Standards which now can provide very stable photodiodes which are absolutely calibrated at a large number of wavelengths between 1100 A and 3000 A to a precision of ± 6%.[6] Other developments, including stable UV light sources, vacuum optical facilities and polarization techniques, have further simplified the calibration problem. The manner in which these new techniques and facilities are combined to provide absolute calibrations in the vacuum ultraviolet to an accuracy of ± 10%, including the standard photodiode uncertainty, are described below.

II. General Description of Method

Light from a stable discharge tube is passed through a premonochromator with a small exit slit to an f/80 concave mirror which can be rastered in two dimensions so that its image can be directed to any point on the entrance slit of the spectrophotometer to be calibrated. Alternatively, the beam can be offset to illuminate about a 1 cm^2 area of a reference photomultiplier tube which is between the mirror and the spectrophotometer. The reference photomultiplier tube to

which the premonochromator beam can be directed is calibrated before and after the spectrophotometer is installed by placing an NBS diode in the spectrophotometer location so that the number of photons in the beam can be determined at all wavelengths of interest. The spectrophotometer is mounted on a gimballed plate with the gimballed axes in the entrance slit focal plane and at the center of the slit. Two-axis motion of the gimballed plate provides the means to direct the narrow calibrated beam to any area of the dispersing element.

With the calibrated monochromatic beam entering the entrance slit, the spectrophotometer is cycled through its wave-length scan a number of times to measure both the spectral signal produced by the detector system and any low level scattered light signal which may be produced by the spectrophotometer.

The above measurements provide a combined determi-nation of the product of the average optical transmission of the spectrometer and the average electronic conversion efficiency of the detector over the full aperture of the spectrophotometer and over the pertinent area of the entrance slit. For example, if the detector is a pulse-counting photomultiplier tube operating at an unknown gain at wavelength λ, the observed pulse count

rate (C_λ) is related to the photon rate S_λ in the calibrated beam by the relationship

$$C_\lambda \text{ (counts/sec)} = S_\lambda \text{ (photons/sec)} Q_\lambda T_\lambda \qquad (1)$$

where Q_λ is the apparent average quantum efficiency of that area of the detector which is illuminated and T_λ is the average transmission of the spectrophotometer.

The product $Q_\lambda T_\lambda$ is not separable by the techniques described herein, nor is separation necessary. More generally, whatever form the detector output signal S_o takes (count rate, current or voltage), the simple relationship

$$S_o = K_\lambda S_\lambda \qquad (2)$$

provides the calibration function. K_λ is a constant for each wavelength only if the detector and the detector electronic circuits are linear over the required dynamic range of the instrument. Although photomultiplier tubes are linear over about 5 to 6 orders of magnitude when used in the current mode and linear sub-picoampere to microampere electrometers are state of the art, pulse-counting circuits do not normally have as wide a dynamic range, or may be purposely designed to be nonlinear for purposes of data compression. In any case, varying S_λ over the

dynamic range in which the spectrophotometer is to be used provides a means of determining the variation of K_λ (or Q_λ T_λ) with light intensity level.

If, in applying the spectrophotometer to an observational problem, incident monochromatic radiation directly fills an entrance slit with area A_s and a dispersing element of projected area A_g the brightness of an extended radiation source is given by

$$B_\lambda = \frac{S_o F^2}{K_\lambda A_s A_g} \qquad (3)$$

where B_λ is the brightness of the source in photons/sec/cm^2/ster

F is the focal length of the spectrometer collimator

If the observed radiation is a uniform spectral continuum, the spectral width $\Delta\lambda$ of the exit slit must also be known, and the relationship can be written

$$B_\lambda/\text{unit wavelength} = \frac{S_o F^2}{K_\lambda A_s A_g \Delta\lambda} \qquad (4)$$

where $\Delta\lambda$ is the spectral width of the exit slit

Note that the length of the exit slit is not a parameter because the calibration procedures described above have indirectly included it.

If the spectrophotometer is employed to measure the continuum spectral flux from a distant star by allowing incident radiation to fall directly on the entrance slit, with no intervening optical system, the incident flux F_λ is given by

$$F_\lambda/\text{unit wavelength} = \frac{S_o}{A_s K_\lambda \Delta\lambda} \qquad (5)$$

III. Polarization Studies

To establish that the gratings in monochromators which we have employed for our rocket and satellite experiments do not introduce

significant polarization we have employed a double vacuum monochromator with a flight prototype grating in the first monochromator and the other with an identical grating, both being replicas from the same master grating.

The experimental equipment for this purpose is shown in Fig. 1. Light from a stable far UV light source is sent through a first vacuum monochromator and then through a second monochromator to a stable photomultiplier tube detector. The mechanical interface between the two monochromators includes a tubular section which permits the second monochromator to be rotated about an axis which is coincident with the central ray of its entrance beam. The vacuum pumping system is attached to a pumping port on the first monochromator and also to a pumping port on the fixed section of the interface tube between the two monochromators. The mirror M in the second monochromator can be substituted for the grating G_2 so that the grating G_1 can be tuned to the peak signal from an emission line of the source. Then the second grating is rotated to the desired grating order and the detector signal measured. Next the entire second monochromator is rotated through an angle of 90° about the common axis and the detector signal again measured. The relative signals from the two positions can be measured to a limit of about 1 or 2%, and to that limit we have not been able to detect any polarization in replica gratings of 3600 g/mm in the range 1200 A to 1800 A from several Bausch and Lomb masters.
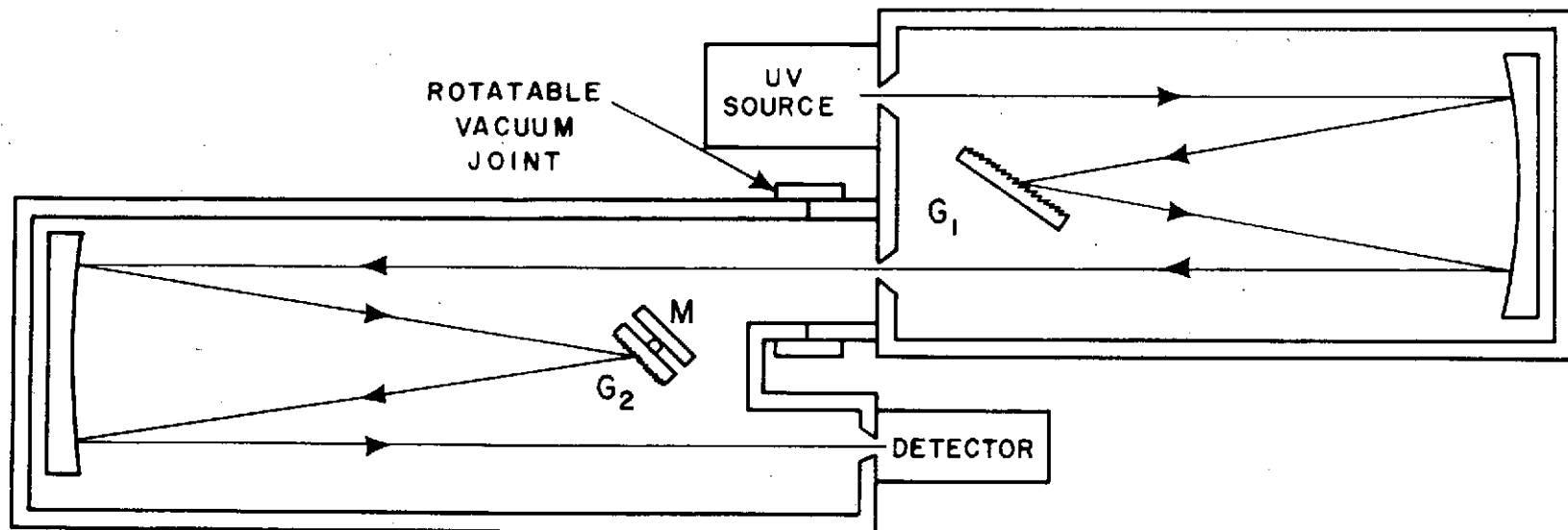
Fig. l   Vacuum Double Monochromator with 90° Rotation Capability between First and Second Monochromator.

IV. Component Evaluation

The equipment shown in Fig. 1 can be used for additional measurements. If the reflectivity of the mirror M is known, the absolute efficiency of the grating G_2 can be determined at any wavelength by measuring the ratio of the detector signal produced by the grating to that from the mirror. Likewise the scattering properties of the grating G_2 can be determined by setting the first monochromator on a bright spectral feature and measuring the detector signal from that spectral feature and the signals obtained for all angular positions of the grating G_2. For the most precise scattered light measurements, it is desirable that the UV source be monochromatic or that its strongest spectral features be employed so that the effect of light scattered by the first monochromator is minimized.

We have also used this test equipment to compare detector systems for flight packages with calibrated laboratory detectors and/or with NBS calibrated diodes. Similarly, we have tested mirrors for flight instruments by the comparison method. In the case of the Apollo 17 ultraviolet spectrometer we were thus able to select the most efficient optical and electronic components for the flight instrument.

V. Light Source for the Far-Ultraviolet Region

The Apollo 17 calibration program required a light source providing line spectra over a range of wavelengths from 1175 A to about 1700 A, which was highly stable for periods approaching 1 hour and which had emission lines or groups of lines within a 1 to 2 A band with equivalent surface brightness of roughly 10^{14} photons cm^{-2} sec^{-1} $ster^{-1}$. The maximum slit area to be illuminated was 0.25 mm^2 and the f-number of the beam was nominally 80. The molecular hydrogen lamp which was developed for this purpose, 30 of which have been made, met these requirements and because of broadly expressed interest details of its properties and method of fabrication are presented below.

The possibility of making a lamp of this type rests upon certain peculiarly fortunate chemical and thermodynamic properties of the physical system consisting of uranium + uranium hydride (UH_3) + hydrogen. The basic properties were first investigated by Spedding et al.[7] and were used by Dieke and Cunningham[8] and Dieke and Crosswhite[9] to produce high-purity spectroscopic light sources of molecular hydrogen, the rare gases and metals, the two latter sources employing the properties of U as a getter. The present lamp is a logical extension of this earlier work.

The properties of the uranium-hydrogen system which are important here are the following: (1), Uranium metal, when properly prepared in very finely powdered form, is an extremely powerful chemical

getter for all gases normally encountered in spectroscopic light sources except the rare gases; (2) the compounds formed between uranium and most elements (hydride, oxide, nitride, etc.) have thermodynamic properties such that the hydride can be formed and dissociated reversibly to yield equilibrium hydrogen pressures useful in discharge light sources (temperatures of 165°C to 227°C give hydrogen pressures from about 0.1 to 2 Torr[7]), while oxides, nitrides, etc. are more tightly bound and require higher temperatures to dissociate them. As a consequence, a mixture of U + UH_3, maintained at temperatures in the range indicated above, can provide a known and controllable pressure of hydrogen, while at the same time the pure uranium metal serves as a continuously acting effective getter for the other chemically active gases.

The physical form and method of operation of the present lamp are indicated in Fig. 2A. The light used for measurement purposes comes from an appreciable length of the positive column of a weak continuous d-c discharge, viewed end-on through the MgF_2 (or LiF) window. The lamp current is controlled to better than $\pm$ 0.05% by a commercially available precision power supply. The temperature of the U + UH_3 is controlled to within approximately $\pm$ 1°C by a feedback circuit using a thermistor temperature sensor in intimate thermal contact with the spherical bulb containing the uranium. The equilibrium temperature is typically about 190°C, corresponding to
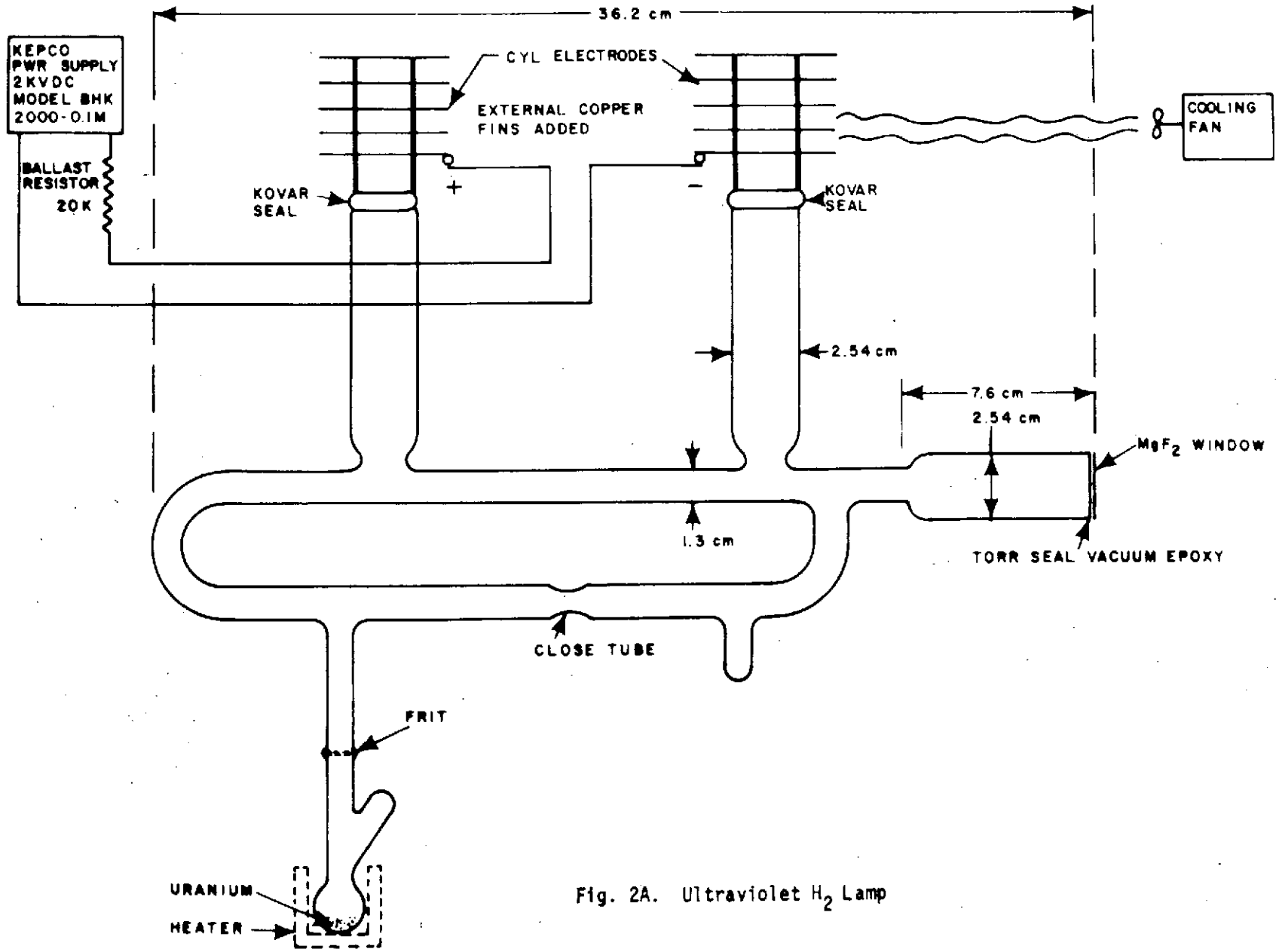
Fig. 2A. Ultraviolet H_2 Lamp

an equilibrium hydrogen pressure of about 0.36 Torr, although stable

operation is possible over a considerable range of both pressure and

current.

The part of the lamp fabrication procedure concerned specifically

with the uranium can be sketched as follows. About 1.3 gm of pure

uranium chips, turnings, or slivers cut from a thin uranium sheet is

carefully cleaned in warm dilute HNO_3 to remove the surface oxide,

washed thoroughly in distilled water and dried, and put into the lamp's

small spherical container before appreciable oxide has reformed (1/2

hour). The lamp is sealed onto the vacuum system and pumped to

about 10^{-6} Torr while the uranium bulb is heated by a small electric

oven to about $200^{\circ}C$ to drive off all moisture. The uranium is cooled

to room temperature, and hydrogen is admitted to a pressure just under

1 atmosphere. (The highest purity of hydrogen is not necessary, but

it should be free of water.) The temperature of the oven is very slowly

increased while the pressure in the system is observed on an accurate

pressure gauge. At temperatures of roughly $130^{\circ}C$ a pressure drop

indicates the beginning of the conversion of the metallic uranium to

the hydride. Depending upon the rate of change of temperature and

the size and surface state of the uranium particles, only part of the

uranium is converted to the hydride in this first step; consequently

the oven temperature should be raised and lowered slowly between

roughly $100^{\circ}C$ and $270^{\circ}C$ several times until the minimum pressure

is approximately constant; as emphasized by Spedding,[7] carrying this step (or the later ones) to completion may require at least 48 hours. Usually 4 hours is sufficient to achieve roughly 80% of any of the reactions involved, and because the quantity of uranium used is more than adequate, it is seldom worth the time to attempt totality of any of the reactions. One gram of uranium requires 0.15 liter-atm. of H_2 for complete conversion to UH_3. It is convenient to provide sufficient volume in the gas-handling system so that the minimum pressure does not drop below about 1/2 atmosphere, because the reaction rate depends fairly strongly on excess hydrogen pressure.

After conversion to the hydride is complete the lamp could be used as a hydrogen source with no further changes, but because the gettering action of pure uranium is also desired   part of the hydrogen must be driven off. The shape of the curves, representing equilibrium dissociation pressure of hydrogen[7] over $U + UH_3$, suggests that U and UH_3 be provided in roughly equal amounts. Consequently the oven tem-perature is raised to about $430^{\circ}C$ and held for several hours, when the UH_3 will be mostly dissociated, leaving pure uranium metal and hydro-gen, at a pressure essentially equal to the initial cold filling pressure. (It is advisable to vary temperature between about $100^{\circ}C$ and $430^{\circ}C$ several times, waiting several hours at each end of the cycle, until the corresponding total change in hydrogen pressure, ΔP, is essen-tially constant.) This value of ΔP is a direct measure of the quantity
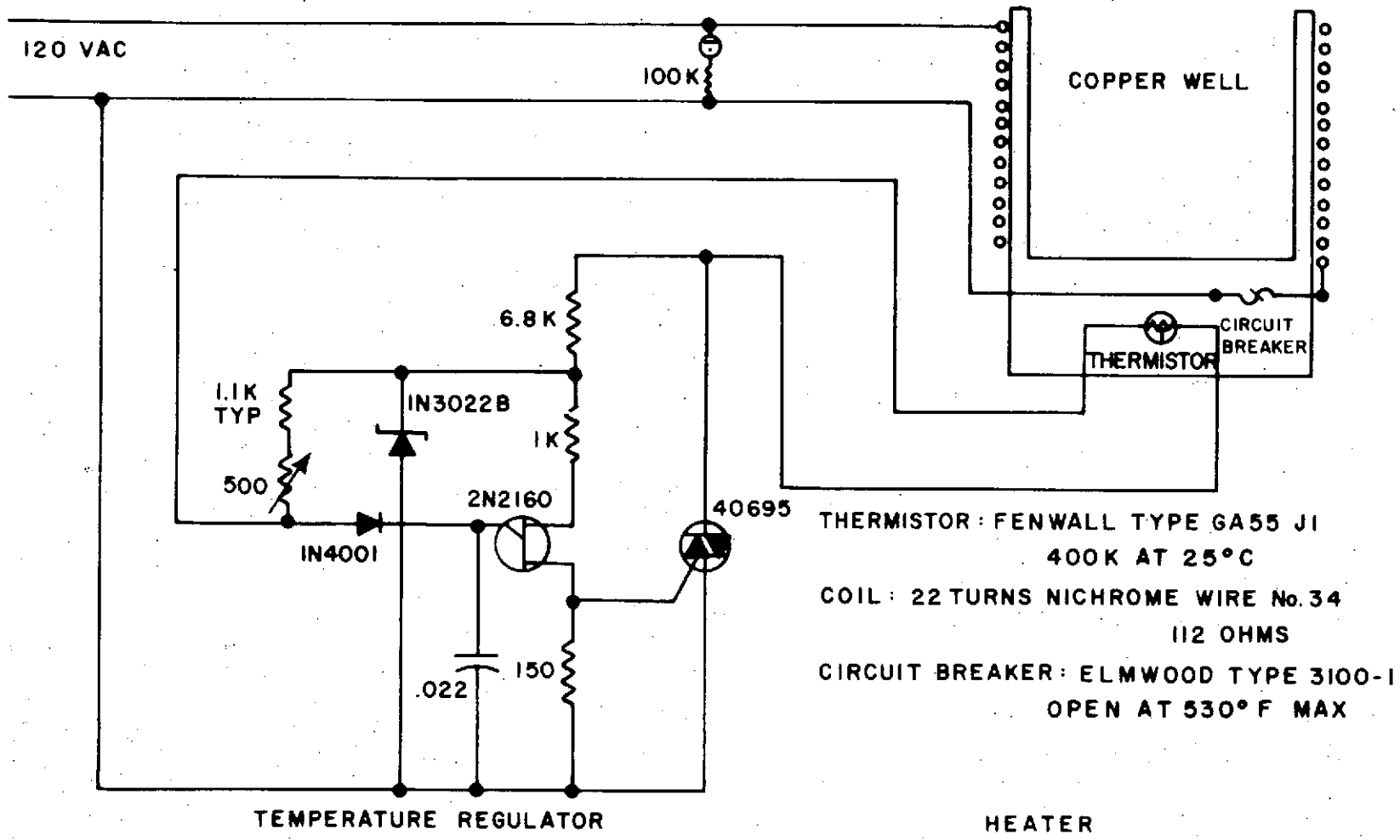
Fig. 2B. Temperature Regulator and Heater

of hydrogen required to convert the uranium completely to the hydride. The last step is to raise the oven temperature to $430^{O}C$, wait for the pressure to stabilize, pump off enough hydrogen to drop the pressure by $\Delta P/2$, cool to room temperature, and seal the lamp off the vacuum system. The uranium bulb then contains a mixture of approximately 50% uranium metal and 50% uranium hydride, in the form of a dark brown or black powder of extremely fine particles. A small electrical heater with a temperature controller is then permanently installed on the spherical bulb. Care should be taken in handling the lamp, for if the processed uranium is exposed suddenly to air it burns to form a fine powder of uranium oxide which should not be breathed.

With the heater control circuit (Fig.2B) set to give a temperature of the uranium bulb of approximately $190^{O}C$ and lamp current up to about 60 ma, the lamp gives a rich spectrum of molecular hydrogen and strong Lyman α at 1216 A, the latter with some self-reversal. Figure 3 shows a sample scan of parts of the spectrum, taken with a spectrometer resolution of 0.08 A. The spectrum has been searched carefully between 1200 A and 1700 A and no traces of impurities have been found. There is a small amount of continuum in the 1600 to 1700 A region which is due to molecular hydrogen. The stability of intensity has proven to be impressive; when a precision current-regulated power supply is used and the temperature is controlled as shown, intensity variation of any spectral feature is less than 1% per hour. Ordinarily
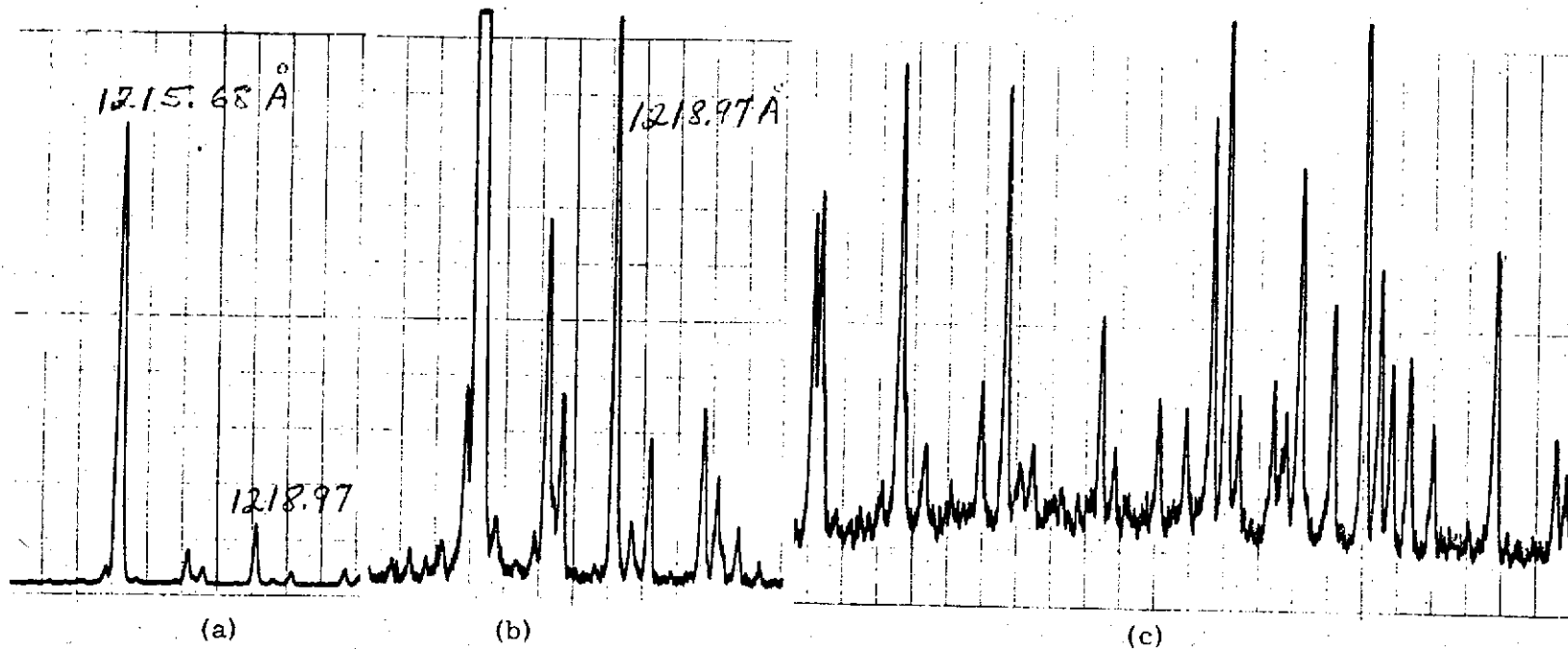
Figure 3. Sample spectra from the hydrogen lamp; (a) and (b), vicinity of 1216 Å with different amplifier gains; (c) approximately 1570-1590 Å.

the temperature control circuit is left running continuously. When the lamp is turned off, then turned on again hours or days later at the same current, the light output quickly returns to the same value it had when turned off.

An interesting and unusual feature of this lamp is revealed in the stability and structure of the striations in the discharge, which are particularly striking in the anode and cathode sections of the discharge. At typical operating pressure and current there may be between 6 and 10 bright stationary striations in this region. After several weeks of operation they cause a slight discoloration of the glass in the form of rings, and the striations hold this pattern indefinitely. In our experience we have never before encountered such stability of striations.

The operating life of these lamps is not known. Some have operated for thousands of hours, with any degradation of performance or eventual termination due to external mechanical damage — breakage, chipping or coating of the window with oil in vacuum-system accidents, etc. Degradation due to vacuum oil coating[10] of the window can be partially reduced by carefully polishing the outer face of the window with sapphire powder.

We have not specifically investigated the effect of ultraviolet radiation from the discharge on the MgF_2 window transmission,[11] but after several hundred hours of operation no degradation in spectral transmission has been observed that is not attributable to external effects mentioned above.

VI. Detailed Description of Calibration Test Equipment

As shown in Fig. 4A the test unit comprises two connected vacuum chambers (a premonochromator chamber and a main chamber which accepts the spectrometer to be calibrated) which are connected by a 3" diameter interface valve. Each chamber has a diffusion pump system with well-baffled liquid nitrogen traps and automatic vacuum control circuits all of which permits recycling the systems independently from high vacuum to atmospheric pressure and back to a vacuum pressure of 2×10^{-5} torr in less than five minutes.

The premonochromator chamber has a vacuum fitting by which a UV source can be mounted at the entrance slit of a 1/4-meter focal length Ebert grating monochromator which has a dispersion of 10 A/mm. The slits are 1/4 mm wide, providing a fixed spectral resolution of 2.5 A/mm. The exit slit can be adjusted in length to a maximum value of 2.5 mm. The exit beam from the premonochromator goes to the folding mirror M_F which is fitted with a square limiting disphragm to provide an f/80 beam. The reflected beam goes to the spherical concave mirror M_T which forms an image of the exit slit at unit magnification in the main chamber at a distance of 1650 mm from M_T. M_T can be adjusted in two axes so that the image can be placed to any point in the focal plane to a positional accuracy of 1/4 mm. This adjustment can be made externally either manually or with an electrical drive system which includes two axis readout dials. The transfer mirror can also be positioned to send the beam to either of the end-on photomultiplier tubes,
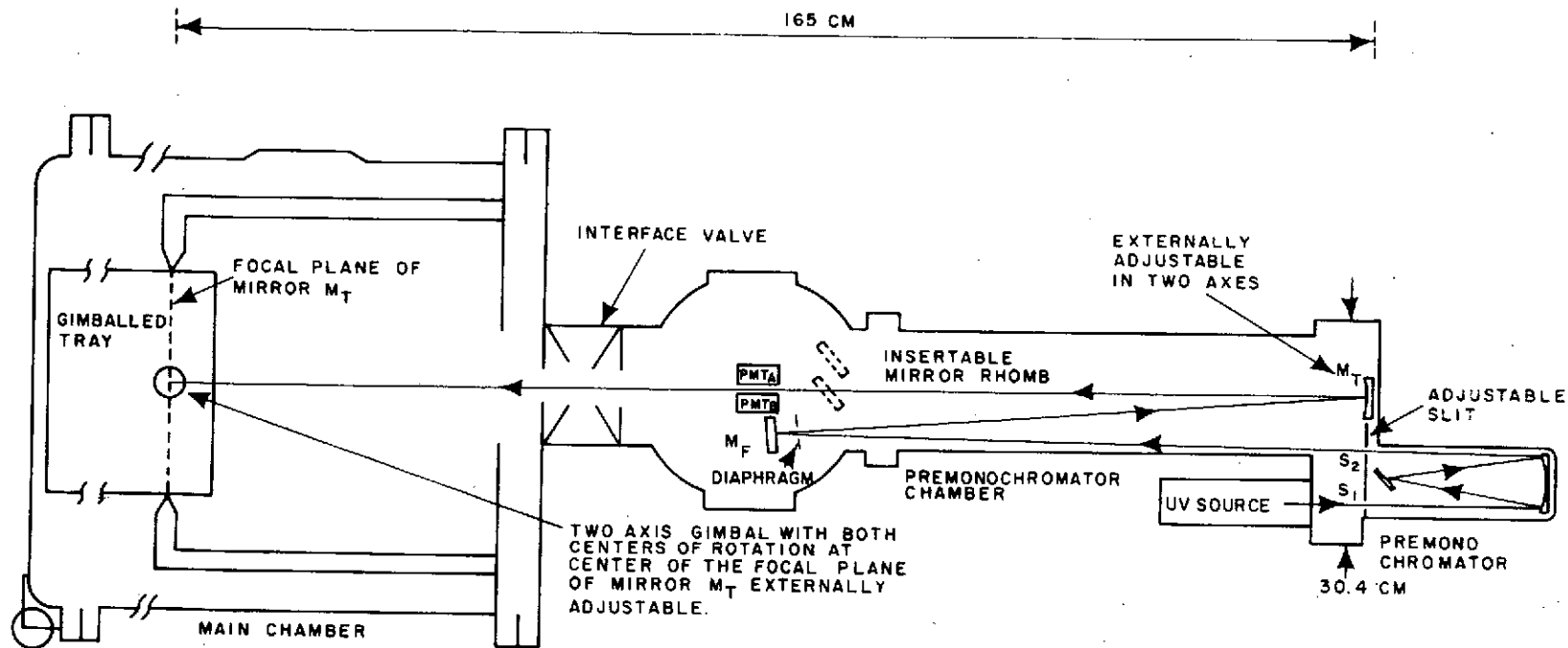
Fig. 4A   Schematic Diagram of Calibration Test Equipment (Plan View).
Optical Elements Laid Out to Scale.

PMT_A or PMT_B, which are about 3° off the central axis and 800 mm from M_T. Thus the beam illuminates a 10 mm by 10 mm area on the tube faces, which have a diameter of 25 mm. One of the reference tubes has a CsI photocathode with a long-wavelength cut-off at about 1700 A, the other a CsTe photocathode with a long-wavelength cut-off at about 3000 A. Both tubes have MgF_2 windows and are mounted on a vacuum cover plate which includes the electrical through connections for the tubes, and which interfaces to the vacuum chamber by means of a flange at the top of the premonochromator chamber.

The cover plate also is equipped with a mechanical through-vacuum means to insert a mirror rhomb in the beam when it is in the central position so that the CsI reference photomultiplier tube (PMT_A) is illuminated. By this means the mirror rhomb reflectivity can be monitored at 1216 A throughout a calibration test to establish that the vacuum environment or vacuum pumping system is not producing optical contamination.

The main chamber, which receives the spectrometer to be calibrated, has a removable end bell mounted on 3 plastic wheels which permit rolling the end bell on the table surface of a laminar flow bench. Thus installation in the main chamber can be performed under clean-room conditions.

The flight spectrometer is placed on the gimballed tray in the main chamber with the center of its entrance slit on the central axis of the calibration beam and with the slit in the focal plane of the transfer mirror M_T. The tray is gimballed about horizontal and vertical axes, both of which pass through the center of the entrance slit. External through-vacuum controls with readout dials are provided so that the spectrometer can be tilted to illuminate any area of the dispersing element with the f/80 calibrated beam,

and with the beam position on the slit being independent of the tilt position to about $\pm$ 0. 25 mm. A vacuum cover plate on a flange in the top of the main chamber provides through-vacuum electrical connection to the spectrometer.

Most of the instruments which have been calibrated employ entrance and exit slits with minimum widths and lengths of a millimeter or more. Instruments which employ slits with submillimeter dimensions must have larger slits substituted for calibration purposes to insure that none of the photons in the calibrated monochromatic beam are cut off by the slits. In either case the calibration procedures call for measuring the instrument output for three positions of the beam on the slit, all of which are within a 0. 5 mm circle to insure that no light is cut off by the slit jaws.

This check is most conveniently made with the spectrometer scan stopped at the wavelength under study. Once the beam position is thus confirmed the spectrometer is scanned through its full wavelength cycle as many times as necessary to provide a total output measurement not limited in its precision by photon statistics. It is desirable to accumulate a total of about 10^5 photoelectrons at the calibration wavelength so that the spectrum can be studied at all wavelengths for scattered light, false reflections and grating ghosts.

Just before a spectrometer calibration, and just afterwards, the reference photomultiplier tubes are absolutely calibrated. An NBS-calibrated photodiode is placed on the tray in the main chamber a distance of 400 mm behind the focal plane of the mirror M_T so that it is illuminated over a 5 mm x 5 mm area. Preliminary visual observations

with the premonochromator grating set in central order and photoelectric

scans of the UV beam had established that the beam illumination was

uniform. This is an essential condition because otherwise nonuniformity

across the face of the photodiode and/or reference photomultiplier tubes

could introduce a calibration error.

On the basis of extensive experience with the detectors and the
(Fig. 4B)
measuring circuits∧ over a period of about three years no error of the

magnitude of the uncertainty in the NBS calibration of the diode (± 6%)

is introduced by the method of calibrating the reference photomultiplier

tubes. Tube calibrations before and after a spectrometer calibration

always agree to within about 2%, although over a period of a year the

reference tube gain may degrade as a result of total photon exposure

by as much as 50%. Likewise, the highvoltage supplies and elec-

trometers are highly stable over the period of several days which

may elapse during a spectrometer calibration. Repeated recalibra-

tions of diodes at NBS show only small variations compared to the

± 6% photodiode calibration uncertainty. This diode stability has been

independently confirmed by repeated calibration of a spectrometer over

a period of about a year during which the spectrometer was sealed in

a chamber filled with very dry highly purified nitrogen.

An almost completely independent check of the validity of these

calibration techniques was obtained by a cross calibration check of the

Apollo 17 prototype spectrometer in the vacuum optical bench at Goddard

| HIGH VOLTAGE POWER SUPPLY ~2500 V FLUKE MODEL 408B | PHOTOMULTIPLIER TUBES EMR 542G or 541F | ELECTROMETER KEITHLEY MODEL 615 | TWO CHANNEL PEN AND INK RECORDER BRUSH MODEL 280 |

PRE MONOCHROMATOR

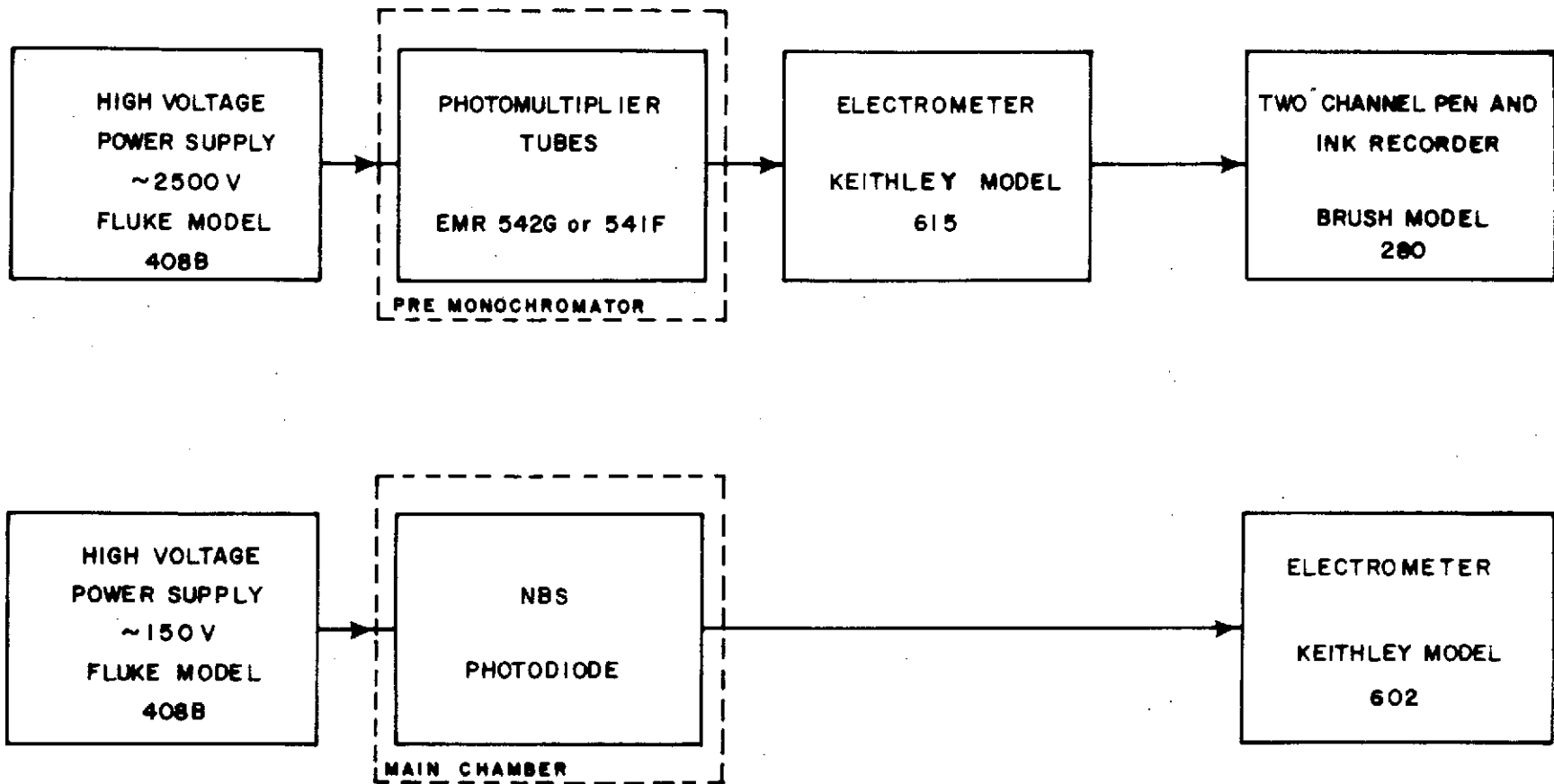| HIGH VOLTAGE POWER SUPPLY ~150 V FLUKE MODEL 408B | NBS PHOTODIODE | ELECTROMETER KEITHLEY MODEL 602 |

MAIN CHAMBER

Fig. 46. Calibration Facility Electronics Block Diagram (Typical)

Space Flight Center which also uses NBS calibrated diodes as standards.
In the spectral range 1350 to 1700 A the two calibrations agreed to
within the limits set by the diodes. At 1216 A a 15 to 20% discrepancy
appeared which was established as being due to the longer vacuum
pumping time employed in the Goddard facility

Apparently the degassing of water vapor from the MgF_2-Al
coated replica grating or the MgF_2-Al mirrors requires about 10 to
20 hours during which period the optical sensitivity at 1216 A increases.
The use of longer pumping times in our facility brought our short wave-
length calibration into agreement with the GSFC vacuum optical bench
calibration. This experience demonstrates that subtleties can creep
into any absolute measurement and suggests that our painstaking efforts
to avoid systematic errors were necessary.

The calibration procedure involves positioning the calibrated
monochromatic beam at various locations in the entrance slit plane.
For a given slit position the gimballed tray on which the spectrometer
is mounted can be tilted to determine the signal coming from various
areas of the dispersing element and the spectrometer focusing elements.

Large variations in sensitivity along the useful area of the detector
at the exit slit of the spectrometer under test or significant nonuniformity
in the optical efficiency of the dispersing element or focusing elements
of the spectrometer disqualify those elements for use in a spectrometer
which is to be employed for precision spectrophotometry. Thus in

practice variations in sensitivity along the slit and across the spectrometer optical elements are relatively small and need to be done at only a few wavelengths. Measurements at the center of the slit and at the center of the optical system for 10 to 15 different wavelengths over a 500 A to 1000 A range are adequate to acquire the needed calibration information.

During the calibration the monochromatic beam is periodically positioned on the appropriate reference photomultiplier tube to confirm that the source output is stable and that the premonochromator wavelength setting is unchanged. Likewise the mirror rhomb is periodically employed to determine that optical contamination has not occurred and the mirror M_T is scanned across the reference photomultiplier to establish that the standard M_T coordinates for the reference tube have not changed.

VII. Calibration Results

During the preparation of the Apollo 17 ultraviolet spectrometer, several calibrations were performed on several instruments over a period of about one year. Throughout the testing period all instruments were stored or transported in an atmosphere of high-purity dry nitrogen, or in a clean-room atmosphere, or in a thermal vacuum chamber. These conditions were also maintained during the testing period at Cape Canaveral and during installation in the spacecraft on the launch pad, and throughout the prelaunch period through the launch phase. The flight instrument was installed in the spacecraft on the launch pad just after final calibration and only six weeks before launch. From the time the flight instrument was first calibrated until minus 48 hours to launch it was always accompanied by a test mirror rhomb whose 1216 A reflectivity was tested at intervals in a special fixture in the main chamber of the calibration test equipment. No degradation in the test rhomb reflectivity was detected to a limit of $\pm$ 2%. Table I shows the reproducibility of the calibration of two of the Apollo 17 units at two wavelengths. Table I also shows the reproducibility of the NBS diode on successive recalibrations at NBS. The repeatability of these calibrations, combined with the maintenance of a benign atmosphere through the launch phase and the monitoring of the reflectivity of the test rhomb, provides a high confidence level in the absolute precision of the photometric results.

TABLE I

Typical Apollo 17 UVS Calibrations
(normalized to 1.00 at each wavelength)

Date	Unit	1463 A	1608 A
7 Jul 72	Flight	1.03	1.02
25 Jul 72	Flight	1.03	.99
31 Jul 72	Flight	.99	.99
7 Aug 72	Flight	.95	1.01
13 Sep 72	Flight	.99	.99
24 Apr 72	Back-up	.99	1.04
1 May 72	Back-up	.99	1.03
22 May 72	Back-up	1.02	.94
25 May 72	Back-up	1.00	1.01

NBS Diode Calibrations (normalized)
Diode #17195 - CsI Photocathode

Date	λ 1216	λ 1608
17 Nov 71	.97	.99
23 Mar 72	1.00	.99
6 Nov 72	1.01	.99
27 Mar 74	1.01	1.02

Figure 5 shows the grating scattering information obtained in the CTE when a point at the center of the entrance slit and the center of the Apollo flight grating were illuminated with Ly α radiation. The exit slit was 2 mm wide, providing a resolution of 10 A. The scattering consists of a family of Rowland ghosts plus a scattering continuum which apparently originates at the grating. The observed scatter signal did not occur when a CaF_2 filter, which is opaque to Ly α radiation, was inserted in the incident beam. This type of laboratory data has proven invaluable in the search for weak emissions from the various objects which were studied during the mission.

One of the experimental results of the Apollo 17 UVS mission was the measurement of the absolute brightness of several stars.[12] We believe, because of the techniques described above, that these measurements provide the most accurate existing UV stellar spectral brightness measurements for these stars.

VIII. Acknowledgements
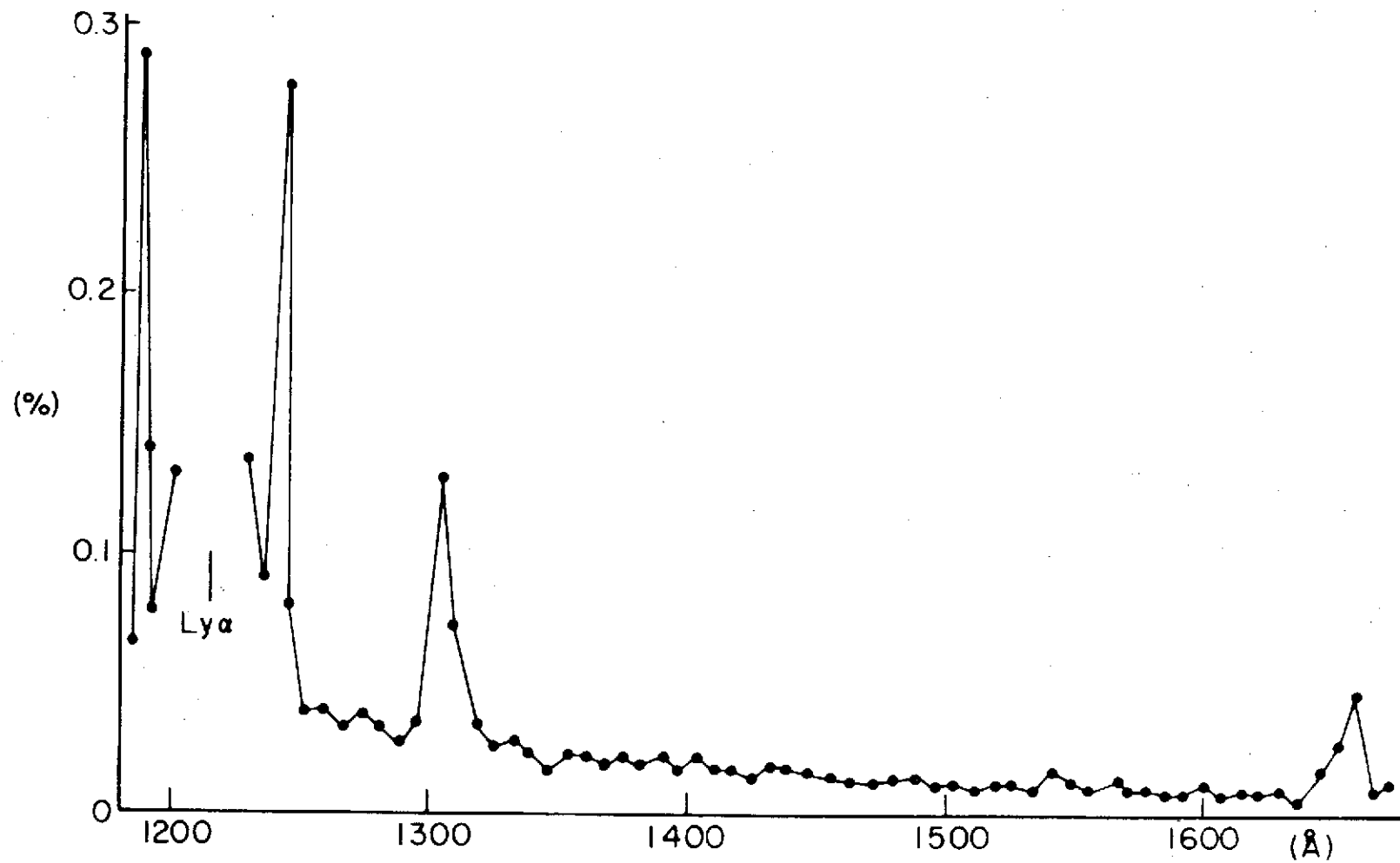
Fig. 5. Measured Percentage of Scattered Ly α from Apollo 17 Flight Grating

in many facets of the program. Mr. Robert Richardson was responsible for final installation and operation of the Calibration Facility. Dr. Robert C. Schaeffer conducted the calibration of all of the Apollo units. Dr. Edward Reed performed the flight simulation test during the mission with a spare instrument. The UV standards group at NBS calibrated the reference diodes under the direction of Dr. Robert P. Madden.

References

1. Fastie, W. G., The Moon 7, 49 (1973).

2. Fastie, W. G., P. D. Feldman, R. C. Henry, H. W. Moos, C. A. Barth, G. E. Thomas and T. M. Donahue, Science 182, 710 (1973).

3. Samson, J. A. R., Techniques of Vacuum Ultraviolet Spectroscopy, Wiley, 1967.

4. Bless, R. C., T. Fairchild and A. D. Code, NASA Report SP-310, 1972.

5. Codling, K. and R. P. Madden, J. Appl. Phys. 36, 380 (1965).

6. Canfield, L. R., R. G. Johnson and R. P. Madden, Appl. Opt. 12, 1611 (1973).

7. Spedding, F. H., A. S. Newton, J. C. Warf, O. Johnson, R. W. Nottorf, I. B. Johns and A. H. Doan, Nucleonics, No. 1, 4 (1949).

8. Dieke, G. H. and S. P. Cunningham, J. Opt. Soc. Am. 42, 187 (1952).

9. Dieke, G. H. and H. M. Crosswhite, J. Opt. Soc. Am. 42, 433 (1952).

10. Taylor, R. G., T. A. Chubb and R. W. Kreplin, J. Opt. Soc. Am. 55, 1078 (1965).

11. P. Warneck, J. Opt. Soc. Am. 55, 921 (1965).

12. Henry, R. C., A. Weinstein, P. D. Feldman, W. G. Fastie and H. W. Moos, Low-Resolution Ultraviolet Spectroscopy of Several Hot Stars from Apollo 17, to be submitted to Ap. J.

ANALYSIS OF BACKGROUND COUNTS

RECORDED BY THE APOLLO 17

FAR ULTRAVIOLET SPECTROMETER EXPERIMENT (S169)[*]

I. INTRODUCTION

During the Apollo 17 mission when the spacecraft was several hundred thousand kilometers from the moon on trans-lunar coast the dark count from the ultraviolet spectrometer (UVS) was observed to be about 3.6 counts per tenth second whereas throughout the test period before launch the spare flight instrument, the prototype and qualification unit plus two spare integrated photomultiplier systems exhibited a background count of about .06 counts per tenth second, one tenth second being the accumulation period over which counts were measured by the instruments. The subsequent history of this background count in lunar orbit and during the trans-earth coast and a tentative analysis of its source is the subject of this report. The implication of the analysis for future ultraviolet observations is discussed.

II. LUNAR ORBIT OBSERVATIONS

In lunar orbit the observed dark count varied with space-craft altitude and attitude but was independent of the position of

---

[*]Prepared by Wm. G. Fastie, Principal Investigator

the spacecraft in lunar orbit, that is, the background signal was clearly not of solar, lunar or earth origin.

For an isotropic source to which the moon is opaque the fraction of the source which would reach the spacecraft as a function of spacecraft altitude is given by the formula

$$F = \frac{1 + \sin \cos^{-1} (R/R + H)}{2} \qquad (1)$$

where R is the lunar radius and H is the altitude of the spacecraft above the lunar surface.

During the early portion of the lunar orbiting period, the spacecraft was in elliptical orbit. Typical count rates observed at various altitudes is shown in Table I, Col. 2.

The UVS was located in the service module near the outer diameter of the module. In lunar orbit the normal spacecraft attitude maintained the UVS on a line which was perpendicular to the axis of the service module and passed through the center of the moon, with the UVS between the moon and the spacecraft axis. Once, when the spacecraft was at about 30 km altitude a 360° roll maneuver was executed. At the 180° roll point, with the spacecraft center line directly between the moon and the UVS, the observed background count signal was increased by 10%, which demonstrates that most of the exciting particles pass through the spacecraft without being lost.

In Table I, Col. 3 shows the expected count rate vs altitude based on Eq. 1.

Table I

Altitude (km)	Observed count (.1 sec)	From Eq. 1
Before orbiting	3. 63	3. 63
312. 5	2. 83	2. 80
226	2. 65	2. 69
126	2. 50	2. 47
26	2. 07	2. 12

III. TRANS-EARTH COAST

During the period after the spacecraft had left the vicinity of the moon until it had reached 5 earth radii at which point it was finally turned off, the dark count rate was about 2.76 counts per second. The reduction in count rate in deep space from 3.6 during trans-lunar coast to 2.76 during trans-earth coast corresponds very closely to the approximately 20% reduction in detector photon sensitivity which was observed during the lunar orbit period. The degradation in light sensitivity was due to excessive

light exposure which reduced the gain of the photomultiplier section of the detector by a factor of about 2.

IV. POISSON DISTRIBUTION

Comparison of the distribution of background counts observed in lunar orbit with calculated Poisson distributions show excellent agreement. See Table II. The small differences between observed and calculated rates can be accounted for by the assumption that a small percentage of the exciting particles produced more than one count.

Table II

Measured and Calculated Count Rate Distribution

Sample I Avg/. 1 sec = 2.8472			Sample 2 Avg. = 2.3076		
Counts	Times Observed	Calc. (Poisson)	Counts	Times Observed	Calc. (Poisson)
0	380	330	0	620	575
1	980	950	1	1375	1320
2	1315	1355	2	1440	1520
3	1230	1285	3	1090	1175
4	875	915	4	675	675
5	520	525	5	3300	310
6	255	245	6	120	120
7	130	100	7	65	40
8	50	40	8	20	10
9	10	5	9	10	5
10	5	0	10	5	0
tal Counts	5750	5750		5750	5750

V. DESCRIPTION OF COUNTING CIRCUIT

As described in APL/JHU Spec. No. 7232-0005D the endon

photomultiplier tube which employed a CSI photocathode and MgF_2

window (3 mm thick) was nominally operated at 5×10^6 gain, that

is, each photoelectron produced 5×10^6 electrons at the collector

in a period of about 10 nanoseconds. If this pulse contained less

than 5×10^5 electrons it was rejected by a discriminator circuit

but all pulses larger than this value were accepted by a pulse

amplifier whose output signal triggered a 16-bit counter. After

a pulse was produced by the pulse amplifier discriminator circuit

(PAD) the circuit could not respond to another photoelectron for an

invariant period of 1. 8 microseconds no matter how many pulses

the photomultiplier tube produced during the dead time, that is

the circuit was non-paralyzing.

VI. ANALYSIS

The correspondence between the degradation of the background

count for trans-lunar and trans-earth coast and the degradations

in the detector sensitivity observed during lunar orbit leads to the

inescapable conclusion that each background count originates as a

single photoelectron at the photocathode. An alternative conclusion

that each observed background count is caused by a group of

particles which produce a single large pulse is rejected on the grounds that if, for example, the background counts were on the average the result of 5×10^7 electrons, the discriminator would have no effect as a pulse rejector and as the gain of the dynode sections degraded each of the very large pulses would still be counted, thus the background count rate would have been the same before and after lunar orbit.

The observation that the observed counts follow a Poisson distribution suggests that all events are completely independent. The only source of particles with enough flux and energy to meet the requirements imposed by the orbiting observations described above are protons of energy greater than 10^8 eV. However, the proton flux in this energy range is only three per cm^2 and since the effective omnidirectional geometric factor of the cathode is ~3 sq cm we would expect a maximum of 0.9 counts for each 0.1 second interval. Furthermore, we would certainly expect that if the de- tector were directly sensitive to 10^8 eV protons, each one would produce much more than one electron in the detector, and the sensitivity degradation argument above precludes that possibility.

We therefore conclude that high energy protons produce optical fluorescence in the magnesium fluoride window, each pro- ton producing many photons but with a fluorescence time which is long compared to one tenth second. The lifetime of the fluorescence

must be less than 10 minutes on the basis that there was no detectable phase lag between the background count rate and the altitude variation in lunar orbit.

VII. CONCLUSIONS

The above analysis, if correct, predicts that the following approaches would not be effective as means to reduce the background count rate:

A. Use of top side discriminator.

The analysis concludes that each observed background count originated as a single photoelectron at the photocathode and therefore produced an average pulse of 5×10^6 electrons.

B. Use of coincidence counter.

The analysis presumes that each high energy proton causes the detector window to "glow" with a relatively long time constant and with random re-emission of photons.

If the analysis is correct the background count can be reduced by reducing the area of the detector. In the Apollo application, which required about only 25% of the photocathode area, a factor of 2 in the minimal detectable signal would have resulted. In other applications, for example LST and IUE, where each element

of the photoreceptor represents a very small area, it would appear superficially that the effect observed on the Apollo 17 UVS is unimportant, but these systems are potentially capable of using observation times which are roughly inversely proportional to the area of the detector element, and therefore the effect may be important. Furthermore, the assumption that the analysis is correct could lead to false conclusions, either way, with respect to these applications.

MgF_2 was chosen as the window for the Apollo 17 UVS detectors on the basis of 1971 data which indicated that MgF_2 was less sensitive to cosmic radiation than LiF, the only other window material which was applicable. It should be emphasized that we have presented no evidence that refutes this information, but if the analysis is correct, it may well be that LiF would have been a better choice for this application but LiF may develop color centers which produce absorbtion bands in the crystal lattice after long exposure to high energy particles. Laboratory and rocket experiments to resolve this question are urgently needed in support of future space experiments.

The Apollo 17 UVS cosmic background observations are in apparent conflict with the observations of the Copernicus Satellite (OAOIII), which preliminarily indicates that each cosmic particle

produced many pulses in a MgF_2 windowed detector. There are, however, a multitude of differences between the two experiments, including earth altitude, electronics and photocathode material and possibly the source of window material.

ADDENDUM

At the request of Dr. Spitzer during a discussion in Princeton
we have summed the dark counts in each spectrum, which repre-
sent 11.5 sec of data, for a more direct comparison with the
14 sec integration time used by Copernicus. Table III lists 20
11.5 sec sums, the average for the 20 sums and the one sigma
value. These data show purely statistical flucuations.

In the discussion at Princeton Dr. Spitzer pointed out that
the magnesium fluoride windowed detectors on Copernicus, which
show poor statistical behavior, employ a bi-alkali photocathode
which is sensitive to the visible. Perhaps each high energy pro-
ton produces a very large number of visible photons in magnesium
fluoride and causes the photomultiplier tube or the electronics to
multiply pulses, whereas CSI photocathodes used on the Apollo
instruments receive a much smaller photon signal from each proton.

Table III

11.5 sec Sample	Total
1	277
2	292
3	282
4	261
5	282
6	280
7	291
8	309
9	253
10	305
11	324
12	266
13	325
14	293
15	305
16	253
17	321
18	293
19	300
20	268

Avg. = 289 $\sqrt{\text{Avg.}}$ = 17

23. Ultraviolet Spectrometer Experiment

William G. Fastie,[a†] *Paul D. Feldman,*[a] *Richard C. Henry,*[a] *H. Warren Moos,*[a] *Charles A. Barth,*[b]
Gary E. Thomas,[b] *Charles F. Lillie,*[b] *and Thomas M. Donahue*[c]

An ultraviolet spectrometer (UVS) on board the Apollo 17 orbiting spacecraft was used in an attempt to measure ultraviolet emissions from the lunar atmosphere. The only emissions observed in the lunar atmosphere were from a transient atmosphere introduced by the lunar module descent engine; 4 hr after the lunar module landed, these emissions were no longer detectable by the spectrometer. The absence of atomic hydrogen (H) expected to be present from the solar wind source leads to the conclusion that solar wind protons are neutralized and converted to molecular hydrogen (H_2) at the lunar surface.

During crossings of the solar-illuminated surface, the spectrometer measured significant variations in surface albedo. These variations are ascribed to variations in the refractive index of the lunar surface material.

The spectrometer made a number of nonlunar observations in lunar orbit and during transearth coast (TEC), including a search for the ultraviolet zodiacal light, solar atmosphere emissions, Earth emissions (including those from the geomagnetic tail), stellar emissions, and galactic emissions. Although significant data were obtained from all these observations, analysis of the data requires precise spacecraft attitude information in galactic coordinates; this information has not yet been received. During TEC, the fluorescence spectrum of H_2 was observed during a purge of the Apollo 17 fuel cells.

INSTRUMENT DESCRIPTION AND CALIBRATION

The Apollo 17 UVS has been described in great

---

[a]The Johns Hopkins University.
[b]University of Colorado.
[c]University of Pittsburgh.
[†]Principal Investigator.

detail elsewhere (ref. 23-1). In summary, it is of the Ebert type, which has been broadly used for space research, but employed new optical and electronic techniques that provided about an order of magnitude improvement in sensitivity. These improvements included exit slit mirrors that provided a 2.5 increase in the signal to the detector pulse-counting electronics (which permitted detection of single photoelectrons) and a precision wavelength scan system that permitted the summation of a large number of spectra without loss of spectral resolution.

The spectrometer is shown in figure 23-1. The triangular stand on which the instrument was mounted (fig. 23-1(a)) was attached to a spacecraft bulkhead that was perpendicular to the spacecraft longitudinal axis. The large baffle over the entrance slit excluded stray light and was designed with multiple angles in several sections to provide a very large capability for rejection of unwanted radiation. There were no external optical components.

As seen in figure 23-1(b), light rays passing through the spectrometer entrance slit are rendered parallel by an area on one side of the spherical Ebert mirror, which directs the rays to the grating. Diffracted rays from the grating go to the area on the other side of the Ebert mirror that focuses the rays through the entrance slit to the face of a solar-blind photomultiplier tube, which transforms each photoelectron produced by a photon into several million electrons. An accumulator circuit counts and stores these pulses for 0.1 sec, and the accumulated pulse count is transmitted to the spacecraft data system as a 16-bit word.

The wavelength scan system consisted of a synchronous, motor-driven, cyclical cam, which encapsulated the pin on a follower arm. The follower arm was attached to the grating shaft. The 3600-lines/mm grating was rotated approximately 5° by the cam drive system to scan the spectral region 118 to 168
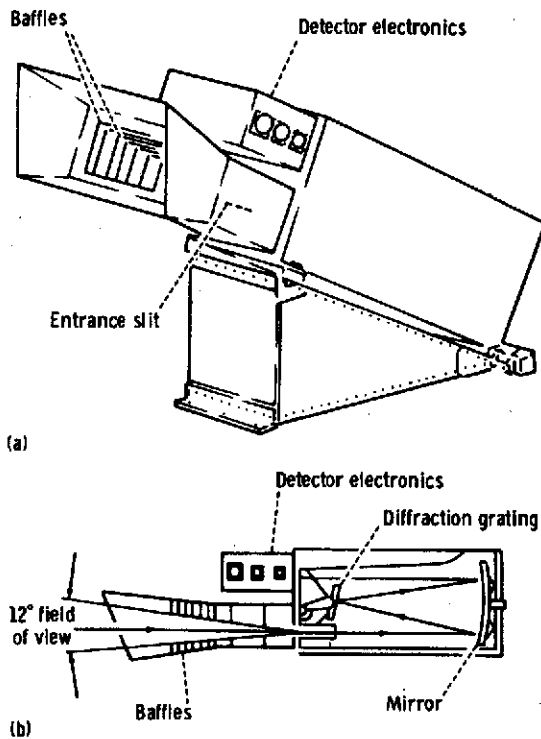
FIGURE 23-1.—Ultraviolet spectrometer. (a) Isometric view of the instrument mounted on a stand, which was attached to a bulkhead in the scientific instrument module bay of the Apollo 17 spacecraft. (b) Optical ray diagram.

nm once every 12 sec. The cam was programed to scan linearly in wavelength at the rate of approximately 7.5 nm/sec except for two 5-nm regions centered at 121.6 and 147.0 nm, where the scan rate was approximately 1.7 nm/sec to give temporal preference to Lyman-alpha radiation (121.6 nm) and to the resonance line of the heaviest atmospheric gas xenon (Xe) at 147.0 nm. The 144.5- to 149.5-nm region also included a fluorescent line of molecular hydrogen and one of carbon monoxide (CO).

The sensitivity S of the spectrometer to a gas column that is emitting 1×10^6 photons/sec-cm^2 (1 R) is given by

$$S \text{ (counts/sec)} = \frac{1 \times 10^6}{4\pi} \frac{A_s A_g}{F^2} QT \qquad (23\text{-}1)$$

where A_s = slit area $\approx$ cm^2 (1-nm resolution)

A_g = grating area $\approx 1 \times 10^2$ cm^2

F = spectrometer focal length = 50 cm

Q = quantum efficiency of the detector ≈ 10 percent

T = transmission of the optical system ≈ 30 percent

or

$$S \text{ (counts/sec)} \approx 100 \text{ photoelectrons/sec/R}$$

$$(23\text{-}2)$$

To provide precision measurements with the spectrometer, it is necessary to measure the value of Q over the exposed area of the photomultiplier tube and to measure the transmission of the optical system over the entire field of view of the spectrometer. No standard source exists for the far ultraviolet region, and a spatially uniform reference source to fill the wide aperture of the spectrometer is beyond the state of the art. A high-precision calibration was accomplished in a specially built vacuum facility, which provided an intense, high f-number, monochromatic beam that could be focused into a very small spot on any point of the entrance slit. The flight spectrometer was mounted in the vacuum chamber on a tilting platform so that the calibrating beam could be directed through the entrance slit to each area of the diffraction grating. A calibrated photomultiplier tube could be inserted in the monochromatic beam to measure the number of photons passing through the entrance slit. A National Bureau of Standards calibrated photodiode was used to calibrate the reference photomultiplier tube before and after each calibration of the spectrometer.

The calibration was performed at a total of 10 wavelengths in the spectral region that the instrument scanned. Successive calibrations provided very reproducible sensitivity values at all wavelengths. A cross-check of the system was provided by calibration of a spare instrument in the vacuum optical bench at the NASA Goddard Space Flight Center, which confirmed the absolute value of the calibration. We believe these careful techniques ensure that the signals observed in flight were measured to an accuracy of ± 10 percent.

LUNAR ATMOSPHERE OBSERVATIONS

The Apollo 17 UVS experiment has as its primary objective the measurement of the density and composition of the lunar atmosphere by observing resonance scattering and fluorescence of solar far ultra-

violet radiation. This technique can provide density measurements in the range 1×10^1 to 1×10^4 atoms/cm^3 for H, H$_2$, atomic oxygen (O), carbon (C), atomic nitrogen (N), CO, carbon dioxide, and Xe but, because of spectral range limitations, could not measure helium, neon, or argon-36, all of which may be present as major constituents of the lunar atmosphere, if the solar wind is the major source for the atmosphere. In addition, radiogenic argon-40 (^{40}Ar) from potassium-40 decay should be present. The present results indicate that the surface concentration of atomic hydrogen is less than 10 atoms/cm^3, almost three orders of magnitude less than predicted (ref. 23-2), whereas the concentration of H$_2$, if present, is less than 6.0×10^3 atoms/cm^3. This is consistent with the hypothesis that the solar wind protons are completely converted into hydrogen molecules at the lunar surface. None of the other observable constituents were detected. A transient atmosphere was observed shortly after lunar module touchdown but disappeared in a matter of hours. No evidence of outgassing was detected in the vicinity of the crater Aristarchus, where many transient optical phenomena have been reported.

Previous measurements of the lunar atmosphere based on an in situ pressure gage (ref. 23-3) indicated that the total surface density at the subsolar point may be as small as 1×10^7 atoms/cm^3. More recently, mass spectrometer measurements from lunar orbit (ref. 23-4) and from the lunar surface (ref. 23-5) have resulted in detection of neon, argon, and helium. Lunar outgassing, the only possible source of a substantial atmosphere, occurs at a rate several orders of magnitude less than the corresponding rate on Earth (ref. 23-6). Apart from ^{40}Ar and radiogenic helium (ref. 23-7), the lunar atmosphere may consist only of neutralized solar wind ions. Thus, the lunar atmosphere would be expected to be composed primarily of neon, argon, hydrogen, and helium, the subsolar surface concentrations of which would lie in the range 2×10^3 to 7×10^3 atoms/cm^3 (ref. 23-7).

The Apollo 17 UVS was mounted in the scientific instrument module (SIM) with the optic axis pointed 23° forward and 18° right of the SIM center line (when looking toward the spacecraft nose). The SIM center line nominally pointed through the center of the Moon when the spacecraft was constrained to local horizontal attitude. Atmospheric observations were made in various spacecraft attitudes as shown in figure 23-2. The principal mode of operation was the
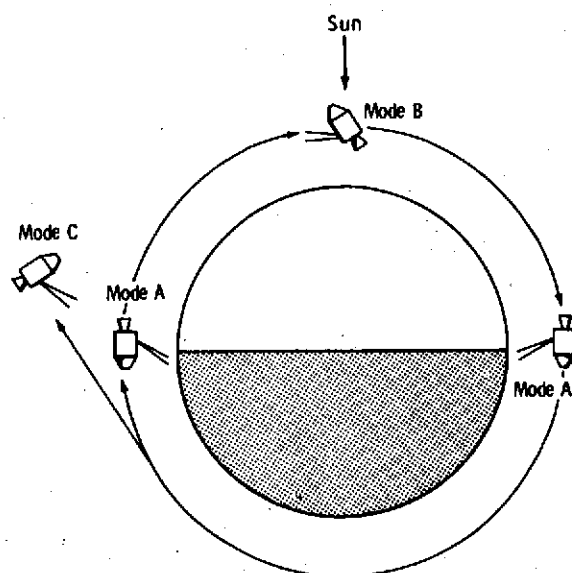

FIGURE 23-2.—Schematic representation of the modes of observation of the lunar atmosphere. Mode A, the principal orbital mode, consists of observation through the illuminated atmosphere above the terminator against the dark side of the Moon. In mode B, a contingency orbital mode, the spectrometer is pointed at a fixed point in space, and the line of sight extends through a tangential slice of illuminated atmosphere. Mode C was used immediately after transearth injection. The Apollo 17 UVS has a field of view of 12° by 12° and looks forward 23° relative to the normal to the spacecraft longitudinal axis.

observation through the illuminated atmosphere above the terminator against the dark side of the Moon (mode A in fig. 23-2). This was done automatically once per revolution if the spacecraft was maintained in the local horizontal attitude (twice if the spacecraft axis reversal was performed between terminator crossings). A total of 1200 of these terminator spectra was obtained.

To allow for the possibility that the atmospheric emissions might be too weak for detection in the principal mode, two special modes were provided to enhance the sensitivity. These modes resulted in most of the upper limits quoted herein. In the first mode, the spectrometer was pointed at a fixed point in space and, as the spacecraft moved in its orbit, the line of sight extended through a tangential slice of illuminated atmosphere (mode B in fig. 23-2). The enhancement provided by this mode is ≈ 20 for H and H$_2$ and ≈ 10 for O, based on Chamberlain's model of an evaporating corona with the lunar

surface as the critical level (ref. 23-8). The second mode (mode C in fig. 23-2) was used immediately after transearth injection (TEI) and is similar to mode A except for the much greater optical path length.

For all atmospheric constituents other than hydrogen (Lyman alpha, 121.6 nm), the sensitivity limit was set by the background count rate (≈ 25 counts/sec), which was caused by solar cosmic ray protons. At 121.6 nm, solar radiation resonantly scattered from hydrogen atoms in the interplanetary medium produces a background of between 200 and 400 R (depending on the viewing direction), in good agreement with previous measurements (ref. 23-9). Emission rates of 6 to 12 R (450 to 900 counts/sec) are obtained when the scattered radiation is observed after reflection from the surface of the dark side of the Moon. Solar Lyman alpha scattered from the Earth hydrogen geocorona and then reflected from the Moon beyond the lunar terminator adds a 1-R contribution to the background for crossings of the terminator facing Earth. During TEC, the fixed areas of space observed in the tangential mode (mode B in fig. 23-2) were again observed to provide a sky background correction for the tangential mode.

We define

$$N_i(z_1, z_2) = \int_{z_1}^{z_2} n_i(z')dz' \qquad (23\text{-}3)$$

where z_1 and z_2 are two altitudes above the lunar

surface, and $n_i(z')$ is the density in atoms per cubic centimeter of atomic species i at altitude z', so that $N_i(0, z)$ is the vertical column density of that atomic species between the surface and altitude z. For observations at an angle θ to the local vertical, the emission rate $4\pi I_i$, in rayleighs, for resonance scattering of solar flux in the ith line is given by

$$4\pi I_i = 1 \times 10^{-6} g_i [N(0,z)][CH(\theta)] \qquad (23\text{-}4)$$

where g_i is the resonance g-factor and $CH(\theta)$ is the Chapman function (ref. 23-10). For molecular species, it is necessary to specify $g_{v',v''}$, where v' and v'' are vibrational quantum numbers of the excited and ground states, respectively. Table 23-I lists the transitions of interest, the resonance g-factors, the instrument sensitivity, and the minimum detectable concentration for the particular mode of observation.

Figure 23-3 shows the difference between the average of the sum of 70 spectra observed in mode B in lunar orbit and the average of 210 spectra obtained during TEC (mode C) when the spectrometer axis was pointed at the same point in space. The spacecraft altitude varied from 70 to 46 km, and the spacecraft was near the subsolar point throughout the observation. Wavelengths corresponding to the resonance transitions of O, C, Xe, and N, to the Lyman bands of H_2, and to the fourth-positive bands of CO are indicated. No emission features are apparent in the spectrum. Figure 23-4(a) shows a sum of 25 spectra

TABLE 23-I.—*Ultraviolet Spectrometer Observations*

Species	Energy-state transition	Wavelength, nm	Resonance g-factor, photon/sec/molecule	Mode of observation[a]	Sensitivity, photoelectrons/sec/R	Observed surface density,[b] atoms/cm³
			Atomic			
H	$2_S - 2_P$	[c]121.6	2.2×10^{-3}	C	75	< 10
O	$3_P - 3_S$	130.4	2×10^{-5}	B	99	< 40
N	$4_S - 4_P$	120.0	3.6×10^{-6}	B	70	< 300
C	$3_P - 3_{PO}$	165.7	2.1×10^{-4}	B	25	< 15
Kr	$1_S - 3_P$	123.6	1.6×10^{-7}	A	85	$< 10\,000$
Xe	$1_S - 3_P$	147.0	1.5×10^{-6}	A	75	$< 1\,000$
			Molecular			
H_2	$B^1\Sigma_u^+ - X^2\Sigma_g^+$ (6, 9)	146.2	4.0×10^{-8}	B	75	$< 6\,000$
CO	$A^1\Pi \quad X^1\Sigma^+$(1, 0)	151.0	7.5×10^{-8}	B	60	$< 20\,000$

[a]See figure 23-2.

[b]At the subsolar point, except for H, krypton (Kr), and Xe, which are terminator values. The entries in this column are based on the spectral feature not exceeding 1 standard deviation in the counting rate.
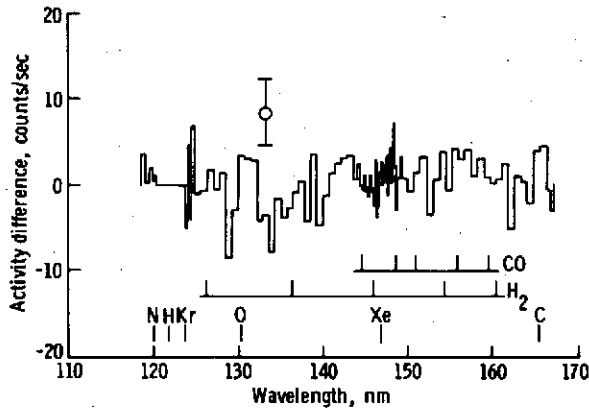
[c]Lyman alpha.

FIGURE 23-3.—The average of 70 spectra obtained during a tangential mode (mode B in fig. 23-2) observation with the sky background (observed during TEC) subtracted. The wavelengths of the principal emission features expected are indicated. The error bar represents 1 standard deviation in the observed counting rate.

obtained at the near-side terminator 2 hr after the lunar module had landed and indicates a slight enhancement at 130.4 nm (atomic oxygen) and at least one band of the CO fourth-positive system. None of these enhancements appear in figure 23-4(b), which shows the sum of 25 spectra obtained on the following orbit, 4 hr after landing.

In figure 23-5, the Lyman-alpha signal (121.6 nm) observed below the spacecraft between the terminator and a point 15° beyond the terminator (270° to 255°) (fig. 23-5(a)) is compared to the signal observed when the spacecraft was in full shadow (255° to 240°) (fig. 23-5(b)). The signal in figure 23-5(b) originated from solar radiation that was resonantly scattered from the solar system hydrogen atmosphere. The difference between the signals shown in figures 23-5(a) and 23-5(b) was initially misinterpreted as being of lunar atmospheric origin (ref. 23-1). More detailed data analysis, particularly of data from mode C (fig. 23-2), shows no signal that can be ascribed to an atomic hydrogen atmosphere to a limit of 10 atoms/cm^3 at the lunar surface. In mode C, the spacecraft altitude was increased by a factor of 5 with no increase in the Lyman-alpha (121.6 nm) signal. The signal difference (figs. 23-5(a) and 23-5(b)) is ascribed to an asymmetry in Lyman-alpha emission in the solar atmosphere. The existence of the asymmetry was confirmed by observations during TEC.

A number of conclusions emerge from the preceding results. The fact that xenon must be at best a minor component of the lunar atmosphere, despite its large mass (131.3), indicates that the mechanism of photoionization loss followed by acceleration in the solar wind electric field dominates over Jean's evaporative escape, at least for the heavy gases. The small concentrations of H, C, N, O, and CO, which are photodissociation products of many gases of volcanic origin, also place severe restrictions on present levels of lunar volcanism.[1] The most surprising result is the absence of atomic hydrogen to an upper limit almost three orders of magnitude below the predicted value (ref. 23-2). The effect of the terrestrial magnetic field in shielding the lunar surface from the incident solar wind proton flux would be important only late in the mission.[2] Other possible ways of accounting for the absence of hydrogen atoms are as follows.

1. Adsorption of solar wind protons in the lunar soil

2. Direct reflection of solar wind protons from the lunar surface

3. Neutralization and rapid escape from the lunar surface as suprathermal hydrogen atoms

4. Recombination to form molecular hydrogen

In current models of the interaction of the solar wind with the lunar soil (ref. 23-13), protons of $\approx$ 1-keV energy penetrate to a depth of $\approx 1 \times 10^{-6}$ cm. They will neutralize to form hydrogen atoms and may combine with other H atoms to form hydrogen molecules. Diffusion to the surface or into the dust grains to a depth of $\approx 1 \times 10^{-5}$ cm may occur. For adsorption within the soil to occur, the diffusion must be retarded, either by the formation of stable hydrides or by trapping in a lattice site. In either case, after sufficient exposure, the soil becomes saturated and diffusion from the surface will occur. Saturation occurs only for the outer surfaces of soil grains, which are exposed to the solar wind for periods ranging from 0.1×10^6 to 20×10^6 yr (ref. 23-14).

---

[1] The limits on the outgassing rates are being described in detail by G. E. Thomas et al.

[2] According to the empirical geomagnetic-tail model of Fairfield (ref. 23-11), the Moon should have entered the Earth bow shock 13 hr before the TEI maneuver. However, according to measurements of the solar wind at the surface of the Moon (ref. 23-12), the proton flux is not appreciably disturbed until the Moon enters the geomagnetic tail. The cut-off of solar wind flux should have occurred at approximately 18:00 G.m.t. on December 18, which was 44 hr after TEI.
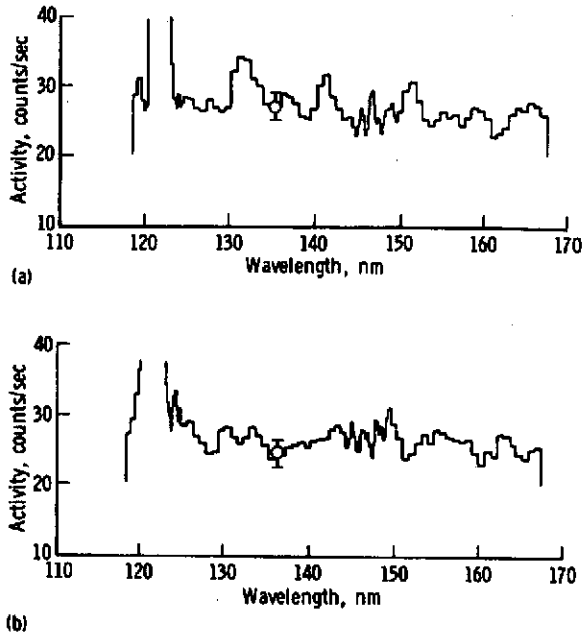
(a)

(b)

FIGURE 23-4.—Comparison of UVS spectra. The error bars represent 1 standard deviation in the observed counting rate. (a) Spectrum obtained 2 hr after lunar module landing, showing mild indication of emission features at 130.4 nm (O) and 151 nm (CO). (b) Spectrum obtained 4 hr after lunar module landing, showing no emission features.

Even for an exposure period of 1 million years (during which the solar wind is assumed constant), complete adsorption of the solar protons would give a density of 4 mg/cm^2 of hydrogen over the entire lunar surface. This value exceeds the measured composition of lunar soil by a factor of $\approx 1 \times 10^5$ (ref. 23-13).

The reflection of solar wind particles has been measured by several solar wind composition experiments on the lunar surface. The albedo for alpha particles is 10 percent (ref. 23-15), and the albedo for protons should not be significantly higher. In addition, significant reflection of solar wind ions would produce measurable perturbations of the solar wind magnetic field that have not been observed from lunar orbit (ref. 23-16).

A "sputtering" atmosphere of atomic hydrogen has been advocated (ref. 23-17), in which hydrogen atoms with average velocities of 15 km/sec are ejected from the lunar surface as a result of energetic ion impact. However, because hydrogen is a minor constituent of the lunar surface, the dominant com-
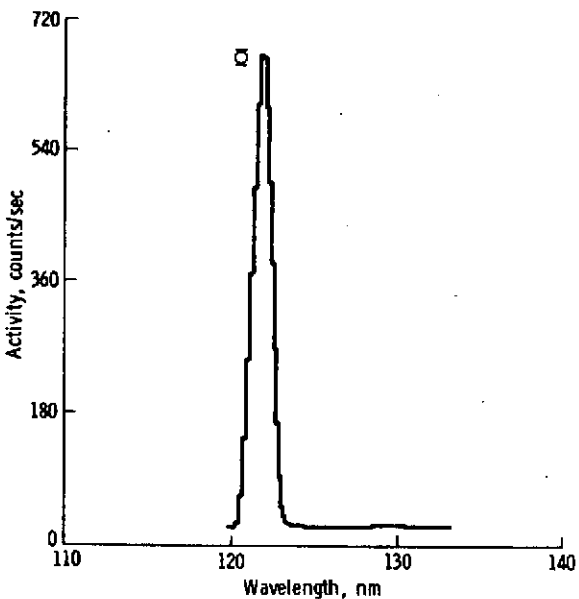

(a)

(b)
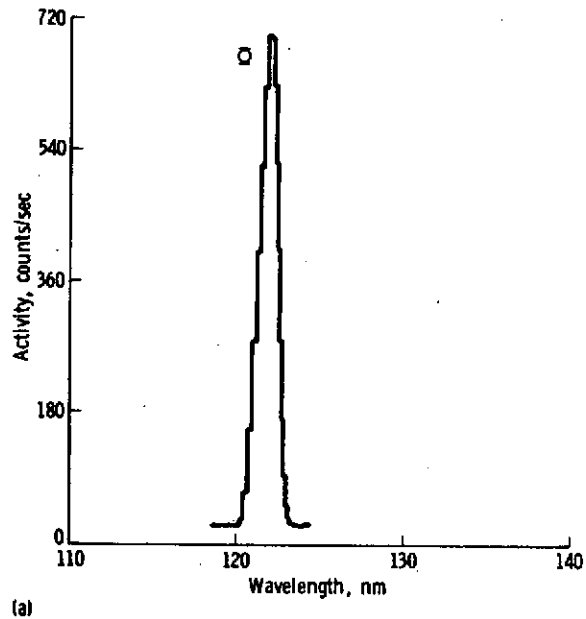
FIGURE 23-5.—Comparison of Lyman-alpha signals obtained on revolution 38. The signals are caused by reflected solar atmosphere radiation; the difference between the signals is due to asymmetry in the reflected solar radiation, not to a lunar H atmosphere. The error bars represent 1 standard deviation in the observed counting rate. (a) Signal observed just beyond the near-side terminator; coverage extends from 270° to 255°. (b) Signal observed when spacecraft was in full shadow; coverage extends from 255° to 240°

position of the sputtered material would probably be that of the lunar soil itself. Even if all the sputtered atoms were hydrogen with the previously mentioned average velocity, the maximum Doppler shift (0.006 nm) of the absorption line would not be sufficient to remove it from the wide solar Lyman-alpha line. The predicted value at the subsolar point of 340 atoms/cm^3 for the previously mentioned sputtering model (ref. 23-17) is far above our detection limit shown in table 23-I.

Thus, efficient surface recombination of solar protons to molecular hydrogen appears to be the most probable explanation for the low atomic hydrogen density. It is reasonable to expect an efficient trapping of kilovolt protons on the lunar surface (ref. 23-18), followed by an upward diffusion of hydrogen atoms. This upward diffusion would promote recombination either within or at the surface of the soil grains. The molecular hydrogen would then be released by the surface at thermal energy. A theoretical model of Hodges (ref. 23-19) predicts H_2 concentrations of 3.6×10^3 atoms/cm^3 at the subsolar point and 2.3×10^4 atoms/cm^3 at the antisolar point.

As shown in table 23-I, the fluorescence in the H_2 Lyman bands from expected density would have escaped detection in the UVS experiment. The expected nighttime density, however, may ultimately be detected by the Apollo 17 neutral mass spectrometer surface experiment (ref. 23-20).

In conclusion, the Apollo 17 UVS experiment has revealed that atomic hydrogen is almost totally absent in the lunar atmosphere. To explain this observation, we believe that nearly 100-percent conversion of solar wind protons to molecular hydrogen probably occurs at the lunar surface. The expected H_2 density would have so far escaped detection. We would also expect that H_2 will predominate over H for the case of Mercury if its atmosphere is thin enough to allow direct solar wind impact on the surface. A related problem on which this result may bear is the formation of interstellar H_2 on dust particles (refs. 23-21 and 23-22).

LUNAR ALBEDO MEASUREMENTS

During the orbital mission, approximately 50 hr of data were obtained with the UVS observing the sunlit side of the Moon and approximately 50 hr of data were obtained on the dark side. Also during the

mission, a rocket experiment conducted by the University of Colorado from the White Sands Missile Range measured the absolute spectral brightness of the Sun in the ultraviolet while the UVS was measuring the sunlit spectrum of the Moon. Thus, we were able to make an absolute measurement of the spectral albedo of the lunar surface.

Before the mission, laboratory measurements had been made of the spectral albedo of lunar dust samples obtained on the Apollo 11, 12, and 14 missions. The laboratory measurements showed that all three lunar samples had an ultraviolet albedo of approximately 2.2 ± 0.2 percent at all wavelengths in the range of 121.6 to 165.7 nm (ref. 23-23). Because almost all minerals are opaque in the spectral region to which the UVS is sensitive, body color plays a small role in the spectral properties of minerals, and refractive index effects probably dominate. Alternatively, metallic sputtering produced by solar wind impact (ref. 23-24) may coat the surface and create the observed grayness in the lunar samples. However, the laboratory-measured albedo is not inconsistent with the assumption that the refractive index, and therefore the mineralogical character of the lunar material, is the factor that controls the far ultraviolet albedo.

Figure 23-6 shows a spectrum obtained from the lunar surface near the subsolar point. The very substantial signals shown, combined with the rocket measurements described previously, permit an accurate measurement of the lunar albedo in the spectral range 118 to 168 nm. This in situ albedo measurement agrees very well with the 2.2-percent value observed in the laboratory.
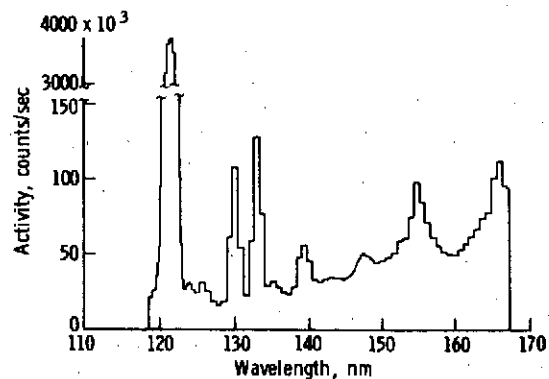

FIGURE 23-6.—Spectrum obtained from UVS observation of the lunar surface near the subsolar point.

Figure 23-7 shows the signal at 147 nm and its variation with lunar longitude during one albedo pass (revolution 28). This curve agrees closely with the behavior of the lunar albedo in the visible region as analyzed by Hapke (ref. 23-25). Figure 23-8 is a plot of the data shown in figure 23-7 divided by the Hapke function for the visible region. Large variations near the terminator are caused by shadowing effects. If the visible Hapke function were the same as the far ultraviolet function, the curve in figure 23-8 would be independent of lunar longitude. In figure 23-9, the residual longitude effect shown in figure 23-8 has been removed by an arbitrary modification of the part of the visible Hapke function that might reasonably be expected to change in the far ultraviolet. Also plotted on figure 23-9 are the normalized data from the next passage across the illuminated surface (revolution 29).

Figure 23-9 demonstrates that the small variations in albedo with longitude are reproducible from one orbit to the next. The most spectacular demonstration is in the crater Neper, which shows an albedo peak in the center of the crater and minimums at the crater edges. However, many other variations are clearly identifiable and are shown to be reproducible in figure 23-9. As might be expected, the variations from point to point on the maria are less pronounced than in other areas. This effect can most clearly be seen in figure 23-7.

Analysis of other bright-side passes demonstrates

that the maria show little albedo variation, but there are exceptions (e.g., the southern portion of Mare Crisium). Perhaps the most important observations at this stage of data reduction are that Neper Crater is an exception, that most craters are not distinguishable in the ultraviolet, and that most of the variations in the ultraviolet albedo seem to occur in regions that show little visible variations. Because we believe the albedo observations may have important geological or mineralogical significance, we are continuing data reduction and analysis and plan a program of intercomparison with other lunar observations.

During the passage of the unilluminated portion of the Moon, we observed a reflected Lyman-alpha signal from solar system hydrogen. We have also observed albedo variations in this signal that may be of particular importance because the signal includes
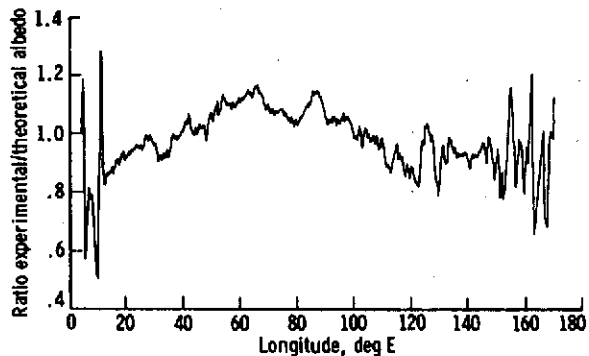
FIGURE 23-8.--Transit data of figure 23-7 divided by visible Hapke function.
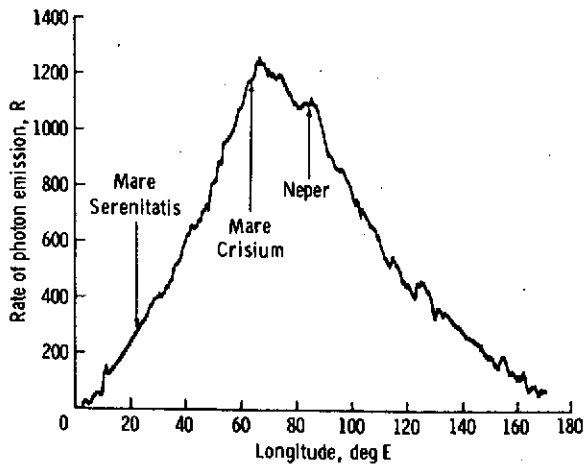

FIGURE 23-7. Variation of brightness with lunar longitude for the signal observed at 147 nm (fig. 23-6) as the spacecraft traversed the illuminated lunar surface on revolution 28.
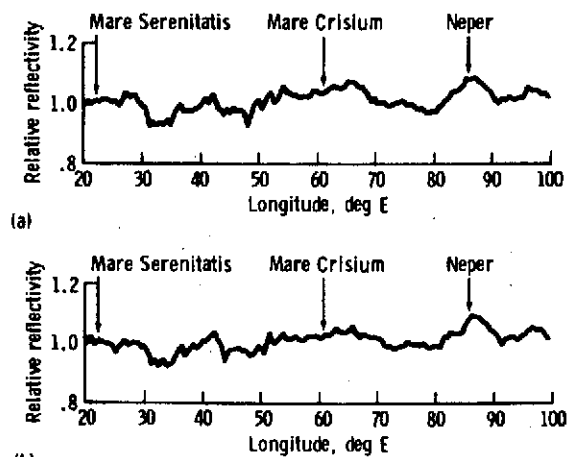

FIGURE 23-9. Lunar transit data divided by far ultraviolet Hapke function. (a) Revolution 28. (b) Revolution 29.

areas that have not been studied in great detail. However, because the signal is so much weaker than the bright-side signal, little analysis of this data has been performed to date.

OTHER OBSERVATIONS

Twice during lunar orbit, when the spacecraft had just entered the shadow behind the terminator, the spacecraft was oriented so that ultraviolet zodiacal light emissions from the inner solar atmosphere could be observed. These data have only been preliminarily analyzed but generally support the ultraviolet zodiacal light observations by Orbiting Astronomical Observatory 2 (OAO-2) (ref. 23-26).

Several times during TEC, the UVS observed the Earth. Preliminary analysis (ref. 23-27) indicates that the data support the Orbiting Geophysical Observatory IV (OGO IV) orbital observations of the ultraviolet Earth airglow and provide an overall view of the Earth for comparison with other planets.

During TEC, the UVS was operated almost continuously to provide a detailed ultraviolet survey of our galaxy and to observe selected stellar spectra. A massive amount of data was obtained, but its analysis awaits viewing direction information in galactic coordinates. Preliminary analysis of the spectra of isolated bright stars demonstrates that significant data were obtained. The observed ultraviolet spectral distributions agree with previous observations and provide the most precise measurement of absolute ultraviolet brightness obtained to date (ref. 23-28).

The full sky survey described previously also provided a measure of the distribution of solar system Lyman-alpha (121.6 nm) emission that is produced by resonance re-radiation of solar radiation by atomic hydrogen in the solar system. The survey also provided an opportunity to search for a geomagnetic tail of atomic hydrogen downwind from the Sun. These data have not been analyzed.

Once during TEC, the UVS was operating during a molecular hydrogen purge of the fuel cells that produced the ultraviolet spectrum shown in figure 23-10. This spectrum arises from absorption by molecular hydrogen of Lyman-beta and Lyman-gamma solar radiation and fluorescent re-radiation of this energy at longer wavelengths. From knowledge of the brightness of these solar emission features and of the Franck-Condon factors for molecular hydrogen, we have calculated the expected fluorescence spec-
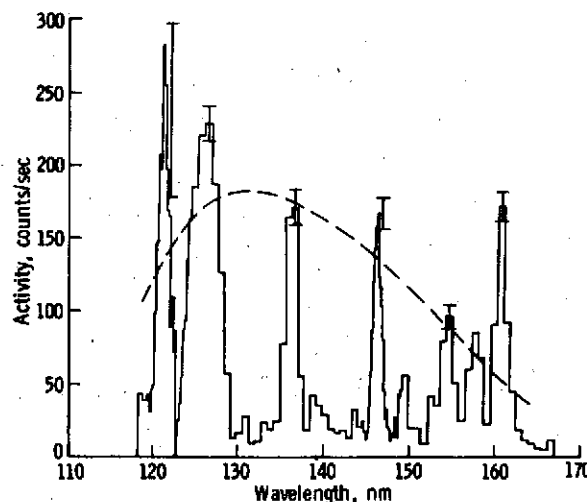
FIGURE 23-10.—Spectrum obtained in TEC during molecular hydrogen purge of fuel cells. The dashed curve represents a brightness of 2 R. The error bars represent 1 standard deviation in the observed counting rate.
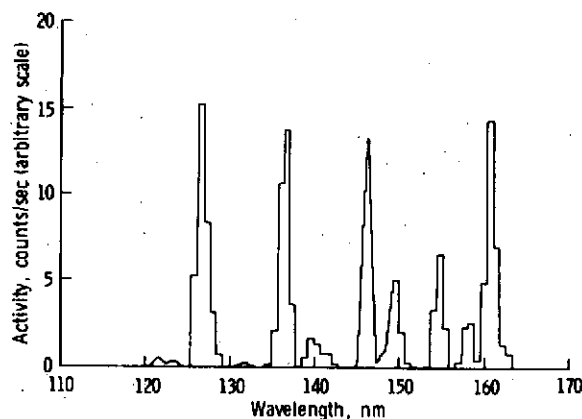
FIGURE 23-11.—Calculated fluorescence spectrum of molecular hydrogen excited by far ultraviolet solar radiation. (Intensity of one band normalized to experimental data (fig. 23-10).)

trum of molecular hydrogen. This theoretical spectrum is shown in figure 23-11 where the intensity of one of the bands has been normalized to the experimental data of figure 23-10. The observed and calculated distributions agree very well. We have also calculated that the observed spectral brightness gives a column density of approximately 1×10^{14} molecules/cm^2, in close agreement with the calculated column density based on a nominal H_2 purge rate and the spacecraft geometry.

The H_2 spectrum provides an internal calibration

of the UVS as a molecular hydrogen sensor and gives high reliability to the upper limit on H_2 at the subsolar point discussed in the section entitled "Lunar Atmosphere Observations" and shown in table 23-I. The H_2 observation is also important as an unambiguous means of identifying molecular hydrogen in the atmospheres of planets and comets (ref. 23-29).

REFERENCES

23-1. Fastie, William G.: The Apollo 17 Far Ultraviolet Spectrometer Experiment. The Moon, vol. 7, nos. 1/2, Mar./Apr. 1973, pp. 49-62.

23-2. Johnson, F. S.: Lunar Atmosphere. Rev. Geophys. Space Phys., vol. 9. no. 3, Aug. 1971, pp. 813-823.

23-3. Johnson, Francis S.; Carroll, James M.; and Evans, Dallas E.: Lunar Atmosphere Measurements. Proceedings of the Third Lunar Science Conference, vol. 3, MIT Press (Cambridge, Mass.), 1972, pp. 2231-2242.

23-4. Hodges, R. R.; Hoffman, J. H.; and Evans, D. E.: Lunar Orbital Mass Spectrometer Experiment. Sec. 21 of the Apollo 16 Preliminary Science Report. NASA SP-315, 1972.

23-5. Hoffman, J. H.; Hodges, R. R., Jr.; and Evans, D. E.: Lunar Atmospheric Composition Results From Apollo 17. Lunar Science IV (Abs. of papers presented at the Fourth Lunar Science Conference (Houston, Tex.), Mar. 5-8, 1973), pp. 376-377.

23-6. Hodges, R. R.; Hoffman, J. H.; Yeh, T. T. J.; and Chang, G. K.: Orbital Search for Lunar Volcanism. J. Geophys. Res., vol. 77, no. 22, Aug. 1, 1972, pp. 4079-4085.

23-7. Hodges, R. R.; Hoffman, J. H.; Johnson, F. S.; and Evans, D. E.: Composition and Dynamics of Lunar Atmosphere. Proceedings of the Fourth Lunar Science Conference, Pergamon Press (New York), Dec. 1973.

23-8. Chamberlain, J. W.: Planetary Coronae and Atmospheric Evaporation. Planet. Space Sci., vol. 11, no. 8, Aug. 1963, pp. 901-960.

23-9. Thomas, G. E.; and Krassa, R. F.: OGO 5 Measurements of the Lyman Alpha Sky Background. Astron. Astrophys., vol. 11, no. 2, Apr. 1971, pp. 218-233.

23-10. Barth, Charles A.: Planetary Ultraviolet Spectroscopy. Appl. Optics, vol. 8, no. 7, July 1969, pp. 1295-1304.

23-11. Fairfield, D. H.: Average and Unusual Locations of the Earth's Magnetopause and Bow Shock. J. Geophys. Res., vol. 76, no. 28, Oct 1, 1971, pp. 6700-6716.

23-12. Neugebauer, M.; Snyder, C. W.; Clay, D. R.; and Goldstein, B. E.: Solar Wind Observations on the Lunar Surface with the Apollo-12 ALSEP. Planet. Space Sci., vol. 20, no. 2, Oct. 1972, pp. 1577-1591.

23-13. Leich, D. A.; Tombrello, T. A.; and Burnett, D. S.: The Depth Distribution of Hydrogen in Lunar Materials. Lunar Science IV (Abs. of papers presented at the Fourth Lunar Science Conference (Houston, Tex.), Mar. 5-8, 1973), pp. 463-465.

23-14. Fleischer, Robert L.; and Hart, Howard R., Jr.: Surface History of Lunar Soil and Soil Columns. Lunar Science IV (Abs. of papers presented at the Fourth Lunar Science Conference (Houston, Tex.), Mar. 5-8, 1973), pp. 251-253.

23-15. Geiss, J.; Buehler, F.; Cerutti, H.; Eberhardt, P.; and Filleux, Ch.: Solar Wind Composition Experiment. Sec. 14 of the Apollo 16 Preliminary Science Report. NASA SP-315, 1972.

23-16. Siscoe, G. L.; and Mukherjee, N. R.: Upper Limits on the Lunar Atmosphere Determined from Solar-Wind Measurements. J. Geophys. Res., vol. 77, no. 31, Nov. 1, 1972, pp. 6042-6051.

23-17. Gott, J. Richard, III; and Potter, A. E., Jr.: Lunar Atomic Hydrogen and Its Possible Detection by Scattered Lyman-α Radiation. Icarus, vol. 13, 1970, pp. 202-206.

23-18. Manka R. H.; and Michel, F. C.: Lunar Atmosphere as a Source of Lunar Surface Elements. Proceedings of the Second Lunar Science Conference, vol. 2, MIT Press (Cambridge, Mass.), 1971, pp. 1717-1728.

23-19. Hodges, R. R.: Helium and Hydrogen in the Lunar Atmosphere. J. Geophys. Res., vol. 78, 1973.

23-20. Hoffman, J. A.; Hodges, R. R., Jr.; and Evans, D. E.: Lunar Atmosphere Composition Results from Apollo 17. Proceedings of the Fourth Lunar Science Conference, Pergamon Press (New York), Dec. 1973.

23-21. Spitzer, L.; Drake, J. F.; Jenkins, E. B.; Morton, D. C.; et al.: Spectrophotometric Results from the Copernicus Satellite. IV, Molecular Hydrogen in Interstellar Space. Astrophys. J. Letters, vol. 181, May 1, 1973, pp. L116-L121.

23-22. Hollenbach, D.; and Salpeter, E. E.: Surface Recombination of Hydrogen Molecules. Astrophys. J., vol. 163, no. 1, Jan. 1971, pp. 155-164.

23-23. Lucke, R. L.; Henry, R. C.; and Fastie, W. G.: Far Ultraviolet Reflectivity of Lunar Dust Samples: Apollo 11, 12, and 14. Astron. J., vol. 78, no. 3, Apr. 1973, pp. 263-266.

23-24. Hapke, B. W.; Cohen, A. J.; Cassidy, W. A.; and Wells, E. N.: Solar Radiation Effects on the Optical Properties of Apollo 11 Samples. Proceedings of the Apollo 11 Lunar Science Conference, vol. 3, Pergamon Press (New York), 1970, pp. 2199-2212.

23-25. Hapke, Bruce W.: A Theoretical Photometric Function for the Lunar Surface. J. Geophys. Res., vol. 68, no. 15, Aug. 1, 1963, pp. 4571-4586.

23-26. Lillie, C. F.: OAO-2 Observations of the Zodiacal Light. The Scientific Results From the Orbiting Astronomical Observatory (OAO-2). NASA SP-310, 1972, pp. 95-108.

23-27. Feldman, P. D.; Fastie, W. G.; Henry, R. C.; Moos, H. W.; et al.: Far Ultraviolet Observations of the Earth's Airglow From Apollo 17. Paper presented at 54th Annual Meeting, Am. Geophys. Union (Washington, D.C.), Apr. 1972.

23-28. Henry, R. C.; Moos, H. W.; Fastie, W. G.; and Weinstein, A.: Low-Resolution Ultraviolet Spectroscopy of Several Stars. Paper presented at 16th Plenary Meeting, COSPAR (Konstanz, W. Germany), June 1973.

23-29. Feldman, P. D.; and Fastie, W. G.: Fluorescence of Molecular Hydrogen Excited by Solar Extreme Ultraviolet Radiation. Astrophys. J. Letters, Oct. 15, 1973.

SCIENCE

A Search for Far-Ultraviolet Emissions

from the Lunar Atmosphere

Wm. G. Fastie, Paul D. Feldman, Richard C. Henry, H. Warren Moos,
Charles A. Barth, Gary E. Thomas and Thomas M. Donahue

A Search for Far-Ultraviolet Emissions from the Lunar Atmosphere

Abstract. *An ultraviolet spectrometer aboard the Apollo 17 orbiting spacecraft attempted to measure ultraviolet emissions from the lunar atmosphere. The only emissions observed were from a transient atmosphere introduced by the lunar landing engine. The absence of atomic hydrogen implies that solar wind protons are converted to hydrogen molecules at the lunar surface.*

The Apollo 17 orbiting far-ultraviolet spectrometer experiment had as its primary objective the measurement of the density and composition of the lunar atmosphere based on observations of the resonance scattering and fluorescence of solar far-ultraviolet radiation. This technique can provide density measurements in the range from 10^1 to 10^4 cm^{-3} for H, H_2, O, C, N, CO, Kr, and Xe, all of which may be present as important constituents of the lunar atmosphere (*1*). The results presented here indicate that the surface concentration of H is less than 10 cm^{-3}, almost three orders of magnitude less than predicted (*2*), whereas the concentration of H_2, if present, is less than 1.2×10^4 cm^{-3}. This is consistent with the hypothesis that the solar wind protons are completely converted into H_2 at the lunar surface. None of the other observable constituents was detected. A transient atmosphere was observed shortly after lunar module touchdown, but this disappeared in a matter of hours. No evidence of outgassing was detected in the vicinity of the crater Aristarchus, where many transient optical phenomena have been reported.

Earlier measurements of the lunar atmosphere made by means of an in situ pressure gauge (*3*) indicated that the total surface density at the subsolar point may be as large as 10^7 cm^{-3}. More recently, mass spectrometer measurements from lunar orbit (*4*) and from the lunar surface (*5*) have resulted in the detection of Ne, Ar, and He. Lunar outgassing, the only possible source of a substantial atmosphere, oc-

curs at a rate several orders of magni-on Earth (*6*). Apart from radiogenic ^{40}Ar and He (*7*), the lunar atmosphere may consist only of neutralized solar wind ions. Thus the lunar atmosphere would be expected to be made up primarily of Ne, Ar, H, and He, whose subsolar surface concentrations would lie in the range from 2×10^3 to 7 $\times 10^3$ cm^{-3} (*7*).

The Apollo 17 spectrometer, designed to scan the wavelength region from 1180 to 1680 A every 12 seconds, with a resolution of 10 A, is described in detail elsewhere (*8*). Observations were made in various command module attitudes as shown in Fig. 1. The principal mode of operation (mode A in Fig. 1) was the observation through
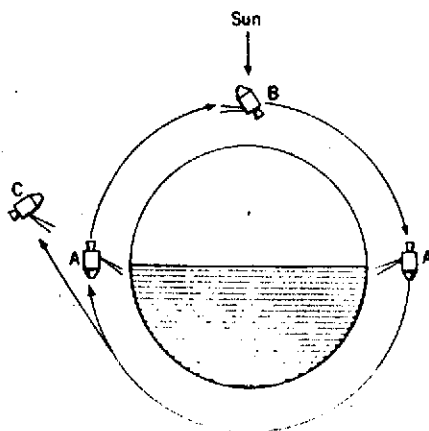

Fig. 1. Schematic representation of the modes of observation of the lunar atmosphere. The Apollo 17 far-ultraviolet spectrometer has a field of view of 12° by 12° and looks forward 23° relative to the normal to the service module axis.

$\approx$ 120 km of illuminated atmosphere tude less than the corresponding rate above the terminator against the dark side of the moon. A total of 1200 of these terminator spectra were obtained.

Two additional modes were employed to enhance the sensitivity. These modes provide most of the upper limits quoted herein. In mode B in Fig. 1 the spectrometer was pointed at a fixed point in space, and, as the spacecraft moved in its orbit, the line of sight extended through a tangential slice of illuminated atmosphere. The enhancement provided by this mode is $\approx$ 20 for H and H_2 and $\approx$ 10 for O, based on an exospheric model with the lunar surface as the critical level (*9*). Mode C in Fig. 1 was used immediately after transearth injection and is similar to mode A except for the much greater optical path length ($\approx$ 550 km).

For all wavelengths other than H Lyman-α (1216 A), the limit on sensitivity was set by the background count rate ($\approx$ 25 count sec^{-1}) which was caused by solar cosmic-ray protons. At 1216 A, solar radiation resonantly scattered from hydrogen atoms in the interplanetary medium produces a background between 200 and 400 rayleighs (depending on the viewing direction), in good agreement with earlier measurements (*10*), or 6 to 12 rayleighs (450 to 900 count sec^{-1}) when observed reflected from the surface of the dark side of the moon. Solar Lyman-α radiation scattered from the earth's hydrogen geocorona and then reflected from the moon beyond the lunar terminator adds a 1-rayleigh contribution to the background for crossings of the terminator facing Earth. During the transearth coast, the fixed areas of space observed during the tangential mode (mode B in Fig. 1) were again observed in order to provide a sky background correction for the atmospheric observation in this mode. Figure 2 shows the result of applying this correction to the tangential mode data obtained near the

Table 1. Experimental upper limits for species in the lunar atmosphere.

Species	Transition	Wavelength (Å)	g Factor (photon sec⁻¹ molecule⁻¹)	Mode of observation*	Sensitivity (photoelectron sec⁻¹ rayleigh⁻¹)	Observed surface density† (cm⁻³)
H	$^2S\text{-}^2P$ (Lyman-α)	1216	2.2×10^{-3}	C	75	< 10
O	$^3P\text{-}^3S$	1304	2×10^{-5}	B	99	< 80
N	$^4S\text{-}^4P$	1200	3.6×10^{-6}	B	70	< 600
C	$^3P\text{-}^3P^o$	1657	2.1×10^{-4}	B	25	< 30
Kr	$^1S\text{-}^3P$	1236	1.6×10^{-7}	A	85	< 20,000
Xe	$^1S\text{-}^3P$	1470	1.5×10^{-9}	A	75	< 2,000
H_2	$B\,^1\Sigma_u^+\text{-}X\,^1\Sigma^+$ (6, 9)	1462	4.0×10^{-5}	B	75	< 12,000
CO	$A\,^1\Pi\text{-}X\,^1\Sigma^+$ (1, 0)	1510	7.5×10^{-6}	B	60	< 40,000

* See Fig. 1.   † Except for H, Kr, and Xe (which are terminator values), these values correspond to measurements obtained at the subsolar point and are based on a 2 σ level in the observed counting rate.

subsolar point and with the spacecraft altitude varying between 45 and 70 km. The error bar represents one standard deviation (1 σ) in the observed counting rate. The H Lyman-α points, representing the difference (Δ) between two large counting rates, have a statistical uncertainty of $\approx$ 60 count sec⁻¹ and are not shown in Fig. 2.

Table 1 lists the transitions of interest, the resonance g factors (11), the instrument sensitivity, and the upper limits of the surface concentrations, based on a 2 σ level. For H the upper limit is derived from the difference between two terminator observations from different altitudes above the lunar surface (modes A and C in Fig. 1). The only positive emission detected was a slight enhancement ($\approx$ 3 σ) at 1304 Å (O) and at several wavelengths of the CO fourth-positive bands observed 2 hours after the landing of the lunar module. None of these spectral features appeared at any other time during the lunar observations.

The most surprising result is the absence of H in the lunar atmosphere. We believe that nearly 100 percent of the solar wind protons are converted to H_2 at the lunar surface. The expected H_2 density of 3.6×10^3 cm⁻³ at the subsolar point and 2.3×10^4 cm⁻³ at the antisolar point (12) would have so far escaped detection (5).

On the basis of the Apollo 17 observations, we would expect that H_2 will predominate over H in Mercury's atmosphere if it is thin enough to allow the direct impact of the solar wind on the surface. A related problem on which this result may bear is the formation of H_2 on interstellar dust particles (13). The upper limits reported here for H, O, C, N, and CO are important in setting new upper limits for the average outgassing rates for H_2O, CO_2, CO, NO_2, N_2, H_2S, and SO_2 (14).

WM. G. FASTIE, PAUL D. FELDMAN*
RICHARD C. HENRY*
H. WARREN MOOS†
Johns Hopkins University,
Baltimore, Maryland 21218
CHARLES A. BARTH, GARY E. THOMAS
University of Colorado,
Boulder 80302
THOMAS M. DONAHUE
University of Pittsburgh,
Pittsburgh, Pennsylvania 15213

References and Notes

1. It is also expected that He, Ne, and Ar are present, but their resonance lines lie outside the spectral range of the spectrometer.
2. F. S. Johnson, Rev. Geophys. Space Phys. 9, 813 (1971).
3. ———, J. M. Carroll, D. E. Evans, Geochim. Cosmochim. Acta 3 (Suppl. 3), 2231 (1972).
4. R. R. Hodges, J. H. Hoffman, D. E. Evans, NASA SP-315 (1972), p. 211.
5. J. H. Hoffman, R. R. Hodges, D. E. Evans, Geochim. Cosmochim. Acta, in press.
6. R. R. Hodges, J. H. Hoffman, T. T. J. Yeh, G. K. Chang, J. Geophys. Res. 77, 4079 (1972).
7. R. R. Hodges, J. H. Hoffman, F. S. Johnson, Geochim. Cosmochim. Acta, in press.
8. W. G. Fastie, Moon 7, 49 (1973).
9. J. W. Chamberlain, Planet. Space Sci. 11, 901 (1963).
10. G. E. Thomas and R. F. Krassa, Astron. Astrophys. 11, 218 (1971).
11. C. A. Barth, Appl. Opt. 8, 1295 (1969).
12. R. R. Hodges, in preparation.
13. D. Hollenbach and E. E. Salpeter, Astrophys. J. 163, 155 (1971).
14. The limits on the outgassing rates will be described in detail by G. E. Thomas et al., in preparation.
15. This work was supported by NASA contract NAS 9-11528.
* Alfred P. Sloan Research Fellow.
† Visiting Fellow 1972-1973. Joint Institute for Laboratory Astrophysics and Laboratory for Atmospheric and Space Physics, University of Colorado, Boulder 80302.
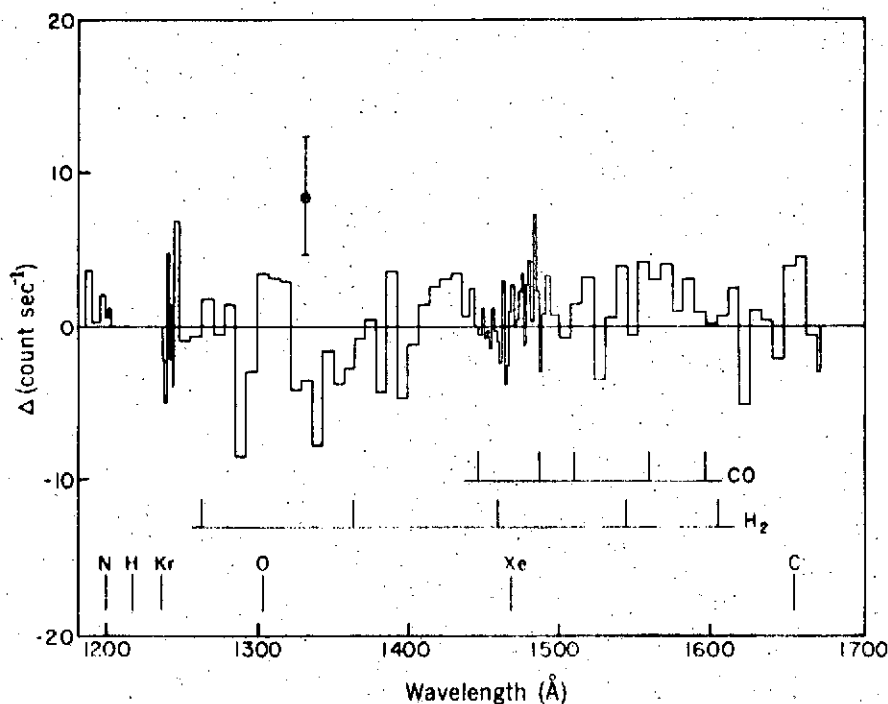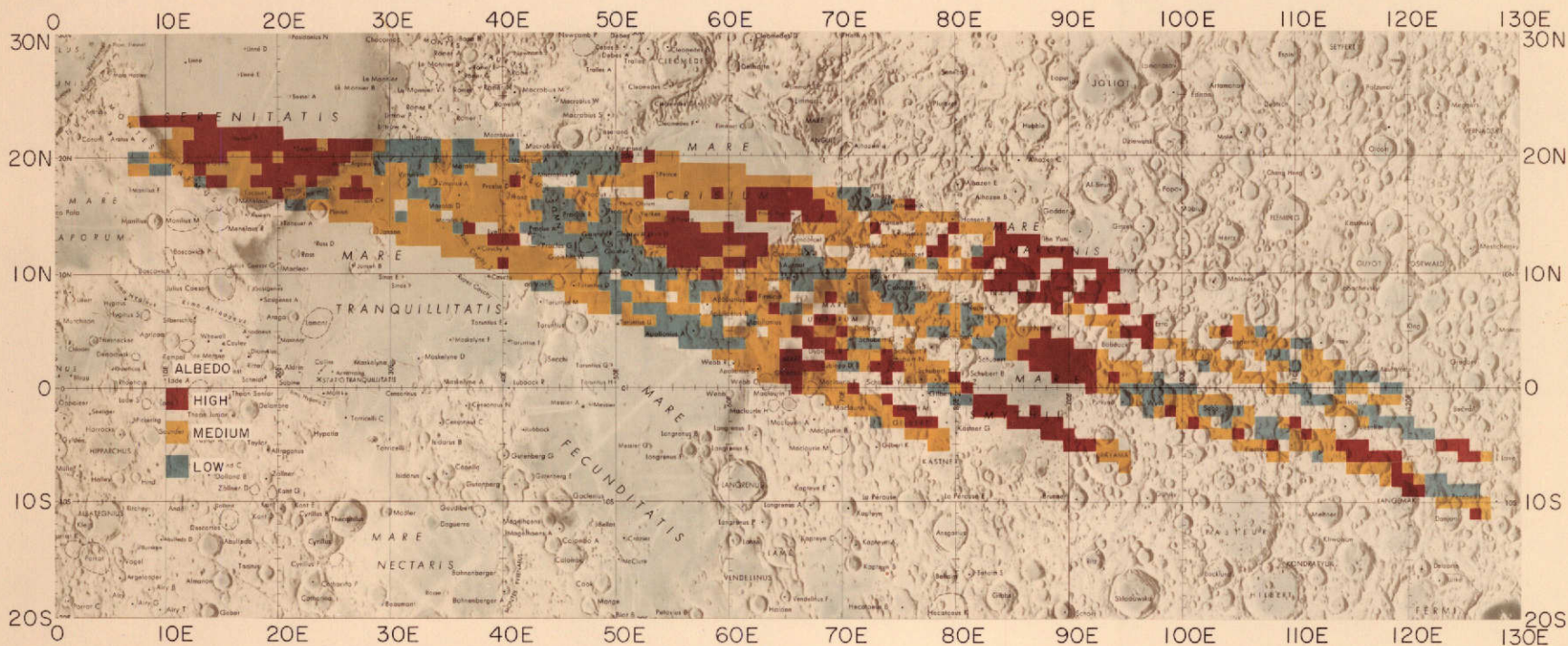
7 June 1973

Fig. 2. The average of 70 spectra obtained during a tangential mode (mode B in Fig. 1) observation with the sky background, observed during transearth coast, subtracted. The wavelengths of the principal emission features expected are indicated.

ULTRAVIOLET (1470Å) LUNAR MAP FROM APOLLO 17

The Apollo 17 Service Module carried an ultraviolet spectrometer which was used to measure the lunar albedo at 1470 Å. Mare areas appear brighter than highland areas, which is exactly opposite to the moon's visual appearance. Variations in albedo in the range ± 2.5% are shown in yellow, greater than 2.5% in red, and less than -2.5% in blue. The overall average normal albedo for the area scanned is about 0.04. The difference may be due to effects of surface age or mineralogical composition. (Robert L. Lucke, Richard C. Henry, and William G. Fastie, 1974, "Far Ultraviolet Lunar Mapping from Apollo 17." In Lunar Science V, pp. 469-471, The Lunar Science Institute, Houston).

ADDENDUM F

LOW-RESOLUTION ULTRAVIOLET SPECTROSCOPY OF SEVERAL HOT STARS FROM APOLLO 17

R. C. Henry[*], A. Weinstein, P. D. Feldman,
W. G. Fastie, and H. W. Moos

Department of Physics
The Johns Hopkins University
Baltimore, Maryland 21218

ABSTRACT

Low-resolution ultraviolet spectra were obtained for
six early-type stars in December 1972, using an Ebert
spectrometer mounted in the service module of the Apollo
17 spacecraft. The spectrometer scanned from 1180 Å to
1680 Å, with a speed that varied with wavelength according
to a program chosen for lunar studies. Spectral resolution
was 11 Å. The ultraviolet absolute calibration of the
instrument was determined by comparison with the National
Bureau of Standards calibrated photodiodes, and is believed
known to ± 10%. Stars observed, with their spectral classes,
were ζ Oph (O9.5), α Vir (B1 V), ζ Tau (B2 IV), η U Ma (B3 V),
α Eri (B5 IV), and α Gru (B5 V). The absolute intensities
are in good general agreement with the observations of
others, and with the predictions of stellar model atmos-
phere calculations.

I. INTRODUCTION

Low resolution far-ultraviolet spectra of six hot stars were obtained using the Far Ultraviolet Spectrometer (experiment S-169) aboard the Apollo 17 service module. This spectrometer (Fastie, 1973) was intended primarily to search for a lunar atmosphere (Fastie et al. 1973 a,b). The grating was rotated by a motor-driven cam from 1180 Å to 1680 Å in 12 seconds, the scan speed being 66.7 Å sec^{-1} except for two 50 Å segments centered on 1216 Å and 1470 Å, where the speed was 16.7 Å sec^{-1}. Detection was by an EMR 542 G MgF$_2$ windowed solar-blind photomultiplier. Data were transmitted directly to earth, or were recorded for later transmission to earth. Data on ζ Oph and ζ Tau were obtained during lunar orbit, while data on the other stars were obtained on Trans-Earth Coast.

II. CALIBRATION

Calibration was performed using the Calibration Test Equipment (CTE) at the Johns Hopkins University. A complete description of the calibration technique is given by Fastie and Kerr (1974). A low-pressure hydrogen lamp

delivers a dispersed f/56 ultraviolet beam to either of two reference photomultiplier tubes, or to the actual Apollo instrument in an evacuated test chamber. The grating was thoroughly mapped using the calibration beam. The reference photomultipliers are calibrated regularly against photodiodes provided by the National Bureau of Standards; these photodiodes have been recalibrated since the Apollo flight and found to be unchanged in sensitivity.

The spectrometer was subjected to a substantial fluence of ultraviolet radiation, predominantly solar $L\alpha$ reflected from the lunar surface, during the six days in lunar orbit. This resulted in a decrease in the sensitivity of the instrument to some degree. The decline was monitored by examining the brightness of the solar system $L\alpha$ scattered from the dark side of the moon over the six day period; by following the brightness of the solar $L\alpha$ and other wavelengths reflected from the lunar surface; by monitoring the dark current (which was predominantly produced by cosmic ray fluorescence in the photomultiplier tube entrance window); and finally by looking at a region of the sky before and after the period of high fluence. All of these methods together give a decline to 0.83 ± 0.04 of the laboratory sensitivity.

The ratio of solar $L\alpha$ reflected from the moon to continuum at longer wavelengths remained constant over the

TABLE 1

SPECTROMETER EFFICIENCY

λ	$\widetilde{OT}$
1192	0.0163
1216	0.0196
1280	0.0263
1336	0.0251
1395	0.0233
1463	0.0200
1518	0.0156
1582	0.0093
1608	0.0079
1639	0.0073
1655	0.0075

whole period. Vidal-Madjar (private communication) reports
that data from the OSO 5 hydrogen resonance cell for this
period show a rise of 10% in the total solar L α flux,
but a decline of 10% in the flux in the core of the
line. Unfortunately only four measurements are available
in the critical period. Comparison of Zurich sunspot
numbers and solar 2800 MHz flux (Lincoln 1973) with corre-
lations of these quantities with solar L α intensity (Vidal-
Madjar et al. (1973)) suggests that the solar L α intensity
did not vary by more than ± 7% during the Apollo 17 orbital
period (Dec. 10-16, 1972). None of this is critical,
because probably the most reliable measure of the decline
in sensitivity is the change in the dark current.

The over-all absolute instrument calibration is
believed known to ± 10% as a result of all of the above
efforts, and is listed in table 1, where QT is the product
of the quantum efficiency of the photomultipliers and the
optical transmission of the system.

III. OBSERVATIONS

Data on the six stars observed are summarized in
table 2. The first column gives the star name, followed
by the HR (Bright Star Catalog) and HD numbers. Visual

TABLE 2

STARS OBSERVED ON APOLLO 17

Star	HR	HD	V	B-V	E_{B-V}	Sp			V sini
ζ Oph	6175	149757	2.56	0.02	0.32	O	9.5	V	350
α Vir	5056	116658	0.96	-0.24	0.02	B	1	V	
ζ Tau	1910	37202	2.99	-0.18	0.06	B	2	IV	310
η UMa	5191	120315	1.86	-0.18	0.02	B	3	V	210
α Eri	472	10144	0.47	-0.17	0.00	B	5	IV	
α Gru	8425	209952	1.73	-0.14	0.02	B	5	V	

magnitudes, spectral types, and B-V colors were chosen
from Blanco et al. (1970). The reddening is as estimated
from the colors and spectral classes. The value of V sin i
(Slettebak 1949, 1954, 1955) is given.

The instrument field-of-view was 12° x 12°, so only
a comparatively small number of bright, isolated stars
could be observed. The wide field of view introduced a
large solar system L α signal, so stellar data were not
obtained near 1216 Å. Details of the background subtrac-
tion for each star are given below.

The spectra have been compared with model atmospheres
computed by Kurucz, Peytremann, and Avrett (1974), and by
Van Citters and Morton (1970). The models have been
reddened, following the interstellar reddening law of
Bless and Savage (1972), and have, in the case of the Van
Citters and Morton model, been folded through the known
resolution of the spectrometer (11 Å). The Smithsonian
Astrophysical Observatory (Kurucz, et al., 1974) models
are broadened by 50 Å as computed. The models are compared
with the rectified stellar data in the figures referred
to below. In order from the hottest star, the stars
observed were:

a) ζ Ophiuchi

This O-type star was observed in lunar orbit just
after sunset in the course of an attempt to measure
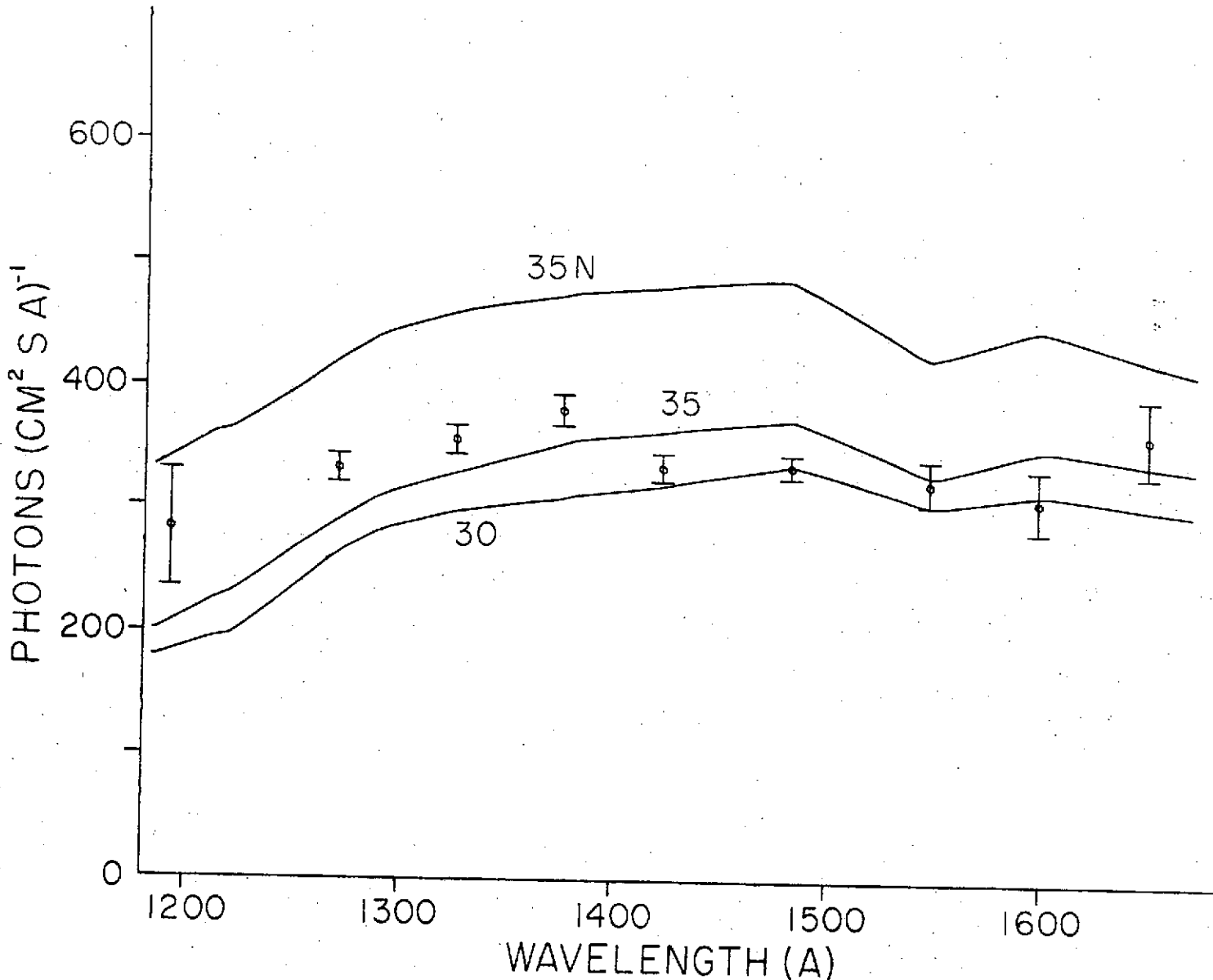
Fig. 1. Observed intensity of ζ Oph is shown as points with 2σ internal statistical error bars, compared with Kurucz et al. (1974) ("SAO") model stellar atmospheres. Models shown are T_e = 35,000°K reddened with the average (A) reddening law of Bless and Savage (1972), and 30 and 35,000°K SAO models reddened with their special ζ Oph reddening law.

zodiacal light near the sun. Five stellar spectra were
obtained, and 24 spectra observed just before (or after)
the stellar observation were averaged to obtain a back-
ground measurement for subtraction. The star was about
4 times background. Because the statistics for this star
were poor, the data have been combined into bins 50 Å
wide, centered on the wavelengths used in the Kurucz et al.
(SAO) models. The result, in figure 1, is compared with
the SAO 35,000° model, reddened according to the average
extinction law of Bless and Savage (1972) and designated
35 A in the figure. (The model here, and in the following
figures, has been matched to the known brightness of the
star at 5475 Å. A comparison, below, of the stellar
angular diameters deduced from these data, and the models,
with the directly observed stellar angular diameters shows
excellent agreement, justifying this procedure.)

Much better agreement between observation and model
is obtained if the special ζ Oph reddening law of Bless and
Savage (1972) is used, and a temperature of either 30 or 35
thousand degrees. The dip in the models at 1550 Å is
produced (at least partly) by the CIV doublet; the data
show no evidence for such a dip, but the statistics are
rather poor. There is clear evidence for a ~ 10% increase
in intensity below 1400 Å, that does not appear in the

models. This also appears in the spectra of some but not all of the other stars observed, as discussed below, and therefore may be a real stellar feature.

b) α Virginis

This B1 main-sequence star was observed both during Passive Thermal Control scans (a "rotisserie" spacecraft mode during trans-earth coast sleep periods) and also during a special maneuver conducted for the sole purpose of observing this star. Background from nearby regions was subtracted, and was very small. Agreement between the spectra obtained by these two different methods was within a few percent, and confirms that stellar data obtained by selecting out the few relevant scans during a rotation of the spacecraft are reliable. Different parts of the grating are illuminated by the star as the spacecraft rotates, and the constancy of the result indicates the uniformity of the grating. During the 10 minute "fixed" observation of α Vir (and of α Eri), the normal spacecraft pointing stability of $\sim 1^{\circ}$ was deliberately relaxed to $\pm \sim 5^{\circ}$, again in order to allow the starlight to wander over the grating and test the uniformity of the system in flight. The star did wander as expected, while the count rate varied less than $\pm$ 3 %.

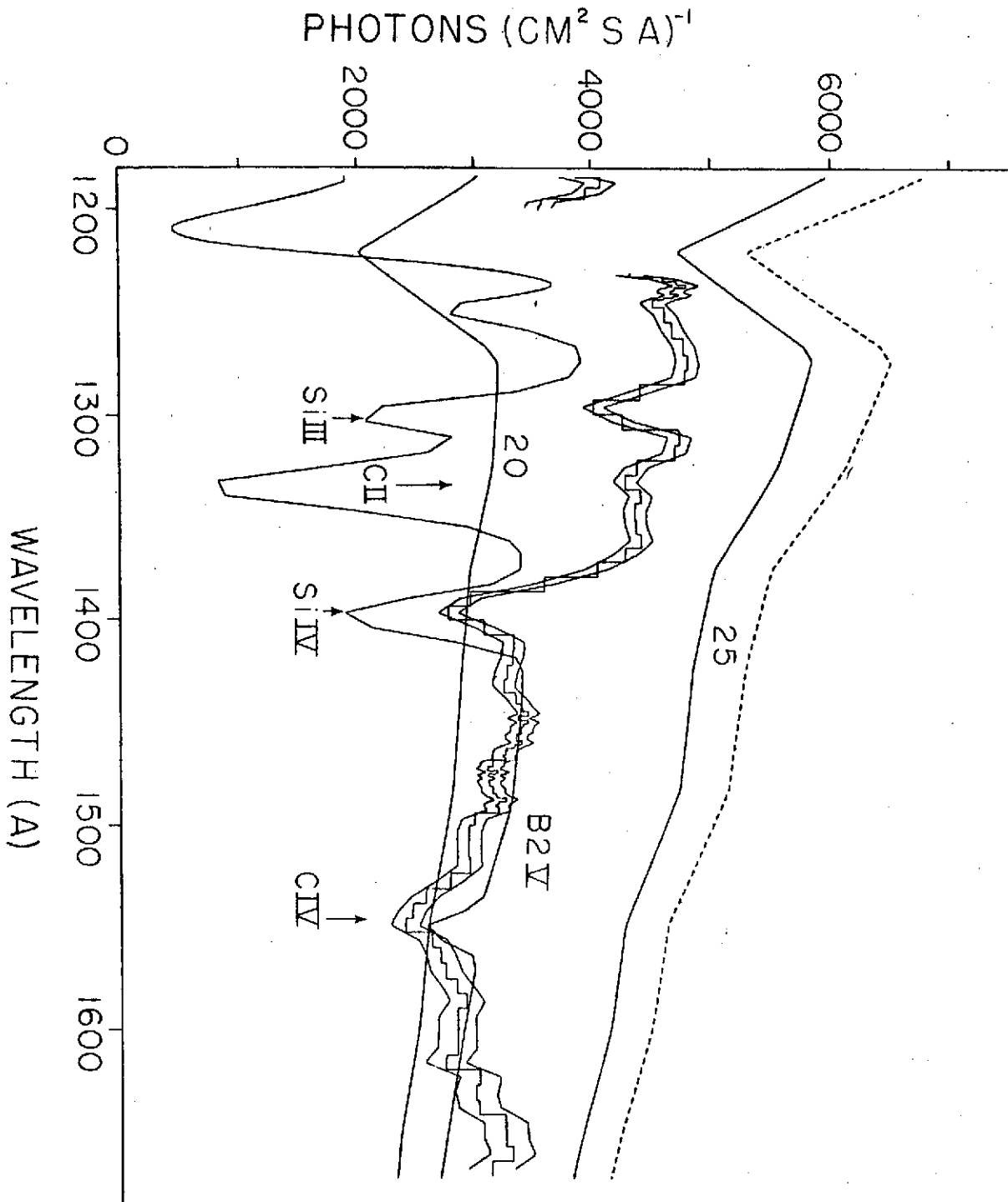Fig. 2.   Observed intensity of α Vir is shown as a histogram
with 2σ internal statistical error bars, compared with unreddened
(dashed lines) and reddened (E_{B-V} = 0.02) 25,000°K SAO models,
and similarly reddened 20,000°K SAO, and B2V Van Citters and
Morton (1970), models.   The SAO models have a resolution of 50 Å,
the data 11 Å, and the B2V model has been broadened 11 Å.   Note
the rise in the data below 1400 Å.

The data obtained are compared with models in figure 2. The data are in the form of a histogram, with 2σ error envelopes reflecting counting statistics in the star and the subtracted background only. Absolute error is believed to be $\pm$ 10%. The dashed line is the 25,000°K SAO model under the assumption that the star is not reddened. The same model is also shown under the assumption that the star is reddened with $E_{B-V} = 0.02$. The 20,000°K SAO model for the same reddening is also shown, as is the Van Citters and Morton (1970) B2V star model, similarly reddened. The latter has an effective temperature of 20,160°K.

Comparison of the observation with the Van Citters and Morton model shows that in the latter the CII and CIII (1247 A) lines are much too strong. This is caused by the assumption of a value for the damping constant 10 times the classical value, which apparently is not valid for these lines. The observed equivalent widths for the Si III, Si IV, and CIV lines, however, agree very well with the predictions of the model. The SAO models do not show lines because the models are averages over 50 Å.

It should be noted that Spica is a spectroscopic binary and is slightly variable (eg., Shobbrook, Lomb, and Herbison-Evans 1972).
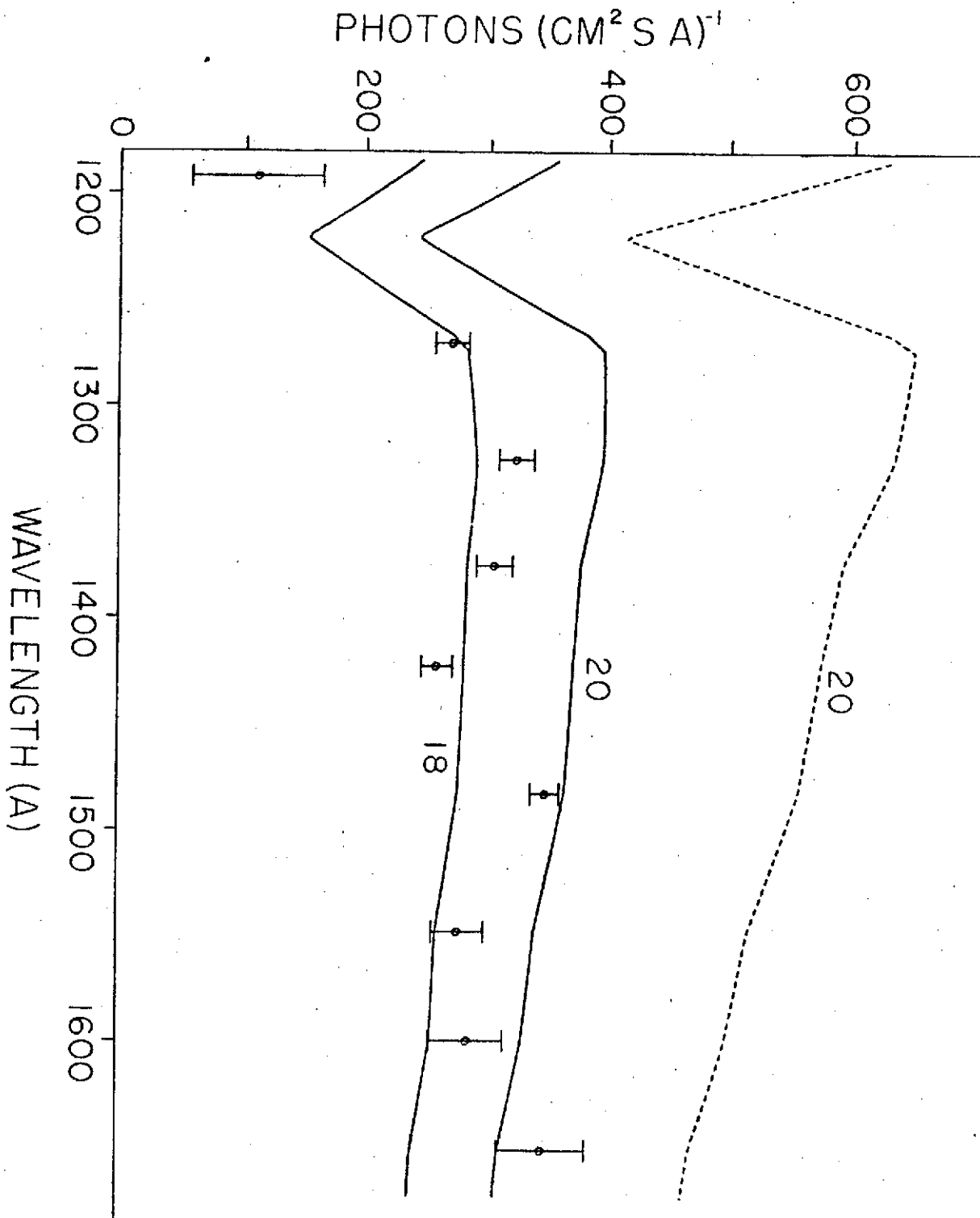
Fig. 3.   Observed intensity of ζ Tau, shown as points
with 2σ error bars, is compared with unreddened and reddened
(E_{B-V} = 0.06) 20,000°K SAO models, and a reddened 18,000°K SAO
model.   There is no indication of a rise below 1400 Å, although
statistics are poor.

c) ζ Tauri

This B2 subgiant was observed briefly during lunar orbit. Only 3 spectra were obtained and 24 background spectra were averaged and subtracted. Figure 3 compares the data, in 50 Å bins, with an SAO unreddened model at 20,000°K, and the same model, and the 18,000°K model, reddened with E_{B-V} = 0.06. No evidence is present for the rise below 1400 Å, although the statistics are rather poor. The observation below 1216 Å falls well below the prediction of the model, which was not the case for the two previous stars. This feature, which is present in all of the following stars, is undoubtedly the effect of the Si III resonance line at 1206.5 Å, and its behavior with temperature is consistent with evidence discussed by B. D. Savage and R. J. Panek (preprint).

ζ Tauri is a spectroscopic binary, and is a shell star.

d) η Ursae Majoris

This B3 main sequence star was observed during the Passive Thermal Control of the very long first sleep period after leaving the moon. Seventy-two scans were obtained. In figure 4, the data are shown as a histogram with 2σ statistical error envelopes, compared with the unreddened 18,000°K, and reddened (E_{B-V} = 0.02) 18,000°K,

Fig. 4. Observed intensity of η UMa is shown with 2σ error envelopes, compared with unreddened and reddened (E_{B-V} = 0.02) 18,000°K and reddened 16 and 15,000°K SAO models.

16,000°K, and 15,000°K SAO models. Agreement with the models is good, apart from the slight rise in stellar brightness below 1400 Å mentioned previously. The Si III 1300 Å and C II 1330 Å lines are clearly present, and the observation falls well below the prediction of the model below 1216 Å, indicating the presence of the Si III 1206.5 Å line. (It must be kept in mind that the models are broadened by 50 Å, while the observations have a resolution of 11 Å.)

e) α Eridani

This B5 subgiant was observed both during a Passive Thermal Control period and during a direct observation, with good agreement. The direct observation gave 106 scans. In figure 5 the data are shown as a histogram with 2 σ statistical error envelopes, compared with an unreddened SAO 15,000°K model, and reddened (E_{B-V} = 0.01) 16,000°K, 15,000°K, and 14,000°K models. This reddening was introduced simply to show the size of the effect; the star is not believed to be actually reddened by this amount. The rise below 1400 Å may also be interpreted as a shallow absorption trough between 1400 Å and about 1550 Å. The Si III 1300 Å and 1206.5 Å and C II 1330 Å lines appear with about the same strength as in η U Ma.
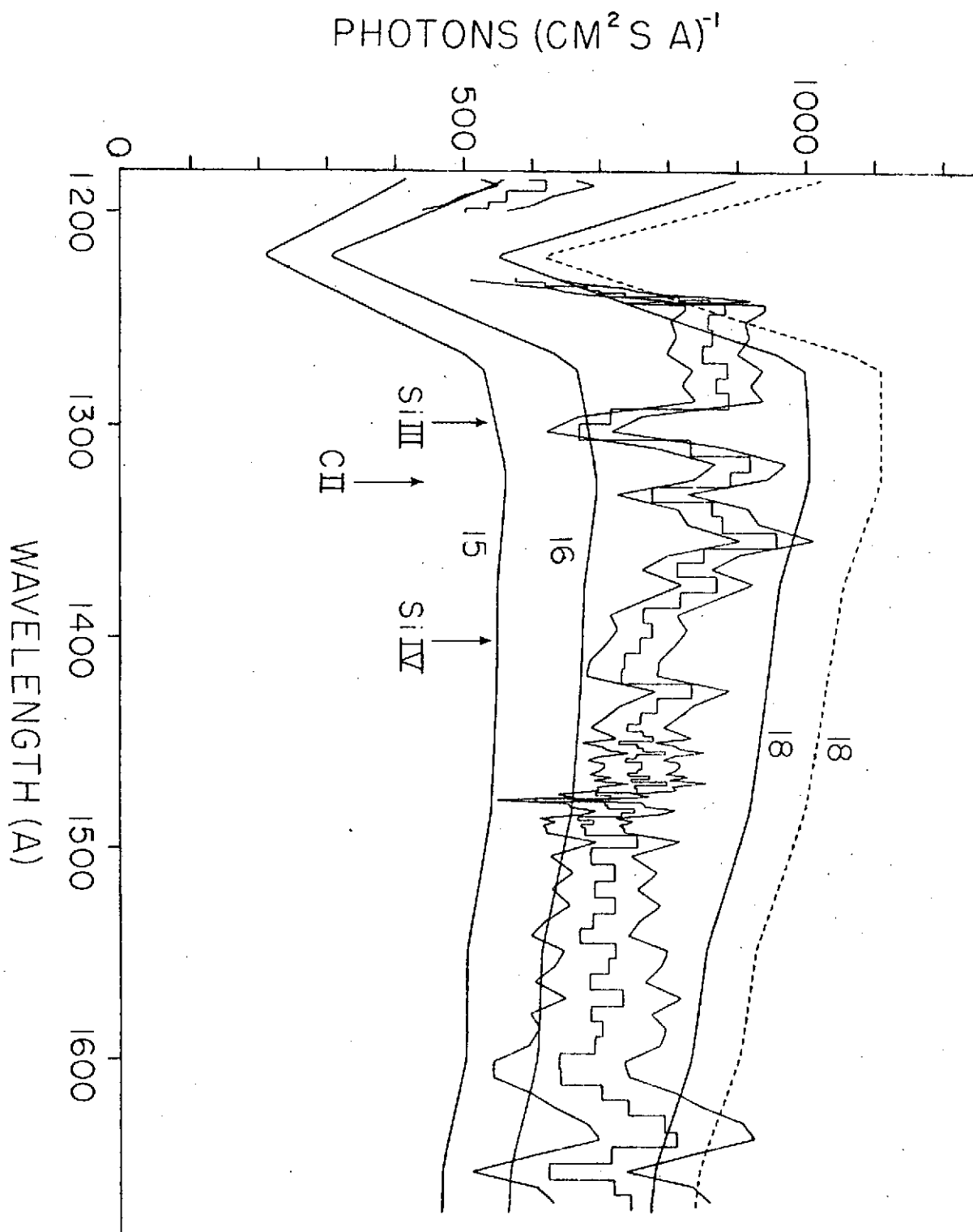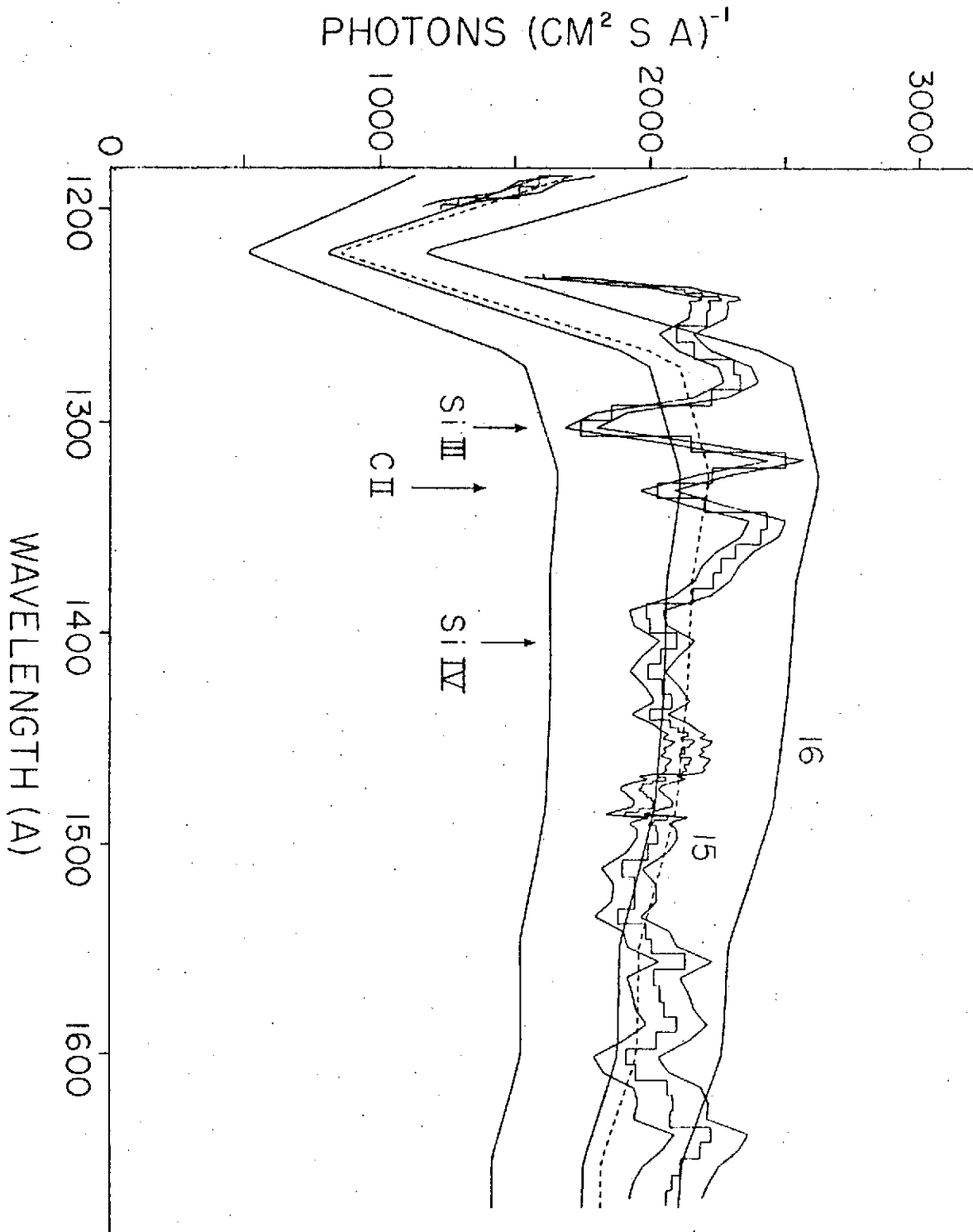
Fig. 5.   Observed intensity of α Eri is shown with 2σ   error envelopes, compared with unreddened 15,000°K and reddened (E_{B-V} = 0.01) 16, 15 and 14,000°K SAO models.

f) α Grus

This B5 main-sequence star was observed during a one-hour Passive Thermal Control period. Seven spectra were obtained, and 25 nearby background spectra were averaged and subtracted. Background was about half the signal while observing this star. In figure 6, the data in 50 $\overset{\bullet}{A}$ bins are compared with the relevant SAO models both assuming the star is unreddened and assuming $E_{B-V} = 0.02$. The agreement with the reddened 13,000°K model is excellent in all respects, except again for the presumed effect of the Si III 1206.5 $\overset{\bullet}{A}$ line.

III. DISCUSSION

In the sections below, we compare the observations systematically with the observations of others, and with the SAO models, and derive effective temperatures and angular diameters for the stars.

a) Comparison with the SAO models

The wavelength 1482 $\overset{\bullet}{A}$ was chosen as relatively free of lines for a comparison of the flux in the far ultraviolet between observation and model, as a function of visible stellar color.
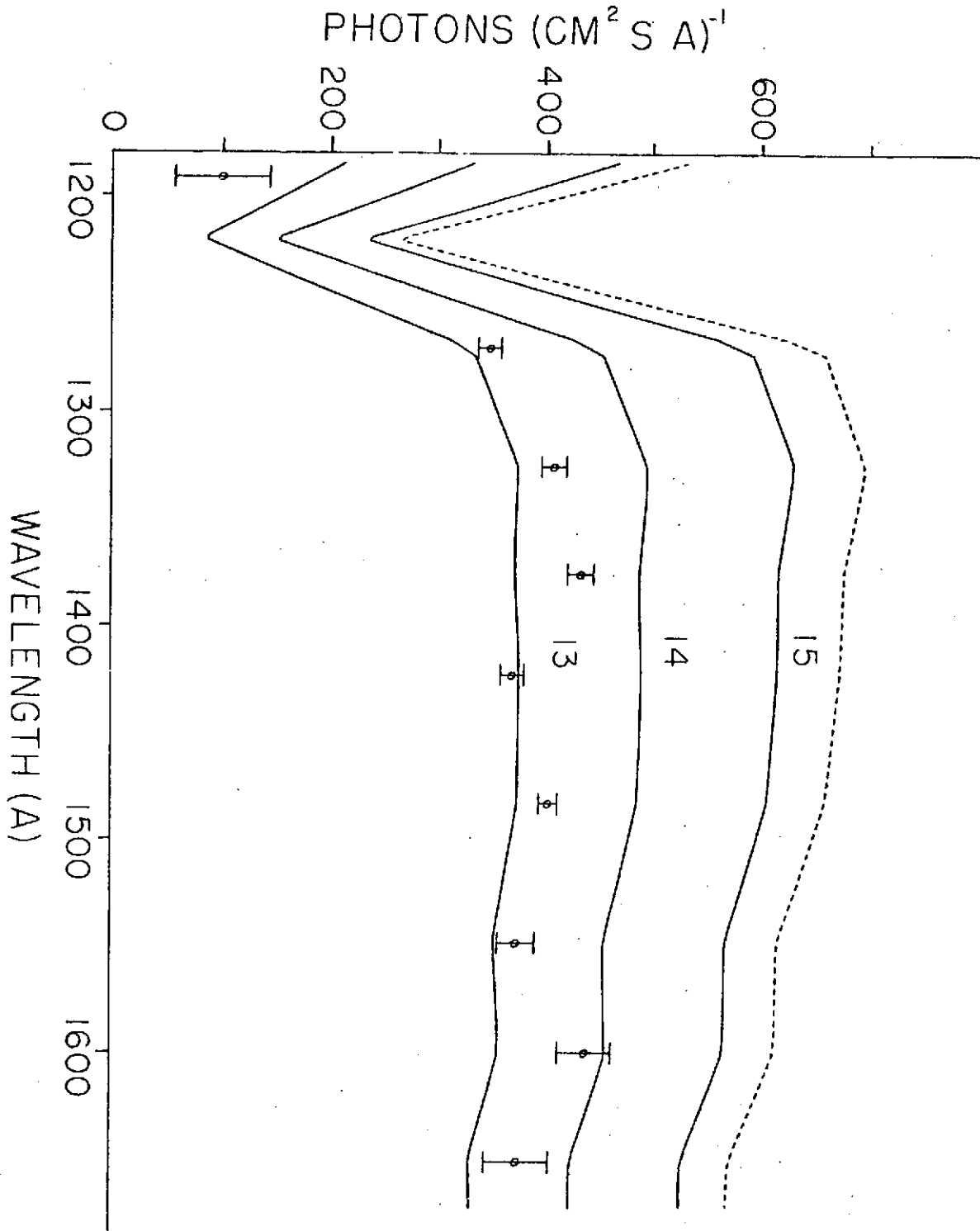
Fig. 6. Observed intensity of α Gru, shown as points with 2 σ error bars, is compared with unreddened 15,000°K, and reddened (E_{B-V} = 0.02) 15, 14, and 13,000°K SAO models.

A color

$$m_{1482} - V = -2.5 \log (F_{1482}/F_{5475}) \tag{1}$$

was formed, where F_λ is the flux in ergs (cm^2 sec Å)$^{-1}$ at wavelength λ. For F_{5475}, the value of Oke and Schild (1970) was used. This color, and the same color with the effects of interstellar reddening removed using the appropriate extinction of Bless and Savage (1972), are listed in table 3. Also, the absolute flux at 1482 Å is given in photons (cm^2 sec Å)$^{-1}$; this has an uncertainty of $\pm$ 10% for α Vir, η UMa, and α Eri, and $\pm$ 15% for ζ Oph, ζ Tau, and α Gru due to the poorer statistics and greater difficulty in judging the appropriate background sub-traction for these three stars. Also listed in table 3 are the effective temperatures deduced for these stars by comparing the present observations with model stellar atmospheres (below), and the uncertainty in these deduced temperatures. The $(m_{1376} - V)_o$ color of Smith (1967) is also given.

Figure 7 plots the 1482 A color as a function of B-V color for the six stars. Each star is shown both under the assumption that it is unreddened, and with reddening removed, assuming the E_{B-V} of table 2. For ζ Oph, reddening is removed under both the "average" and the "ζ Oph" (dot-dash line) extinction laws of Bless and

TABLE 3

ULTRAVIOLET FLUXES OF STARS OBSERVED ON APOLLO 17

Star	Scans	Flux at 1482 Å Ph $(cm^2 s A)^{-1}$	Te deduced		$m_{1482}-V$	$(m_{1482}-V)_o$	$(m_{1376}-V)_o$ Smith
ζ Oph	5	330	35,000 ± 5800		-2.80	-4.52	-4.86
α Vir	95	3200	22,300	1400	-3.66	-3.75	-3.61
ζ Tau	3	320	18,500	760	-3.19	-3.45	-3.24
η UMa	72	750	17,100	580	-2.98	-3.07	-3.24
α Eri	106	2080	15,800	640	-2.71	-2.71	-2.19
α Gru	7	435	13,350	360	-2.26	-2.35	
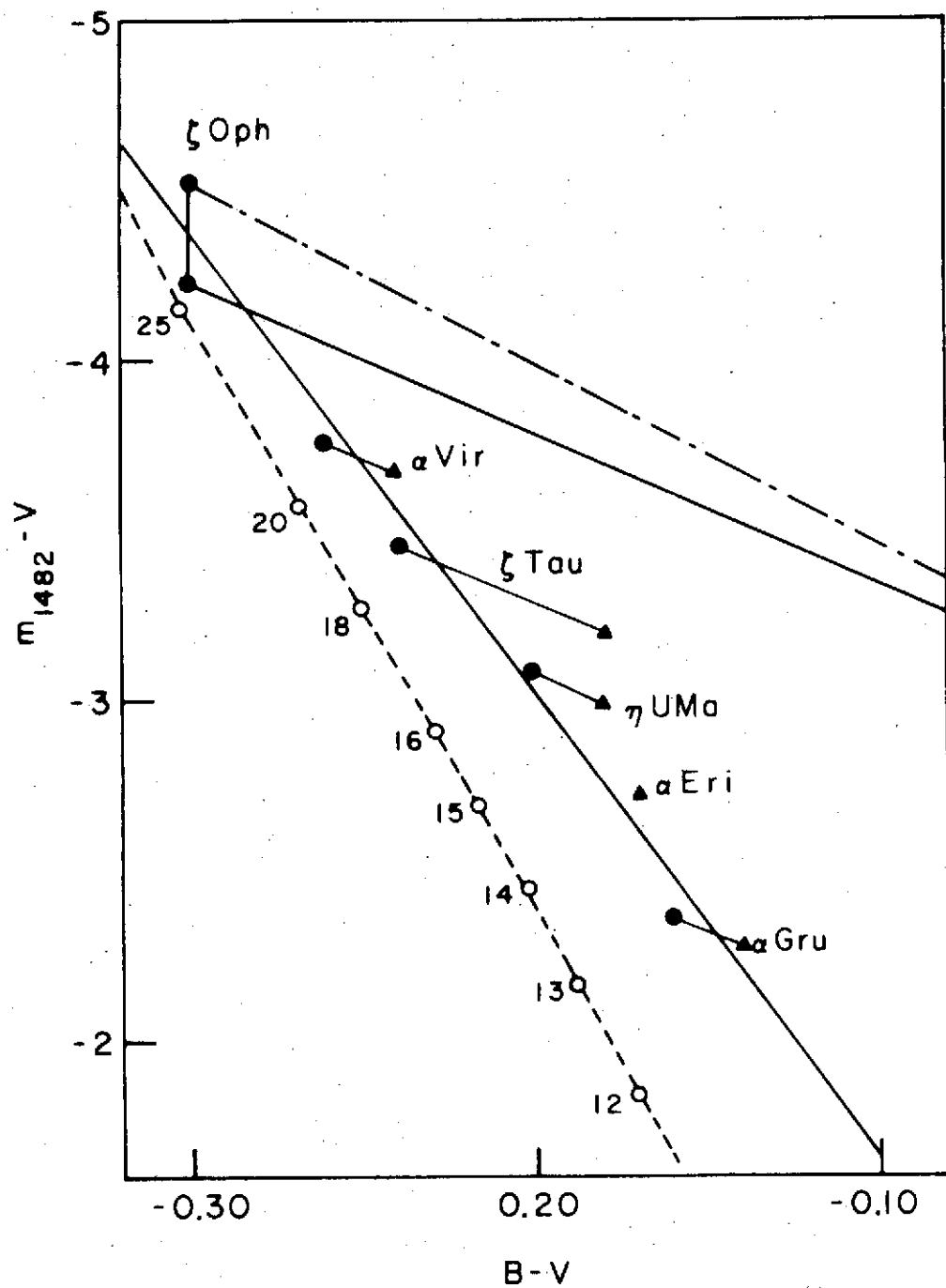
Fig. 7. An ultraviolet-visible color, obtained from the present data, is compared with the B-V color of the stars. Triangles are the observed colors, and filled circles the colors corrected for the interstellar reddening of table 2. The open circles show a similar comparison for the SAO models. The solid line is the adopted Apollo 17 calibration of the far-ultraviolet brightness of the early-type stars (see text).

Savage (1972). The SAO models are plotted as open circles
in the diagram. They differ systematically from the
observations in a manner that has already been pointed
out by Troy, Johnson, Young, and Holmes (1974): the B-V
colors of the models are apparently the cause of the
discrepancy. A solid line drawn through the observations
defines the adopted Apollo 17 calibration for the absolute
brightness of early B type stars:

$$m_{1482} - V = 13.73 \ (B-V)_o \ -0.26 \qquad (2)$$

or

$$\log_{10} F = 2.54 - 5.49 \ (B-V)_o, \qquad (3)$$

for a $V = 0.0$ star, where F is now photons $(cm^2 \ sec \ \overset{\bullet}{A})^{-1}$.
The use of photons has the virtue that the calibration
is virtually independent of wavelength over at least the
range 1250 to 1650 $\overset{\bullet}{A}$ (see figures 1 through 6).

In figure 8, the data and models are similarly compared
using the U-B colors. We have used the value U-B = -0.759
of Crawford (1963) for ζ Tau, rather than the value -0.66
of Iriarte et al. (1965). The value of Mendoza (1958),
-0.77, is similar to that of Crawford. A discrepancy,
presumably in the colors of the models, again appears.
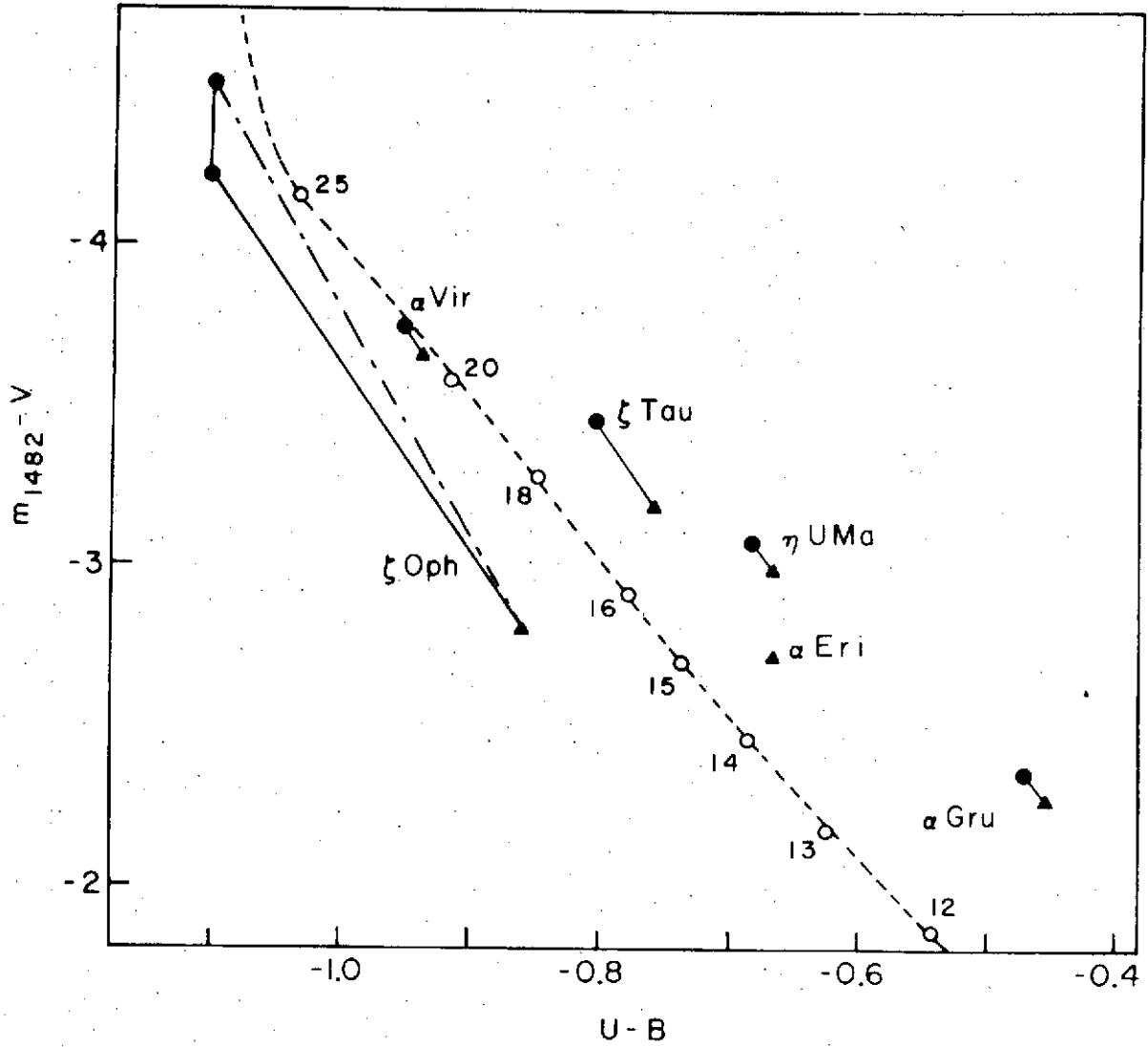
Fig. 8. The ultraviolet-visible color of Figure 7 is compared with U-B color. Symbols are as in Figure 7. The models differ systematically from the observations, probably because of deficiencies in the visible colors of the models.

b) Comparison with Observations of Others

The far ultraviolet colors listed in table 3 may be compared with the $(m_{1376}-V)_o$ colors of Smith (1967), also listed in table 3. Values given are slightly revised by Smith (personal communication). For the five stars observed in common, the average value of $(m_{1482}-V)_o$ - $(m_{1376}-V)_o$ = -0.07 $\pm$ 0.34, an absolute agreement which is clearly fortuitous in view of the overall uncertainty of 50% stated by Smith. The scatter of $\sim$ 30%, however, is puzzling.

In figure 9, the present data for η U Ma, integrated in 50 $\overset{\bullet}{A}$ bins, are compared with a number of other observations, and with the SAO 16,000^{o}K model, both unreddened and reddened assuming E_{B-V} = 0.02. A typical ($\pm$10%) error bar is placed on one of the observed Apollo 17 points. The observation of Opal et al. (1968) falls somewhat, but perhaps not significantly, below the present observation, although below 1216 $\overset{\bullet}{A}$ the disagreement is serious. The observation of η U Ma by Bless, Fairchild, and Code (1972; as revised by Code, private communication) lies above the present observation, although again perhaps not significantly in view of the uncertainties in the absolute calibrations of the two experiments. The observation of Bohlin, Frimout, and Lillie (1974) at somewhat longer wavelengths extrapolates rather better to join the
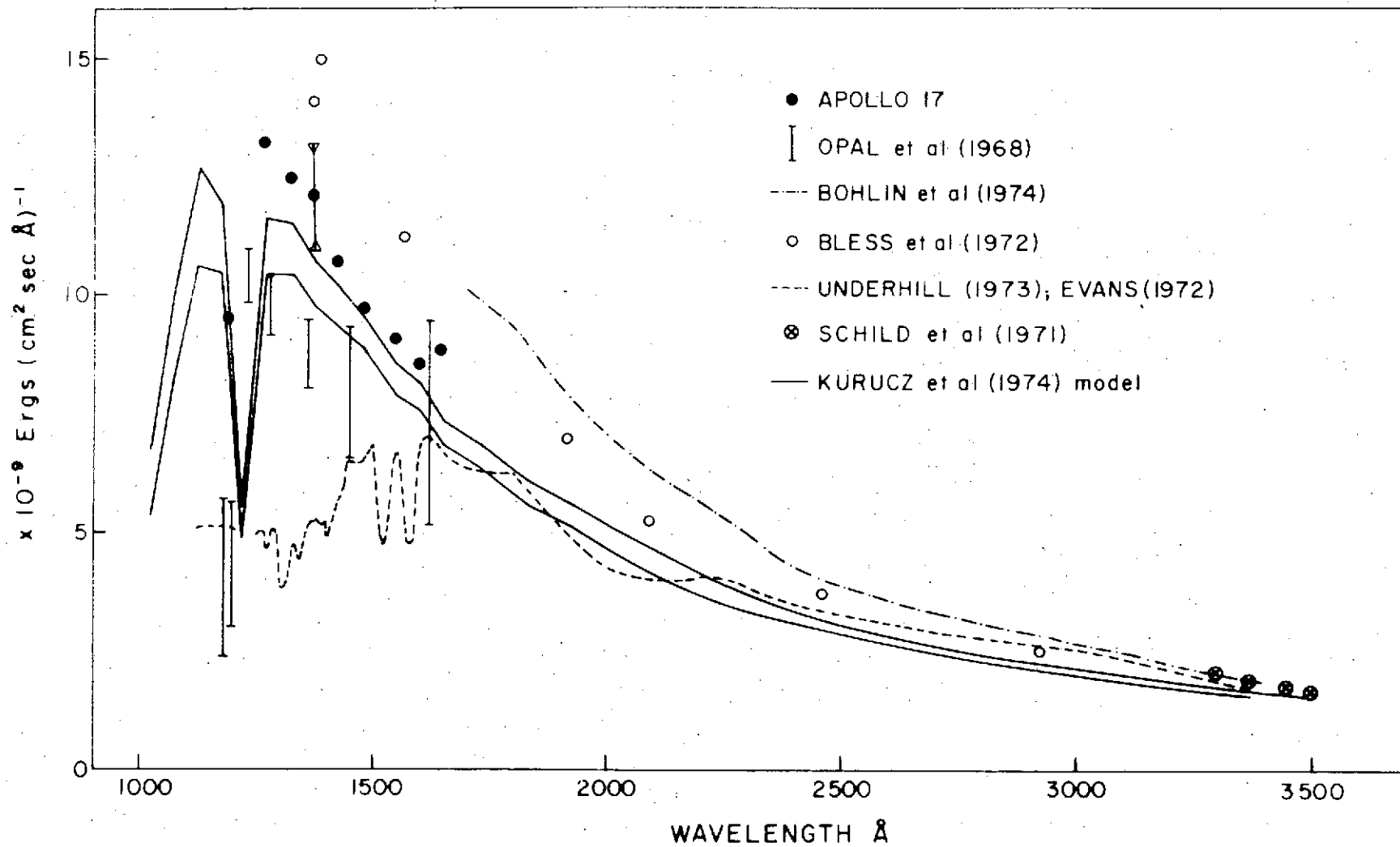
Fig. 9. Apollo 17 brightness of - UMa is shown as filled circles. The SAO (Kurucz et al. 1974) models are 16,000°K, unreddened and reddened with $E_{B-V} = 0.02$. All models in all figures in this paper are log g = 4. This figure compares the present observation with the observations of others.

Bless et al. observation than the present observation, especially if one is guided by the models. The SAO 18,000°K model provides an excellent fit to this combination of observations. The combination by Underhill (1973) of OAO-2 spectral scans with the absolute calibration of Evans (1972) falls below the present observation.

c) Effective Temperatures

Using figure 1 through 6, an effective temperature for the six stars may be deduced. In each case we have decided that the star is actually reddened by the amount indicated in table 2. The deduced effective temperatures are given in table 3, with an uncertainty that includes the 10% uncertainty in absolute calibration of the experiment. These effective temperatures are compared in figure 10 with the effective temperature scale of Adams and Morton. The data suggest that the stars could be somewhat cooler than that calibration indicates, but the error bars show that this is not at all certain.

Statistical precision and agreement in shape between observation and model were not good enough to provide much discrimination with regard to surface gravity, given the temperature. The log g = 2 SAO models could usually be ruled out, but the log g = 3 and log g = 4 models fit about equally well.
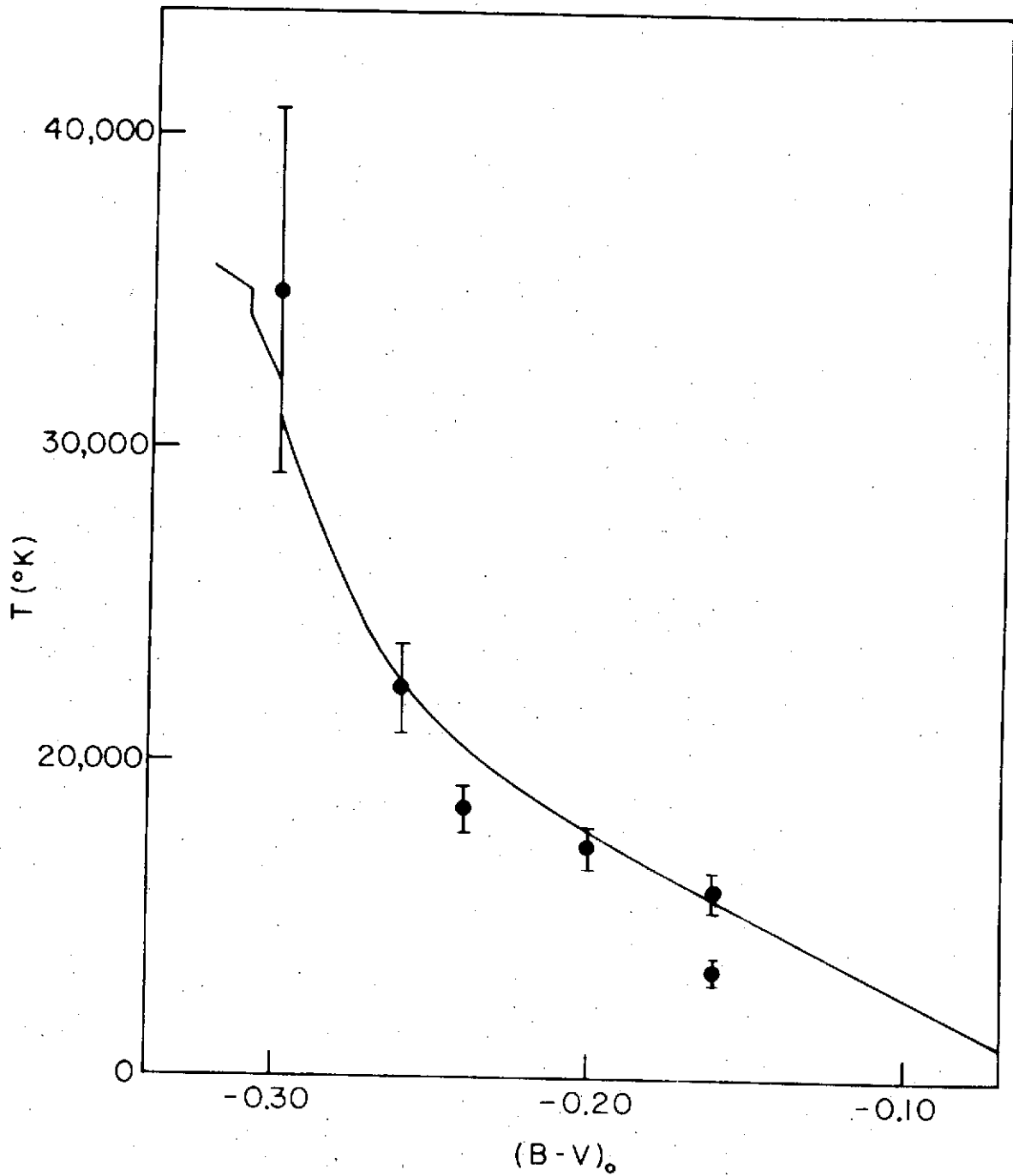
Fig. 10. Effective temperatures derived from a comparison of the present data with the SAO model are shown as a function of B-V color. The solid line is the effective temperature scale of Adams and Morton (1968).

d) Angular Diameters

The observed brightness of the stars at earth may be combined with the predicted (stellar model) brightness at the surface of the star to deduce an angular diameter for the star. We have

$$\theta = 2 \ (f_\lambda / \pi F_\lambda)^{1/2} \ , \tag{4}$$

where f_λ is the observed flux in erg $(cm^2 \ sec \ \mu)^{-1}$ and F_λ is the value from the SAO tables. In table 4, the deduced angular diameters are compared with the directly observed (stellar interferometer) angular diameters for the four stars that were observed by Brown, Davis, and Allen (1974). Angles are in milliseconds of arc, and the last column gives the number of standard deviations between the two determinations. Agreement is satisfactory.

e) Spectral Lines

The present data are of spectral resolution (11 A) comparable to that of the OAO-2 Wisconsin experiment. Only for three stars, however, are our statistics good enough to reveal the character of the stronger lines, which are listed in table 5. Details concerning the atomic origin of the specific lines are given by Morton (1965). Agreement with Code and Bless (1970) regarding the strength of the Si IV and C IV lines is quite reasonable.

TABLE 4

ANGULAR DIAMETERS OF THE STARS

Star	θ present	θ direct	Δ, σ
♉ Oph	0.47 ± 0.07	0.51 ± 0.05	0.5
α Vir	1.00 ± 0.10	0.87 ± 0.04	1.2
α Eri	1.61 ± 0.08	1.92 ± 0.07	2.9
α Gru	1.19 ± 0.03	1.02 ± 0.07	2.2

TABLE 5

EQUIVALENT WIDTHS OF STRONG LINES

Star	α Vir	η UMa	α Eri
Spectral Type	B1 V	B3 V	B5 IV
Line			
C III 1247	0.5:		0.9:
Si III 1300	2.8	4.5	4.6
C II 1330	0.7:	2.7	2.2
Si IV 1400	4.9		0.8
C IV 1550	5.2		

IV. CONCLUSION

The observations obtained of the ultraviolet spectra of six hot stars may be interpreted in a reasonable fashion using the models by Kurucz, Peytremann, and Avrett (1974). The visible colors of these models appear to leave something to be desired (in fact the plot of the calculated U-B versus B-V for the models does not agree well with the observed colors of Johnson (1963)), and an absorption trough between 1400 and 1550 or 1600 A (or possibly just a rise below 1400 A) appears in some of the stars, a feature which does not appear in the models.

REFERENCES

Adams, T. T., and Morton, D. C. 1968, <u>Ap. J.</u>, 151, 611.

Blanco, V. M., Demers, S., Douglass, G. G., and Fitzgerald, M. P. 1970, <u>Publ. U. S. Naval Obs.</u>, Second Series, Vol. XXI.

Bless, R. C., Fairchild, T., and Code, A. D. 1972, in <u>The Scientific Results from the OAO-2</u>, <u>ed.</u> A. D. Code, NASA SP-310.

Bless, R. C., and Savage, B. D. 1972, <u>Ap. J.</u>, 171, 293.

Bohlin, R. C., Frimont, D., and Lillie, C. F. 1974, Astron. and Astrophy., submitted.

Brown, R. H., David, J., and Allen, L. R. 1974, <u>M. N.</u>, 167, 121.

Code, A. D., and Bless, R. C. 1970, in <u>Ultraviolet Stellar Spectra and Related Ground-Based Observations</u>, ed. L. Houziaux and H. E. Butler, Reidel Dordrecht - Holland.

Crawford, D. L. 1963, <u>Ap. J.</u>, 137, 523.

Evans, D. C. 1972, in <u>The Scientific Results from the OAO-2</u>, <u>ed.</u> A. D. Code, NASA SP-310.

Fastie, W. G. 1973, <u>The Moon</u>, 7, 49.

Fastie, W. G., Feldman, P. D., Henry, R. C., Moos, H. W., Barth, C. A., Thomas, G. E., and Donahue, T. M. 1973 a, <u>Science</u>, 182, 710.

Fastie, W. G., Feldman, P. D., Henry, R. C., Moos, H. W., Barth, C. A., Thomas, G. E., Lillie, C. F., and

Donahue, T. M. 1973 b, in <u>Apollo 17 Preliminary Science Report</u>, NASA SP-330.

Fastie, W. G., and Kerr, D. E. 1974, preprint.

Iriarte, B., Johnson, H. L., Mitchell, R. I., Wisniewski, W. K. 1965, <u>Sky and Telescope</u>, 30, 21.

Johnson, H. L. 1963, in <u>Basic Astronomical Data</u>, vol. III of <u>Stars and Stellar Systems</u>, ed. B. P. Kuiper, Univ. of Chicago Press, Chicago.

Kurucz, R. L., Peytremann, E., Avrett, E. H. 1974, <u>Blanketed Model Atmospheres for Early-Type Stars</u>, Smithsonian Astrophysical Observatory (in press).

Lincoln, V. 1973, <u>J. Geophys. R.</u>, 78, 1739.

Mendoza, V. 1958, <u>Ap. J.</u>, 128, 207.

Morton, D. 1965, <u>Ap. J.</u>, 141, 73.

Oke, J. B., and Schild, R. E. 1970, <u>Ap. J.</u>, <u>161</u>, 1015.

Opal, C. B., Moos, H. W., Fastie, W. G., Bottema, M., and Henry, R. C. 1968, <u>Ap. J. (Letters)</u>, 153, L179.

Smith, A. M. 1967, <u>Ap. J.</u>, 147, 158.

Schild, R., Peterson, D. M., and Oke, J. B. 1971, <u>Ap. J.</u>, 166, 95.

Shobbrock, R. R., Lomb, N. R., and Herbison-Evans, D. 1972, <u>M. N.</u>, 156, 165.

Slettebak, A. 1949, <u>Ap. J.</u>, 110, 498.

Slettebak, A. 1954, <u>Ap. J.</u>, 119, 146.

Slettebak, A. 1955, <u>Ap. J.</u>, 121, 653.

Troy, B. E., Johnson, C. Y., Young, J. M., and Holmes, J. C. 1974, <u>Ap. J.</u>, submitted.

Underhill, A. B. 1973, <u>Astron. and Astroph.</u>, 25, 175.

Van Citters, G. W., and Morton, D. C. 1970, <u>Ap. J.</u>, <u>161</u>,
    695.

Vidal-Madjar, W., Blamont, J. E., and Phissamay,B. 1973,
    <u>J. Geophys. R.</u>, 78, 1115.

FLUORESCENCE OF MOLECULAR HYDROGEN EXCITED BY SOLAR EXTREME-ULTRAVIOLET RADIATION

PAUL D. FELDMAN AND WM. G. FASTIE

PRECEDING PAGE BLANK NOT FILMED

FLUORESCENCE OF MOLECULAR HYDROGEN EXCITED BY SOLAR EXTREME-ULTRAVIOLET RADIATION

PAUL D. FELDMAN* AND WM. G. FASTIE

Physics Department, Johns Hopkins University, Baltimore
Received 1973 June 8; revised 1793 August 6

ABSTRACT

The ultraviolet fluorescence spectrum of H_2 excited by solar extreme-ultraviolet radiation was observed by the *Apollo 17* Ultraviolet Spectrometer during a purge of the hydrogen fuel cells. Absorption of $L\beta$ and $L\gamma$ in the nearly resonant (6, 0) and (11, 0) Lyman bands completely accounts for the observed spectrum.

Subject headings: molecules — spectra, ultraviolet

During trans-Earth coast, the *Apollo 17* Ultraviolet Spectrometer was scheduled to make observations of the far-ultraviolet background in selected regions of the sky. In the course of one of these observations the spacecraft fuel cells were routinely purged of excess hydrogen and water vapor. The spectrum obtained during 4 minutes of purge, subtracted from the sky background spectrum obtained immediately preceding and following the purge, is shown in figure 1a. The interpretation of this spectrum is straightforward, involving the absorption of solar $L\beta$ and $L\gamma$ radiation in nearly coincident Lyman bands, but the results are quite significant for investigations of the atmospheres of the Moon, planets, and comets by ultraviolet spectroscopy.

The *Apollo 17* Ultraviolet Spectrometer is a $\frac{1}{2}$-meter Ebert-type spectrometer designed to scan the region 1180–1680 Å with 10 Å resolution every 12 seconds. A complete description of the instrument has been given by Fastie (1973). In order to make optimum use of the Apollo Scientific Data System, the scan rate was variable during a complete spectrum scan. The "histogram" effect in the spectrum of figure 1a is the result of only three data samples per spectral resolution element during the fast portion of each scan. Instrument sensitivity is shown in the figure. The effluent from the fuel-cell purge consisted of equal parts, by mass, of hydrogen and water vapor. A waste-water dump 10 minutes before the fuel-cell purge did not produce a detectable spectrum other than $L\alpha$, so we may assume that the observed spectrum is due to H_2 alone.

We consider absorption only from the lowest vibrational level $(v = 0, J)$ of the ground electronic state $X\ ^1\Sigma_g{}^+$ to level (v', J') of the $B\ ^1\Sigma_u{}^+$ state and the subsequent fluorescent decay to ground-state level (v'', J''). A column of N_J molecules cm^{-2} along the line of sight will produce a column emission rate of $4\pi I_{v'v''}{}^{J'J''}$ in the $(J'J'')$ line of the $(v'v'')$ band given by

$$4\pi I_{v'v''}{}^{J'J''} = g_{0v'}{}^{JJ'} \left(A_{v'v''}{}^{J'J''} \Big/ \sum_{v'',J''} A_{v'v''}{}^{J'J''} \right) N_J \text{ photons s}^{-1}\text{ cm}^{-2} \text{ (column)}$$

and

$$g_{0v'}{}^{JJ'} = \pi J_{0v'}{}^{JJ'} (\lambda_{0v'}{}^{JJ'})^2 \frac{\pi e^2}{mc^2} f_{0v'}{}^{JJ'} \text{photons s}^{-1} \text{ mol}^{-1}, \qquad (1)$$

where $\pi J_{0v'}{}^{JJ'}$ is the solar flux in photons cm^{-2} s^{-1} A^{-1} at wavelength $\lambda_{0v'}{}^{JJ'}$; $f_{0v'}{}^{JJ'}$ is the absorption oscillator strength; and $A_{v'v''}{}^{J'J''}$ is the line emission probability. At

* Alfred P. Sloan Research Fellow.
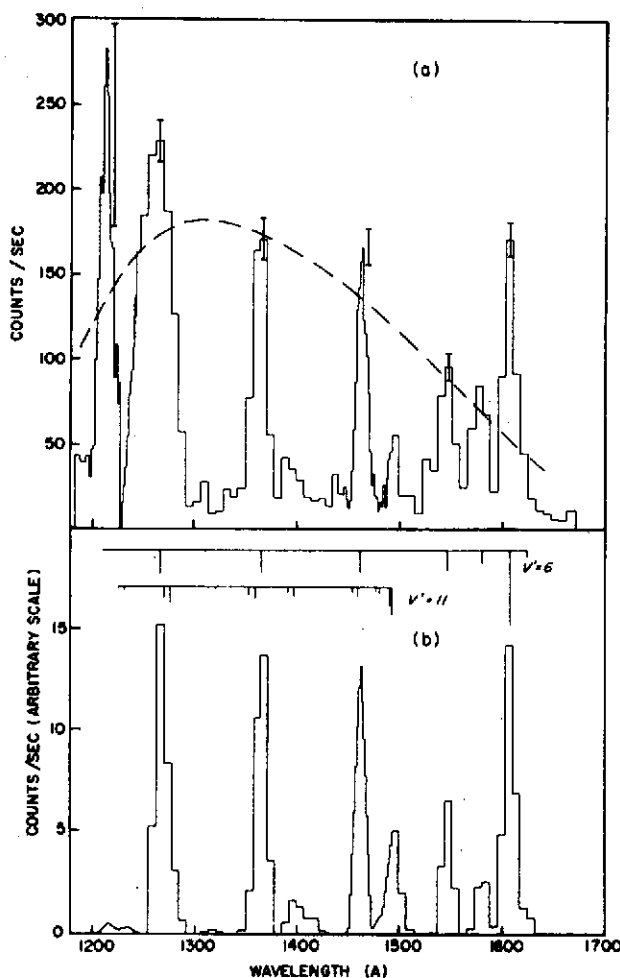
FIG. 1.—(a) The sum of 21 spectra obtained during a hydrogen purge of the *Apollo 17* fuel cells. The sky background spectrum observed before and after the purge has been subtracted. Error bars represent 1 standard deviation in the observed count rate. The dashed curve represents the response of the spectrometer to a source of uniform spectral brightness of 2 R. (b) Relative transition probabilities for the $v' = 6$ $P(1)$, and $v' = 11$ $R(1)$ and $P(3)$, progressions of the H_2 Lyman bands and the synthetic spectrum, with the two progressions taken in the ratio of 4 to 1, respectively.

$300°$ K only the $J = 0, 1$, and 2 rotational levels need be considered. The relevant parameters for those lines in the Lyman bands which are nearly coincident with solar emission lines are given in table 1. The band oscillator strengths are from Allison and Dalgarno (1970), and the Lyman-band wavelengths are computed from the rotational and vibrational constants of Herzberg and Howe (1959). The Doppler shift, due to the relative motion between the Sun and spacecraft, is -0.003 Å. The spectral flux may be directly evaluated only at $L\beta$, using the measured line profile of Tousey (1963) and the flux measurements of Hinteregger (1970).

The relative emission probabilities are shown in figure 1*b* for the $v' = 6$ and 11 progressions (Allison and Dalgarno 1970). Absorption of the C II line, which gives

TABLE 1

Band, Line (v', v'')	Wavelength (Å)	$f_{0v'}{}^{JJ'}$	Solar Line	Flux (photons cm^{-2} s^{-1} A^{-1})	$g_{0v'}{}^{JJ'}$
(5,0), $R(1)$	1037.15	0.0168	C ɪɪ (1037.02 Å)	7×10^{8}*	5×10^{-8}*
(6,0), $P(1)$	1025.935	0.0091	Lβ (1025.72 Å)	6.7×10^{9}	5.6×10^{-7}
(11,0), $R(1)$	972.633	0.0120	Lγ (972.537 Å)	3×10^{9}†	2×10^{-7}†

* Based on identification of (5, 8) band at 1436 Å.
† Allows for 40% decay to the ground-state vibrational continuum.

rise to the $v' = 5$ progression, is neglected, since, if we identify the weak feature in figure 1a at 1436 Å as the (5, 8) band, the rate factor g_{05} is found to be an order of magnitude smaller than g_{06}. The summation over v'' includes only the discrete ground vibrational levels, and ignores transitions to the vibrational continuum ($v'' > 14$) (Stecher and Williams 1967). Dalgarno and Stephens (1970) estimate that for $v' = 6$, less than 3 percent of the transitions lead to dissociation and may be neglected, while for $v' = 11$ nearly 40% of the transitions are to the continuum. A good fit to the data is obtained by assuming that the $v' = 6$ and $v'' = 11$ progressions contribute in a ratio of 4 to 1. A synthetic spectrum of emission from an optically thin region of H_2, including the instrument response function, is given in figure 1b and agrees quite well with figure 1a. The solar spectral flux at 972.6 Å, derived from the observation, and including the dissociative loss, is given in table 1.

The Lα feature in figure 1a represents a 2 percent increase over the background of solar Lα resonantly scattered by interplanetary hydrogen, and is most likely the result of photodissociation into the $2p$ state. From the observed column emission rate at 1608 Å of 8.3 R [1 rayleigh $= 10^{6}$ photons s^{-1} cm^{-2} (column)], using the numerical factors given in table 2, the H_2 density along the line of sight is found from equation (1) to be 8.1×10^{13} cm^{-2}. The Lα emission rate factor, based on the observed rate of 5.2 R, is found to be 6.5×10^{-8} s^{-1} molecule^{-1} at 1 a.u. For Venus,

TABLE 2

A. Emission Rate Factors at 1 a.u.

Transition	λ(Å)	g
(6, 5)	1265.7	4.9×10^{-8}
(6, 7)	1365.7	4.6×10^{-8}
(6, 9)	1462.0	4.4×10^{-8}
(6, 11)	1546.7	4.7×10^{-8}
(6, 13)	1607.5	1.6×10^{-7}

B. Relative Population of the $J = 1$ Level

T (°K)	$n_{J=1}/\Sigma_J n_J$
200	0.72
300	0.66
400	0.58
500	0.51
700	0.41

this number is 1.24×10^{-7} s^{-1}, which may be compared with the value of 6.3×10^{-8} of Dalgarno and Allison (1969) and 8.6×10^{-8} of Barth, Wallace, and Pearce (1968), derived from theoretical and experimental photodissociation cross-sections, respectively. However, Dalgarno and Allison found that photodissociation yielded atoms predominantly in the metastable $2s$ state. Mentall and Gentieu (1970) observed that the rate of photodissociation directly into $2p$ was less than 15 percent of the total rate. In a planetary atmosphere, collisional transfer from $2s$ to $2p$ ensures that the quantum efficiency for Lα emission will be near unity. However, in the present case, the possibility that the H$_2$ cloud is collisionless beyond a certain distance from the exit nozzle questions the reliability of the derived column density and hence the absorption g-factor. The major source of uncertainty is the solar Lβ line, which, like the well-studied Lα line, is variable in line width across the disk of the sun, and is variable in intensity with time. However, if the g-factor were to be reduced by an order of magnitude, the contribution of the solar continuum to the fluorescence would produce a spectrum noticeably different from that of figure $1a$. Another possible source of the high Lα emission is the fluorescence of H$_2$O or the reflection of solar Lα from ice crystals in the ejecta. However, during the waste-water dump preceding the purge, the Lα signal was similarly 5 R, but the H$_2$O flow rate was a factor of 200 higher, so this possibility must be excluded. Further high-resolution observations of solar Lβ, similar to the Lα data recently reported by Bruner et al. (1973) are needed to quantitatively establish the fluorescence g-factors.

Nevertheless, Lyman-band fluorescence provides an unambiguous means of identification of molecular hydrogen in the upper atmospheres of the planets and comets. For investigation of comets, care must be taken to ensure that the Doppler shift due to the relative motion between the comet and the Sun does not displace the solar Lβ line completely outside the H$_2$ absorption line. In this regard, viewing conditions are most favorable after perihelion.

REFERENCES

Allison, A. C., and Dalgarno, A. 1970, *Atomic Data*, **1**, 289.
Barth, C. A., Wallace, L., and Pearce, J. B. 1968, *J. Geophys. Res.*, **73**, 2541.
Bruner, E. C., Parker, R. W., Chipman, E., and Stevens, R. 1973, *Ap. J. (Letters)*, **182**, L33.
Dalgarno, A., and Allison, A. C. 1969, *J. Geophys. Res.*, **74**, 4178.
Dalgarno, A., and Stephens, T. L. 1970, *Ap. J. (Letters)*, **160**, L107.
Fastie, W. G. 1973, *Moon*, **7**, 49.
Herzberg, G., and Howe, L. L. 1959, *Canadian J. Phys.*, **37**, 636.
Hinteregger, H. E. 1970, *Ann. Geophys.*, **16**, 547.
Mentall, J. E., and Gentieu, E. P. 1970, *J. Chem. Phys.*, **52**, 5641.
Stecher, T. P., and Williams, D. A. 1967, *Ap. J. (Letters)*, **149**, L29.
Tousey, R. 1963, *Space Sci. Rev.*, **2**, 3.

NATIONAL DATA CENTER INFORMATION

Apollo 17 Ultraviolet Spectrometer Experiment

Data Format

The data from the Apollo 17 Ultraviolet Spectrometer Experiment (S-169) are contained on five magnetic tapes covering the following time periods:

Tape 1:	81:37:30	- 94:58:21	CTE
Tape 2:	110:51:58	- 188:55:06	CTE
Tape 3:	188:55:18	- 234:54:00	CTE
Tape 4:	235:04:08	- 273:08:39	CTE
Tape 5:	273:09:19	- 299:31:22	CTE

Each 12-second spectrometer scan is represented by one physical record containing 125 36-bit integer words. The record format is given in Table I. The data words represent the number of photoelectrons per 0.1 second, and the wavelengths corresponding to each data word are given in Table II. Note that at large counting rates, the data words must be corrected for counter dead-time according to the following expression:

$$C_{actual} = \frac{C_{obs}}{1 - (C_{obs}\tau)} \tag{1}$$

where C_{actual} is the real count rate per 0.1 second

C_{obs} is the observed count rate per 0.1 second

and $\tau = 1.83 \times 10^{-5}$.

Data records that have flagged data dropouts or do not match the synch words have been eliminated from the final tape.

To convert the actual count rate to brightness, we use the expression

$$S = B \cdot \frac{10^{-6}}{4\pi} \frac{A_s A_g (QTPG)}{F^2}$$

where   S is the signal in counts <u>per second</u>

              B is the brightness in Rayleighs

              A_s is the slit area = 1.14 cm²

              A_g is the grating area = 104 cm²

              F is the focal length = 50 cm.

The product of quantum efficiency and transmission, QTPG, is given in Table III at 11 wavelengths, along with the instrument sensitivity in photoelectrons/second/Rayleighs.

During the mission, the sensitivity of the instrument deteriorated due to continuous exposure to solar Lyman-α radiation reflected by the moon. During trans earth coast the sensitivity was reduced to 83% of the value given in the calibration table.

A detailed description of the instrument is given in Fastie, The Moon, <u>7</u>, 49 (1973). Preliminary results are given in the <u>Apollo 17 Preliminary Science Report</u>, NASA SP-330, p. 23-1 (1973) and by Fastie <u>et al.</u>, Science <u>182</u>, 710 (1973).

Sensitivity

During lunar orbit the UVS sensitivity decreased linearly with time from the values shown above to 83% of those values. During transearth coast the sensitivity was constant at 83% of the listed values.

Dark Count

The dark count rate varied by the same percentages with which the UVS sensitivity varied. However, the dark count rate was also sensitive

to the spacecraft altitude above the moon as described in Addendum C of the UVS final report. During transearth coast the dark count rate was constant at 2.76 counts per tenth second.

Scattered Light

During several periods in transearth coast the UVS was observing interstellar space or a background of very weak stars with the interference of solar system Ly α scattered by the grating. This scatter signal consisted of a family of Rowland Ghosts and an apparent spectral continuum. Analysis of weak spectra observed during transearth coast requires the subtraction of 2.764 counts from each tenth second word plus the subtraction of a percentage of the peak Ly α signal from each tenth second word as shown in Table IV. Because of the uncertainty in the UV background correction, the values listed in Table IV may be too high by as much as 0.07×10^{-3}.

In order to make use of the above data it is necessary to know the viewing direction of the UVS during the observation periods. This information has also been filed. Scientific data analysis indicated that there are some small but significant errors in the aspect information from 260 hours CTE until the end of the mission. Further analysis is in progress. If the errors can be resolved, this information will be subsequently submitted.

TABLE I.   Record Format (S-169)

Word	
0	Johns Hopkins "green" word - ignore
1	synch word = 65514
2	synch word = 21
3	motor step count (typically 4800)
4	synch word = 21
5	synch word = 65514
6- 120	data words
121	original tape number
122	⎰record and word location on original
123	⎱tape of first synch word
124	time (CTE) in integer milliseconds of word one

TABLE II. Wavelengths Corresponding to Each 0.1 Sec Word

Word no.	Wavelength interval, nm		Word no.	Wavelength interval, nm	
	From –	To –		From –	To –
6	118.400	118.409	66	143.997	144.357
7	118.409	118.905	67	144.357	144.595
8	118.905	119.450	68	144.595	144.808
9	119.450	119.767	69	144.808	144.967
10	119.767	119.946	70	144.967	145.144
11	119.946	120.133	71	145.144	145.316
12	120.133	120.299	72	145.316	145.454
13	120.299	120.522	73	145.454	145.634
14	120.522	120.738	74	145.634	145.808
15	120.738	120.935	75	145.808	145.959
16	120.935	121.114	76	145.959	146.141
17	121.114	121.285	77	146.141	146.318
18	121.285	121.461	78	146.318	146.464
19	121.461	121.627	79	146.464	146.603
20	121.627	121.788	80	146.603	146.744
21	121.788	121.972	81	146.744	146.913
22	121.972	122.148	82	146.913	147.054
23	122.148	122.312	83	147.054	147.251
24	122.312	122.480	84	147.251	147.387
25	122.480	122.638	85	147.387	147.535
26	122.638	122.776	86	147.535	147.694
27	122.776	122.916	87	147.694	147.853
28	122.916	123.040	88	147.853	148.022
29	123.040	123.211	89	148.022	148.196
30	123.211	123.403	90	148.196	148.378
31	123.403	123.571	91	148.378	148.567
32	123.571	123.711	92	148.567	148.742
33	123.711	123.867	93	148.742	148.887
34	123.867	124.017	94	148.887	149.015
35	124.017	124.131	95	149.015	149.289
36	124.131	124.224	96	149.289	149.883
37	124.224	124.315	97	149.883	150.648
38	124.315	124.683	98	150.648	151.448
39	124.683	125.410	99	151.448	152.222
40	125.410	126.182	100	152.222	152.978
41	126.182	126.987	101	152.978	153.681
42	126.987	127.711	102	153.681	154.402
43	127.711	128.399	103	154.402	155.092
44	128.399	129.164	104	155.092	155.821
45	129.164	129.870	105	155.821	156.591
46	129.870	130.616	106	156.591	157.371
47	130.616	131.383	107	157.371	158.071
48	131.383	132.109	108	158.071	158.784
49	132.109	132.826	109	158.784	159.589
50	132.826	133.543	110	159.589	160.334
51	133.543	134.209	111	160.334	161.074
52	134.209	134.998	112	161.074	161.778
53	134.998	135.722	113	161.778	162.505
54	135.722	136.376	114	162.505	163.287
55	136.376	137.059	115	163.287	163.987
56	137.059	137.790	116	163.987	164.764
57	137.790	138.513	117	164.764	165.535
58	138.513	139.216	118	165.535	166.247
59	139.216	139.908	119	166.247	166.972
60	139.908	140.643	120	166.972	167.157
61	140.643	141.363			
62	141.363	142.087			
63	142.087	142.793			
64	142.793	143.484			
65	143.484	143.997			

TABLE III. Calibration Data

Wavelength (A)	QTPG	Photoelectrons/sec/R
1192	.0163	61.5
1216	.0196	74
1280	.0263	99
1336	.0251	95
1395	.0233	88
1463	.0200	75.5
1518	.0156	59
1582	.0093	35
1608	.0079	29.8
1639	.0070	26.4
1655	.0078	29.4

TABLE IV. Scattered Light Fraction*

Word	Fraction	Word	Fraction	Word	Fraction
6	1.48×10^{-3}	61	.44	97	.37
7	1.87	2	.47	8	.29
8	1.87	3	.48	9	.32
9	2.21	4	.33	100	.33
10	2.11	5	.41	1	.29
		6	.42	2	.23
30	1.81	7	.39	3	.48
1	1.54	8	.51	4	.33
2	1.48	9	.41	5	.21
3	1.77	70	.25	6	.37
4	1.95	1	.39	7	.23
5	1.79	2	.43	8	.19
6	1.95	3	.49	9	.33
7	2.19	4	.48	110	.36
8	1.95	5	.46	1	.33
9	1.46	6	.33	2	.26
40	1.25	7	.44	3	.23
1	1.07	8	.32	4	.42
2	.73	9	.38	5	.33
3	.64	80	.39	6	.53
4	.63	1	.34	7	.67
5	.73	2	.46	8	.75
6	1.49	3	.49	9	.67
7	1.10	4	.38	120	.65
8	.65	5	.39		
9	1.11	6	.39		
50	1.31	7	.42		
1	.99	8	.36		
2	.85	9	.48		
3	.74	90	.41		
4	.55	1	.33		
5	.54	2	.26		
6	.44	3	.48		
7	.41	4	.39		
8	.53	5	.34		
9	.49	6	.33		
60	.32				

*To determine word count to be subtracted multiply above fractions for
each word by Ly α peak count rate. The listed values may include a
component due to a weak stellar or interstellar UV continuum of the order
of 0.07×10^{-3}.